EVALUATING 3D PRINTABILITY OF SOY PROTEIN-WHEAT GLUTEN-EPIGALLOCATECHIN GALLATE COMPLEXES

SHIVANI MITTAL

Department of Bioresource Engineering

McGill University, Montréal, Canada

AUGUST 2024

A thesis submitted to McGill University in partial fulfillment of the requirements of the degree of Master of Science

Abstract

This study aims to perform a multivariate assessment of the impact of various 3D printing parameters on the printability of protein-polyphenol complexes and to predict the printability of these complexes. It explores the potential of 3D printing technology in producing functional and customizable plant-based protein products, focusing on soy protein isolate (SPI), wheat gluten (WG), and epigallocatechin gallate (EGCG) complexes. Factors studied include EGCG concentration, nozzle speed, nozzle diameter, and height/diameter (H/D) ratio.

Using a fractional factorial design, the research examined the effects of these parameters across 144 experimental runs, with variations in EGCG concentration (0%, 0.25%, 0.5%, 1%), nozzle diameter (1.5 mm, 4 mm), nozzle H/D ratio (0.85, 1, 1.25), and nozzle speed (50 mm/sec, 58 mm/sec, 65 mm/sec, 228 mm/sec, 235 mm/sec, 245 mm/sec). Protein-polyphenol inks were prepared by mixing SPI, WG, oil, and water in a 5:3:2:33.3 ratio, followed by the addition of EGCG at specified concentrations. Two-dimensional line filaments and three-dimensional cylindrical structures were printed to assess dimensional stability and print quality. Image analysis was conducted using MATLAB to quantify line width, thickness, and cross-sectional area from the two-dimensional line filaments, while ImageJ was used to determine the dimensional stability of the three-dimensional structures by comparing the change in the inner diameter of hollow cylinders to the actual design specifications. A four-way ANOVA was applied to statistically analyze the significance of factors and their interactions on printability, revealing that EGCG concentration, nozzle diameter, and H/D ratio significantly influenced the structural integrity and consistency of the printed products. The results demonstrated that optimal settings for print quality were a 1% EGCG concentration, a 4 mm nozzle diameter, and a 0.85 H/D ratio. Additionally, machine learning techniques were employed to predict printability, demonstrating that a Linear Discriminant Analysis (LDA) model could effectively predict the quality of extruded filaments based on the parameters used.

This research contributes to enhancing the precision and quality of 3D-printed plant-based protein products, offering valuable insights for the development of sustainable, nutritious food alternatives. The findings support the advancement of 3D food printing technology and material formulation, paving the way for innovative and efficient production processes in the plant-based food industry.

Résumé

Cette étude vise à réaliser une évaluation multivariée de l'impact de divers paramètres d'impression 3D sur l'imprimabilité des complexes protéines-polyphénols et à prédire l'imprimabilité de ces complexes. Elle explore le potentiel de la technologie d'impression 3D dans la production de produits protéiques végétaux fonctionnels et personnalisables, en se concentrant sur les complexes d'isolat de protéines de soja (SPI), de gluten de blé (WG) et de gallate d'épigallocatéchine (EGCG). Les facteurs étudiés comprennent la concentration d'EGCG, la vitesse de la buse, le diamètre de la buse et le rapport H/D. En utilisant un plan factoriel fractionnaire, la recherche a examiné les effets de ces paramètres sur 144 essais expérimentaux, avec des variations de concentration d'EGCG (0, 0,25, 0,5, 1), de diamètre de buse (1,5 mm, 4 mm), de rapport H/D de buse (0,85, 1, 1,25) et de vitesse de buse (50, 58, 65, 228, 235, 245 mm/sec). Les encres à base de protéines et de polyphénols ont été préparées en mélangeant du SPI, du WG, de l'huile et de l'eau dans un rapport de 5:3:2:33,3, suivi de l'ajout d'EGCG à des concentrations spécifiées. Des filaments de lignes bidimensionnels et des structures cylindriques tridimensionnelles ont été imprimés pour évaluer la stabilité dimensionnelle et la qualité d'impression. L'analyse d'image a été réalisée à l'aide de MATLAB pour quantifier la largeur, l'épaisseur et la section transversale des filaments de ligne bidimensionnels, tandis qu'ImageJ a été utilisé pour déterminer la stabilité dimensionnelle des structures tridimensionnelles en comparant le changement du diamètre intérieur des cylindres creux aux spécifications de conception réelles. Une ANOVA à quatre facteurs a été appliquée pour analyser statistiquement la signification des facteurs et de leurs interactions sur l'imprimabilité, révélant que la concentration d'EGCG, le diamètre de la buse et le rapport H/D influençaient de manière significative l'intégrité structurelle et la cohérence des produits imprimés. Les résultats ont démontré que les paramètres optimaux pour la qualité d'impression étaient une concentration d'EGCG de 1 %, un diamètre de buse de 4 mm et un rapport H/D de 0,85. De plus, des techniques d'apprentissage automatique ont été utilisées pour prédire l'imprimabilité, démontrant qu'un modèle d'analyse discriminante linéaire (LDA) pouvait prédire efficacement la qualité des filaments extrudés en fonction des paramètres utilisés.

Cette recherche contribue à améliorer la précision et la qualité des produits protéiques végétaux imprimés en 3D, offrant des informations précieuses pour le développement d'alternatives alimentaires durables et nutritives. Ces résultats soutiennent l’avancement de la technologie d’impression alimentaire 3D et de la formulation des matériaux, ouvrant la voie à des processus de production innovants et efficaces dans l’industrie alimentaire d’origine végétale.

Acknowledgments

I would like to express my deepest gratitude to my supervisor, Professor Michael Ngadi, for generously providing the space and equipment from his lab that were essential for conducting my experiments. His invaluable guidance and unwavering support throughout this research have been instrumental in its success. I also extend my heartfelt thanks to my co-supervisor, Dr. Idaresit Ekaette, whose insights and advice have greatly enriched this work.

I am profoundly thankful to Dr. Michael Osadebey for dedicating countless hours to assist with the statistical analysis. My sincere appreciation also goes to Md Hafizur Rahman Bhuiyan for his diligent corrections and edits to this work.

I extend my heartfelt thanks to my friends Chinwendu Eze, Bikramjeet Singh, Ishwinder Kaur, Revathi Kollipara, Amy Milne, and my brother Ansh Mittal for their unwavering support and assistance whenever I encountered difficulties. Your encouragement and help have been immensely valuable.

To my parents, Sanjeev Mittal and Dolly Mittal, I owe everything. Your unwavering support and the resources you provided for my education have enabled me to achieve this milestone. I dedicate this work to you both with profound gratitude and love.

Contribution of Authors

This thesis comprises two manuscripts, both of which I am the primary author. I conducted the research work, collected data, analysed the data, and wrote the manuscripts. My supervisor, Dr. Michael Ngadi is also an author in both manuscripts.

He provided overall guidance and concepts for the work as well as reviewed the manuscripts. Md Hafizur Rahman Bhuiyan edited and corrected the 2^{nd} chapter of the thesis. Dr. Michael Osadebey had direct participation in the statistical analysis of the results as reported in the 4^{th} chapter. His contributed not only in data analysis but also in decision regarding the better-fitting models, and interpreting the meaning and significance of the model parameters.

Chapter 3 has been accepted and presented at the Future of Food: Innovation, Challenges and Perspectives Symposium. Chapter 2 has been published in MDPI scientific publication in December 2023.

Signed: Shivani Mittal

Date: August 2024

Table of Contents

List of Tables

List of Figures

Nomenclature

°C	-	Celsius degrees
3D	-	3 Dimensional
SPI	-	Soy protein isolate
EGCG	-	Epigallocatechin-3-gallate
WG	-	Wheat gluten
C-N	-	Carbon-Nitrogen
%	-	Percentage
EU	-	European Union
GHG	-	Greenhouse gas emissions
CAD	-	Computer-aided design
ASTM	-	American Society of Testing and Materials
%w/w	-	Weight per weight
mm^2/sec	-	Millimeter square per second
CS	-	Corn starch
W	-	Water
CO	-	Canola oil
XG	-	Xanthan gum
RS	-	Rice starch
µm	-	Micrometer
RC	-	Red cabbage
SEM	-	Scanning electron microscope
WPI	-	Whey protein isolate
pI	-	Isoelectric point
Pa.s	-	Pascal second
TSP	-	Textured soy protein
DSP	-	Drawing soy protein
SPAH	-	Soy protein acid hydrolysate
g	-	Gram
MC	-	Methylcellulose
s	-	Second
mm	-	Millimeter
G’	-	Storage modulus

G”	-	Loss modulus
Hz	-	Hertz
T_{gase}, TG	-	Transglutaminase
min	-	Minutes
NaCl	-	Sodium chloride
KCl	-	Potassium chloride
$CaCl_2$	-	Calcium chloride
$CaSO_4$	-	Calcium sulphate
mL	-	Milliliters
PPI	-	Pea protein isolate
rpm	-	Revolutions per minute
W	-	Watts
h	-	Hour
IDDSI	-	International Dysphagia Diet Standardization Initiative
PP	-	Pea protein
MBPI	-	Mung bean protein isolate
H_2O_2	-	Hydrogen peroxide
MD	-	Microwave drying
CID	-	Catalytic infrared drying
HAD	-	Hot air drying
NP	-	Nanoparticles
HPLC	-	High Performance Liquid Chromatography
USA	-	United States of America
mm/sec	-	Millimeter per second
ANOVA	-	Analysis of Variance
H/D	-	Height/Diameter
AIC	-	Akaike Information Criterion
MATLAB	-	Matrix Laboratory
EOS	-	Electro-Optical System
SLR	-	Single Lens Reflex
RGB	-	Red, Green and Blue
HSV	-	Hue, Saturation and Value

R_a	-	Arithmetic mean
RMS	-	Root mean square
MSE	-	Mean squared error
MAE	-	Mean absolute error
Rq	-	Root mean square average deviation
TPR	-	True positive rate
TNR	-	True negative rate
PRA	-	Precision accept
PRR	-	Precision reject
LDA	-	Linear discriminant analysis
GLM	-	Generalized linear model

I. General Introduction

1.1 Overview

The recognition of food security issues and the growing global population drive the quest for sustainable and environmentally friendly high-nutrition foods. This includes the exploration of alternative protein sources. It leads to growing concerns regarding the negative impacts of animal-derived foods on the environment, health, and religious beliefs, resulting in a rising inclination towards plant-based diets. Consequently, numerous scholars are investigating the feasibility of substituting animal-derived functional components with plant-based alternatives, focusing on plant-based proteins that accurately mimic the physicochemical, functional, sensory, and nutritional attributes of real animal-based products (Han *et al.* 2022).

Proteins constitute vital macronutrients in human nutrition, as reported by Adenekan *et al.* (2018). The nutritional value of a protein source exhibits significant variation, contingent upon factors such as bioavailability, digestibility, amino acid profile, purity, presence of antinutritional factors, and processing effects (Sa *et al.* 2020). There is an increasing global trend for highly nutritious, affordable, safe and easy-to-obtain plant protein-based diets. While numerous studies indicate that the majority of plant protein sources offer sufficient quantities of essential amino acids for human nutritional requirements (López *et al*., 2018; Sun-Waterhouse *et al.,* 2014), there is a common perception that plant proteins are incomplete or nutritionally inferior compared to animal proteins (Hughes *et al.,* 2011; Millward, 1999). Nevertheless, it is crucial to acknowledge that plant proteins play a significant and valuable role in human nutrition.

The fast-evolving plant-based food market ignites the development of technologies that can increase the functionality of essential plant-based constituents. 3D printing technology provides sustainable functionality to plant-based ingredients. This pioneering technology enables the generation of foods with personalized shapes, structures, compositions, and nutritional profiles through an additive manufacturing approach (Sun et al., 2018). In particular, this technology can be applied to create personalized food for diverse populations, such as athletes needing specific nutrients, children with a preference for sweets, elderly individuals with chewing or swallowing difficulties, and pregnant women requiring tailored nutritional requirements for their well-being (Godoi *et al.* 2016). Many start-ups like Novameat developed a process for producing 3D-printed meat by extruding filaments composed of peas, seaweed, and rice, replicating the flavor and texture of traditional meat (Montes *et al.*, 2018). Similarly, Legendary Vish 3D-printed salmon fillets utilize plant-based components such as mushroom proteins and algae extracts (Holmyard, 2020). While numerous companies and researchers have successfully created plant-based meat substitutes, there remains a gap when compared to animal meat in terms of attributes such as color, aroma, taste, flavor, mouthfeel, texture, and nutritional properties (Wen *et al.* 2023). In practice, the primary challenges associated with 3D printing innovative foods arise from various factors, including material characteristics, printing process parameters (such as nozzle size, printing speed, printing height, infill percentage, etc.), and post-processing considerations (Portanguen *et al*., 2019). Addressing these challenges is crucial for the continued advancement of 3D printing in the plant protein domain. Developing objective methods for assessing and improving the 3D printing process becomes paramount. This involves refining the composition of plant-based materials, optimizing printing parameters, and enhancing the overall quality of the printed products.

Plant-based meat analogues are a high source of protein (Singh et al 2021) and possess extensive thermo-mechanical properties, such as varying storage and loss modulus under constant force as a function of temperature, making them ideal for 3D printing (Baune et al 2021). Soy protein, in particular is becoming increasingly popular due to its advantages in 3D printing, such as self-supporting ability, water absorption, emulsification, and gelling properties (Yu et al 2022). Soybeans primarily create textured vegetable protein, providing fibrous chewiness, hardness, and mouthfeel to meat analogues (Chiang et al 2019). However, controlling the gelation rate of soy protein isolate (SPI) is challenging.

Epigallocatechin-3-gallate (EGCG), the main polyphenol found in green tea, offers potential solutions. EGCG possesses many health benefits, including fighting inflammation, antioxidative, antibacterial, and anticancer activities (Xu et al 2020). Its incorporation into plant-based 3D printing formulations could improve the quality and nutritional profile of the final product.

In conclusion, pursuing sustainable and high-nutrition foods drives the development of plant-based protein alternatives. With advancements in 3D printing technology, there is a growing potential to create plant-based foods that meet consumers' nutritional and sensory demands while addressing environmental and health concerns.

1.2 Thesis Structure

This thesis report is organized into five chapters, each addressing key aspects of plant-based proteins and their application in 3D printing technology. Chapter 1 provides an overview of the current landscape of plant-based proteins globally, highlighting their importance in contemporary diets. It discusses the existing challenges associated with the 3D printing of plant proteins and underscores the necessity of developing objective methods to enhance 3D printing techniques. Chapter 2 presents a brief history of 3D printing of plant proteins and provides a detailed description of previous research conducted in this area, exploring the advancements and milestones achieved in the field, and laying the foundation for the current study. Chapter 3 offers a comprehensive understanding of how 3D printing parameters affect the printability of SPI-WG-EGCG complexes. It investigates the individual and combined effects of adjusting nozzle diameter, nozzle H/D ratio, and nozzle speed on the 3D printability of the ink. In Chapter 4, predictive models are developed to estimate material printability based on polyphenol concentration and various printing parameters. These models aim to provide insights into optimizing the 3D printing process for better accuracy and efficiency. This research will help optimize printing parameters for improved control and precision in 3D food printing. Chapter 5 provides a general summary of the study, concluding with key findings on optimizing 3D printing parameters for plant-based proteins. It also discusses potential future research directions and the importance of continued innovation in this field to meet the evolving demands of customized, nutritious, and sustainable food production.

1.3 Scope of the Study

The present study focuses on optimizing the 3D printing of plant-based protein formulations, particularly those incorporating SPI and EGCG. By systematically analyzing the effects of key 3D printing parameters — nozzle diameter, nozzle H/D ratio, and nozzle speed—on the printability and structural integrity of these formulations, the study aims to enhance the quality and nutritional value of the printed products. The expected outcomes include the development of predictive models that accurately guide the selection of optimal printing settings for consistent, high-quality food production.

The results of this study are expected to benefit food manufacturers, researchers, and consumers by enabling the production of customized, nutritious, and sustainable plant-based foods. This research offers food manufacturers a framework to improve product consistency and reduce production costs by identifying optimal printing parameters. Researchers will gain valuable insights into the relationships between material properties and printing parameters, contributing to advancements in the field of 3D food printing. Consumers will benefit from healthier, environmentally friendly food options that meet specific dietary requirements.

References

1. Adenekan, M. K., Fadimu, G. J., Odunmbaku, L. A., & Oke, E. K. Effect of isolation techniques on the characteristics of pigeon pea (Cajanus cajan) protein isolates. *Food Science and Nutrition*, **2018**, 6(1), 146–152. https://doi.org/10.1002/fsn3.539.
2. Dick, A., Bhandari, B., Dong, X., & Prakash, S. Feasibility study of hydrocolloid incorporated 3D printed pork as dysphagia food. *Food Hydrocolloids*, **2020**, 107, Article 105940. https://doi.org/10.1016/j.foodhyd.2020.105940.
3. Godoi, F.C., Prakash, S., Bhandari, B.R. 3D printing technologies applied for food design: status and prospects. *J Food Engineering*, **2016,** 179:44–54, doi: https://doi.org/10.1016/j.jfoodeng.2016.01.025.
4. Han, S.; Cui, F.; McClements, D.J.; Xu, X.; Ma, C.; Wang, Y.; Liu, X.; Liu, F. Structural Characterization and Evaluation of Interfacial Properties of Pea Protein Isolate–EGCG Molecular Complexes. *Foods* **2022**, 11, 2895. https:// doi.org/10.3390/foods11182895.
5. Han, X., Liang, Z., Tian, S., Liu, Lu., Wang, S. Epigallocatechin gallate (EGCG) modification of structural and functional properties of whey protein isolate, *Food Research International*, **2022,** 158, 111534, doi: https://doi.org/10.1016/j.foodres.2022.111534.
6. Holmyard, N. (2020). Legendary Vish creates 3D-printed salmon analogs made from mushroom proteins. Algae extracts https://www.seafoodsource.com/ news/foodservice-retail/legendary-vish-creates-3d-printed-salmon-analogs-made-from-mushroom-proteins-algae-extracts.
7. Hughes, G. J., Ryan, D. J., Mukherjea, R., & Schasteen, C. S. Protein digestibility corrected amino acid scores (PDCAAS) for soy protein isolates and concentrate: Criteria for evaluation. *Journal of Agricultural and Food Chemistry*, **2011**, 59 (23), 12707–12712. https://doi.org/10.1021/jf203220v.
8. López, D. N., Galante, M., Robson, M., Boeris, V., & Spelzini, D. Amaranth, quinoa and chia protein isolates: Physicochemical and structural properties. International *Journal of Biological Macromolecules,* **2018**, 109, 152–159. https://doi.org/10.1016/j. ijbiomac.2017.12.080.
9. Millward, D. J. The nutritional value of plant-based diets in relation to human amino acid and protein requirements. Proceedings of the Nutrition Society, **1999**, 58, 249–260.
10. Montes, L., & Moynihan, Q. (2018). This meat substitute is printed with a pea and rice protein paste and a 3D printer. In Business Insider. https://www. businessinsider.com/this-fake-meat-is-printed-in-a-lab-using-vegetables-and-a-3d-printer-2018-11?r¼US&IR¼T.

11. Portanguen, S., Tournayre, P., Sicard, J., Astruc, T., Mirade, P.S. Toward the design of functional foods and biobased products by 3D printing: A review. *Trends in Food Science and Technology*, **2019**, 86, 188-198, https://doi.org/10.1016/j.tifs.2019.02.023.
12. Sa, A.G.A., Moreno, Y.M.F., Carciofi, B.A.M. Plant proteins as high-quality nutritional source for human diet. *Trends in Food Science and Technology*, **2020**, 97, 170-184, https://doi.org/10.1016/j.tifs.2020.01.011.
13. Sun, J., Zhou, W., Yan, L., Huang, D., & Lin, L. Extrusion-based food printing for digitalized food design and nutrition control. *Journal of Food Engineering*, **2018**, 220, 1–11. https://doi.org/10.1016/j.jfoodeng.2017.02.028.
14. Sun-Waterhouse, D., Zhao, M., & Waterhouse, G. I. N. Protein modification during ingredient preparation and food processing: Approaches to improve food processability and nutrition. *Food and Bioprocess Technology*, 7(7), **2014**, 1853–1893. https://doi. org/10.1007/s11947-014-1326-6.
15. Wen, Y., Chao, C., Che, Q.T., Kim, H.W., Park, H.J. Development of plant-based meat analogs using 3D printing: Status and opportunities. *Trends in Food Science and Technology*, **2023**, 132, 76-92, https://doi.org/10.1016/j.tifs.2022.12.010.
16. Zhao, J., Su, G., Zhao, M., Sun, W. Physicochemical changes and in vitro gastric digestion of modified soybean protein induced by lipoxygenase catalyzed linoleic acid oxidation. *J. Agric. Food Chem.*, **2019,** 67(50), 13978−13985, doi: http://dx.doi.org/10.1021/acs.jafc.9b05843.

II. General Literature Review

2.1 Introduction

Three-dimensional (3D) printing is a process that lays down the physical objects from a digital blueprint layer-by-layer and fuses them together (Lille *et al* 2018). Three-dimensional printing first came to light in the 1980s after which it started offering new opportunities in the fields of medicine, education, and aerospace (Derossi *et al* 2017). Three-dimensional food printing is used to give customized shapes, colors, textures, and different nutritional compositions to food products. In particular, it can be used to design food for target populations that require personalized meals.

In 3D printing, the ink is a crucial component. Several inks have been formulated to give different customized shapes to printed food products which can be made of complex formulations such as fruits, vegetables, animal products, and dairy. Amongst a broad spectrum of materials, plant protein is gaining attention as a raw material used in 3D printing to produce meat analogs, satisfy the personalized needs of consumers, and reduce the environmental impact of livestock rearing (Wang *et al* 2022). Proteins are macromolecules comprising amino acids linked by peptide bonds (C-N) and are generally classified into fibrous (keratin, silk) and globular proteins (soy, albumin) (Mu et al 2021). The demand for reliable and environmentally friendly protein sources is driven by the increase in the world population. The growing awareness of the inefficiency in protein conversion during the production of meat from livestock sparked the creation of plant-based foods as an alternate source of protein. Food consumption accounts for 30% of EU (European Union) greenhouse gas emissions (GHG), and plant-based meals typically emit fewer GHGs than animal-based foods. Plant-based meat analog production is a way of mimicking meat in terms of nutrition, texture, and sensory properties (Wen *et al* 2023). Plant-based meat is a high source of protein and thus can meet high protein requirements (Singh *et al.* 2021). But, in order to work with plant-based proteins as a raw material, it is important to understand the relation between raw material and the printed material to be produced.

The processes of 3D printing are as follows: designing custom shapes using computer-aided design (CAD), pre-treating the inks to have suitable rheological parameters, feeding ink capsules, slicing designs, extruding ink from the nozzle, and depositing the structure on the printed bed (Liu *et al.* 2019). In accordance with the American Society of Testing and Materials

(ASTM), 3D printing depends on seven technologies including selective laser sintering, direct energy deposition, material extrusion, ink jetting, sheet lamination, binder jetting, and vat polymerization; however, not all the techniques apply to plant-protein inks (Mu *et al.* 2021). Food incorporation in 3D printing is a bit challenging due to the variation in physiochemical properties (Mantihal *et al.* 2020). Therefore, several studies classified the 3D technologies into four major categories, (1) selective laser sintering/hot-air sintering, (2) hot-melt extrusion (used to create customized 3D chocolate products, cheese, and humus) and room temperature extrusion (used for pizza printing), (3) binder jetting (used for sugar printing), and (4) inkjet printing (used for decoration or surface fill in cake, pastry, or cookie fabrication) (Sun *et al.* 2015).

The rheological characteristics of protein-based inks, additives, and printing conditions have affected printing results in different ways by providing printing stability, structural support, and nutrition and have been the main research topic over the years. The objective of this review was to gather and examine information on the technical specifications for 3D printing, 3D printing parameters, printing materials, and the role of proteins in 3D printing. Additionally, the current status and prospectus of different types of plant-protein-based inks were also discussed.

2.2 Trends of Plant-Protein-Based 3D Printing

Three-dimensional printing is a cutting-edge technology to design and personalize food products to cater to consumer needs and to meet market demand. Amongst the wide availability of printers, extrusion-based ones are the most commonly used ones for plant-based proteins. Plant-based foods are gaining popularity as their positive effects on human health gain wider recognition. Researchers have been exploring various plant-derived materials for 3D printing, including proteins from sources like soy, peas, and other legumes. Advances in material science contribute to the development of printable and functional plant-based materials. The number of original studies on plant-based printable materials surged to a rise in the past few years (Figure 2.1). This is because the current trend in 3D food printing involves providing a broader range of personalized and visually appealing food designs, utilizing digitized nutritional information to cater to specific health-focused lifestyle preferences.

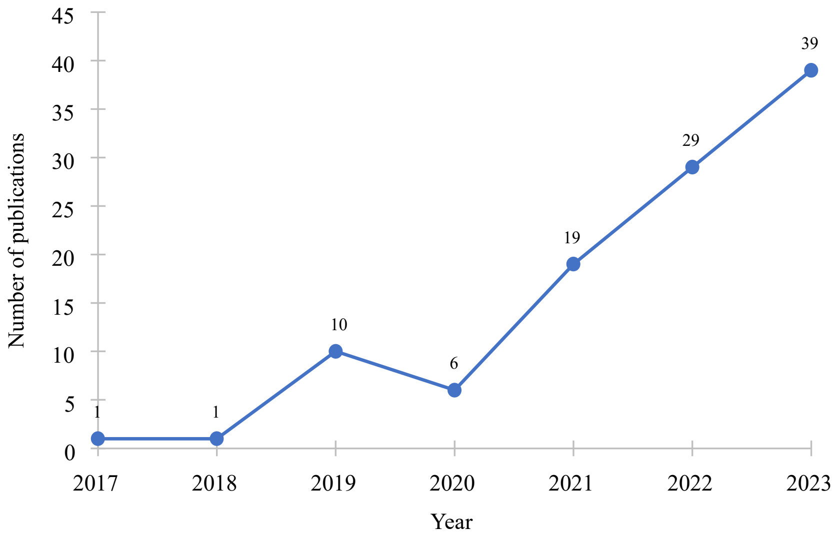

Figure 2.1. Number of scientific publications on plant-protein-based 3D printing (source: Web of Science, accessed in 2023).

Three-dimensional printing goods and services are projected to have a yearly growth rate of roughly 26% and a projected value of 40 billion US dollars by 2024 on a global scale.

2.3 Three-Dimensional Printer Parameters

Three-dimensional printer is the heart of the modern food industry producing personalized meals (Figure 2.2). Printability is one of the most important parameters in extrusion-based 3D printing and is characterized to handle dimensional stability, i.e., whether the material is capable of supporting its own weight (Godoi *et al.* 2016). It is the most important factor to consider in food printing, as it directly influences the formation of food products. The printability of a material (ink) is highly dependent on the properties of the food system and the 3D printer parameters used. Three-dimensional printing is not only affected by the properties, physicochemical and rheological, of the printing materials but also by the processing parameters such as the nozzle height, nozzle diameter, infill percentage, printing speed, extrusion rate, and temperature (Perez *et al.* 2019). The temperature of the nozzle can affect the flowability of the material; an increase in the temperature can decrease the viscosity (Chen *et al.* 2022). Past studies explored the relationship between printing parameters and the quality of 3D-printed food.

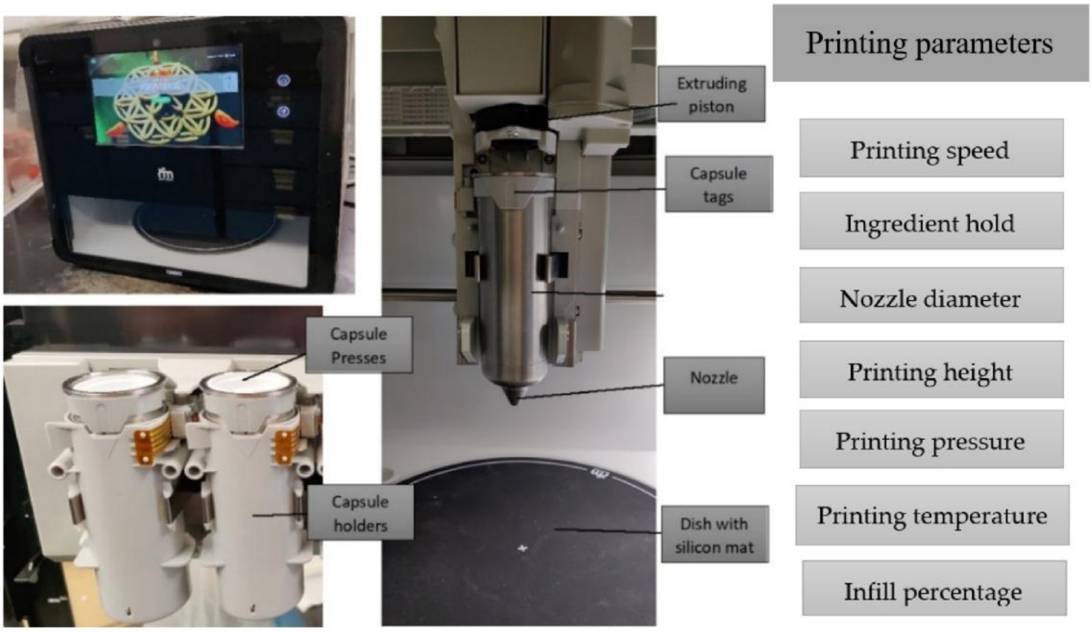

Figure 2.2. Commercial (Foodini) 3D food printer and major printing parameters.

Liu *et al.* 2021 studied the effect of the extrusion rate and printing speed on the printability of whey protein isolate (WPI) as shown in Table 2.1. Printing speed and extruding rate impact 3D printing simultaneously during the printing process because they alter the quantity of printed paste per unit length per unit time. It was reported that the extruding rate must be increased with increasing printing speed to feed the paste in time. Also, the printing quality decreased with the increasing printing speed.

The force applied by the commercial 3D printer (Foodini) can be modified to "hold back" the ingredient in the capsule as it moves to the first print area once the ingredient detection over the test cup is finished. The suggested default value of the ingredient hold is 4.2. It is recommended to increase the initial ingredient hold if there is an ingredient dropping from the test cup to the first print (Advanced user setting Natural Machines).

Table 2.1 Effect of printing speed and extruding rate on the printability of WPI (Liu *et al.* 2021).

Ingredient Ratio (w:w:w:w)					Oil Content (%, *w/w*)	Manufacturer-Defined Printing Speed (Actual Printing Speed, mm/s)	Manufacturer-Defined Extruding Rate (Actual Extruding Rate, mm^3/s)	Printed Shape	Printing Quality Score
No.	CS	W	CO	WPI					
A	20	25	25	25	26.3	100 (21.1)	100 (20.0)		1
B	22	25	25	25	25.8	100 (21.1)	100 (20.0)		3
C	25	25	25	25	25.0	100 (21.1)	120 (26.8)		3
D	25	25	25	22	25.8	100 (21.1)	110 (23.3)		2
E	25	25	25	20	26.3	100 (21.1)	100 (20.0)		4
F	25	28	25	25	24.3	100 (21.1)	100 (20.0)		2

CS: corn starch; W: water; CO: canola oil; WPI: whey protein isolate

Huang *et al.*2019 studied the effect of the nozzle diameter and reported that a bigger nozzle size resulted in a bigger deviation in the diameter of printed objects. Thus, decreasing the nozzle diameter would print samples closer to the designed ones. Shi *et al.* 2023 evaluated the influence of structural geometry (nozzle diameter and porosities) of soy protein isolate–xanthan gum–rice starch (SPI-XG-RS)-based printed samples on a texture profile analysis. It was reported that the printed samples with 200 µm filaments have a higher shape fidelity than that of samples with 600 µm filaments (Figure 2.3). Moreover, decreasing nozzle diameter not only marks precision but also increases printing time and feed pressure. A 3D printing system that is overloaded due to excessive printing pressure may experience machine wear. The printing procedure requires more pressure to print edible ink at lower nozzle diameters, which could lead to irregular deposition of the printable substance (Wang *et al.* 2018).

The nozzle height is the distance between the bottom of the nozzle and the printer bed in the printing process. The nozzle height has been identified by numerous prior studies as a significant factor influencing the printing accuracy (Severeni *et al.* 2016). However, Yang *et al.* 2018 have carried out a number of thorough experiments to confirm that the nozzle height should be the same as the nozzle diameter in the 3D-printing process.

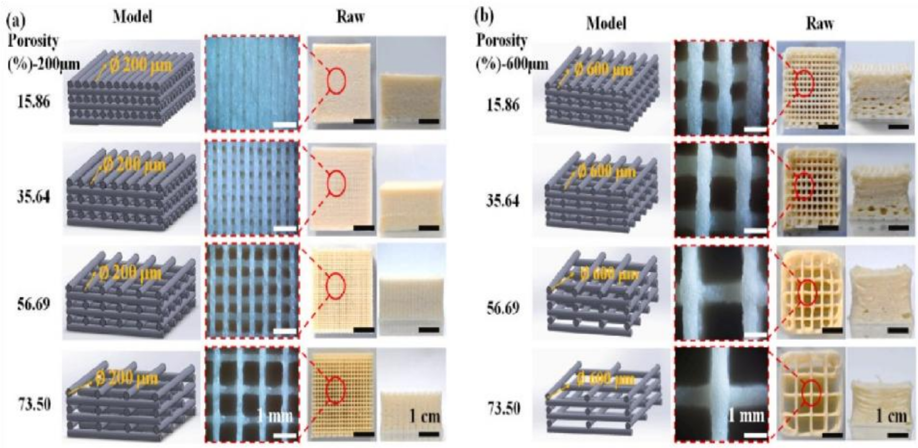

Figure 2.3. Comparison of SPI-XG-RS-based samples having different nozzle sizes and printing porosity (Shi *et al.* 2023).

Printing temperature in 3D food printing is an important aspect influencing the rheological characteristics of food, which is likely to have an impact on the material's 3D printability (Liu *et al.* 2019). Chen *et al*. 2022 studied the effect of three printing temperatures of 25, 35, and 45 ˚C on the rheological properties of SPI-based pastes. The effect of the printing temperature on the microstructure and texture of 3D-printed protein pastes cylinders varied greatly according to the gelatin content in the SPI-based paste. It is reported that increasing the temperature reduced the viscosities of pastes, thus improving the rheological properties and printability (Figure 2.4).

Sample	T (℃)	Printing		0h		6h		Solid Cylinder
		1	2	Side view	Top view	Side view	Top view	
S	25							
	35							
	45							
SAG-2	25							
	35							
	45							
SAG-6	25	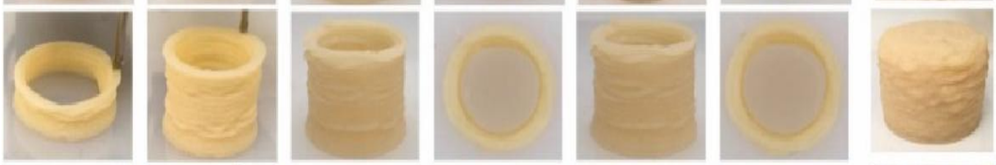						
	35	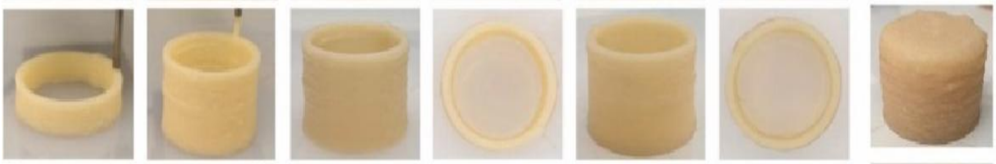						
	45	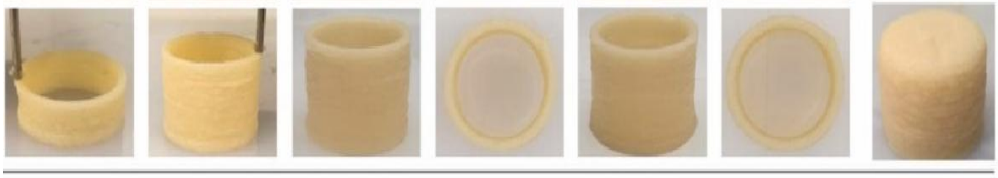						

Figure 2.4. The 3D printing behavior of SPI-based pastes at 25, 35, and 45 ˚C (12). (S: control; SAG-2: 2% gelatin, 0.5% sodium alginate; SAG-6: 6% gelatin, 0.5% sodium alginate).

Figure 2.5 shows the effect of different infill percentages (12.5, 25, and 50%) on the inner structure and post-stability of the soy protein isolate (SPI)-red cabbage (RC) inks. It was reported that the interior structure of the samples was unaffected by the various infill percentages (12.5, 25, and 50%). As for the dough composition, increased RC concentration reduced the number of cavities and made the structure more compact (Carranza *et al.* 2023).

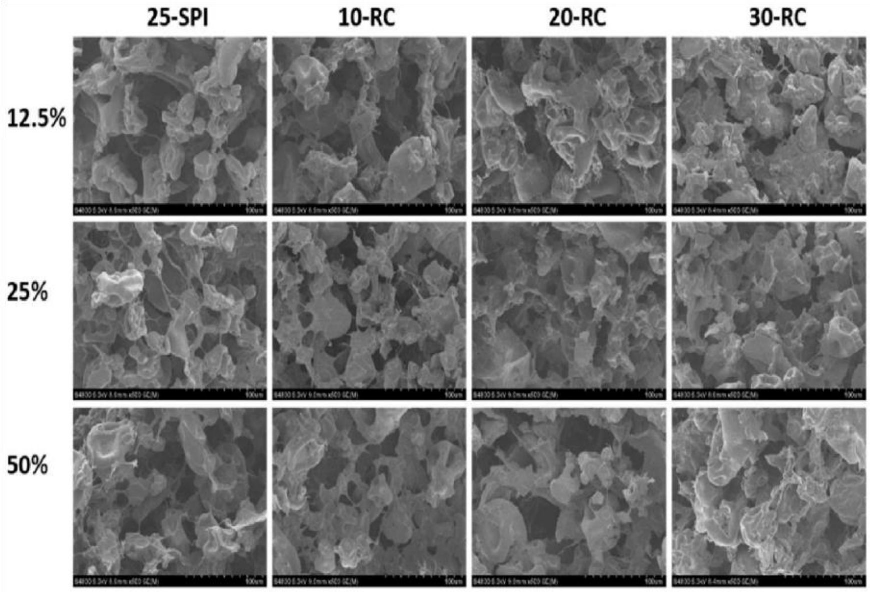

Figure 2.5. Cross-sectional SEM images for 25-SPI doughs with different RC contents as a function of infill rates (12.5, 25, and 50%). Abbreviations used include: SPI (Soy protein isolate); RC (Red cabbage).

2.4 Technological Feasibility of Protein-Based 3D Printed Food

The 3D printing of plant protein presents an opportunity to expand additive manufacturing applications in the food industry. High precision characteristics of 3D printing give a way to produce plant-based meat which is subjected to mimic the taste, texture, appearance, and nutritional values of traditional meat. Amongst these, the texture still remains the challenging one (Ramachandraiah *et al.* 2021). So, for this, technological feasibility plays a major role. In terms of printer-related challenges, the main technological considerations for 3D printing are the dispensing mechanism and the 3D positioning method. The designing software (CAD) controls the positioning system that creates 3D structures. In the case of the dispensing system, the extruder type, which can have a single or a double nozzle, is the most common (Dick *et al.*

2019). Furthermore, different operational settings may be required depending on the type of material. Three-dimensional printing of food products is limited due to the lack of suitable materials for printing because of the instability of plant-based proteins. These challenges can be overcome by taking care of the technical requirements of 3D printing.

In addition to processing parameters and sources of protein, the rheological property of printing ink plays a pivotal role in deciding the successful printing according to the present pattern and is related to the accuracy and results of the printing (Figure 2.6). Viscosity plays a major role in rheology in the self-supporting and stacking properties of materials while printing (Kim *et al.* 2018). Three-dimensional printing involves the extrusion of material from the nozzle to deposit on the surface. The ink is required to present a shear-thinning behavior, i.e., less viscosity during extrusion so that it can be easily extruded from the nozzle; however, it is expected to regain its viscosity and maintain the structure after deposition (Malda *et al.* 2013 and Gao *et al.* 2018). The viscoelastic properties of the ink, measured by a series of rheological tests, have a significant role in determining the printing performance, including the extrudability, filament fidelity, and sol-gel transition (Mu *et al.* 2021). Xu *et al.* 2023 studied the effect of enzyme-assisted apricot polysaccharide (EAP) on soybean protein isolate (SPI) gel preparation. It was reported that the dynamic rheological properties, i.e., the viscoelasticity of gels, are related to the printing accuracy and is concentration-dependent. It was demonstrated that the degree of crosslinking of SPI-apricot polysaccharide increased with increasing EAP content, thus exhibiting stronger solid-like behavior.

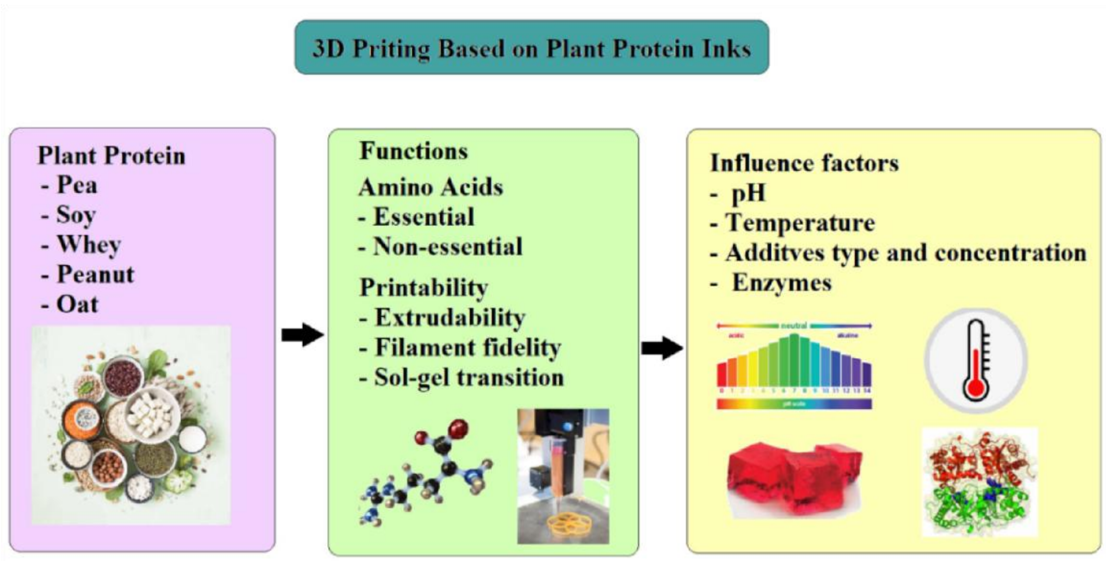

Figure 2.6. Steps to be considered while 3D food printing: sources of plant protein, functions, and influencing factors.

2.4.1. Extrudability

The efficiency with which an ink is extruded from the dispensing nozzle is termed extrudability, and viscosity is a key indicator of extrudability. Viscosity depends on the concentration of the protein isolate, molecular weight, and inter and intra-molecular interactions which are influenced by factors such as temperature, protein concentration, ion strength, and pH. Viscosity is inversely proportional to shear rate, shown by the rheological flow curve called shear-thinning behavior, which is necessary for 3D printing. For example, Yu *et al.* 2022 reported that the viscosity of the inks decreased with the addition of polysaccharides such as guar gum and xanthan gum into the soy protein isolate (SPI) emulsion gels, thus exhibiting shear-thinning behavior. Another study used SPI-WG-RP (soy-protein isolate-wheat gluten-rice protein) pastes and reported a decrease in apparent viscosity with an increasing rice-protein ratio (Qiu *et al.* 2023). Also, in accordance with the same study, it could be seen that the apparent viscosity decreased with the increasing shear rate for all types of ink as shown in Figure 2.7 (Qiu *et al.* 2023). Also, various pre- or post-treatments can improve the viscosity of the sample. For instance, a study reported the effect of microwave pre-treatment on 3D printing of soy–strawberry ink increased the viscosity, which is more suitable for 3D food printing (Fan *et al.* 2020).

The structure of the material largely depends on the pH of the solution. Protein denaturation, protein-protein, and protein–water interactions are affected by pH and proper pH can prevent the collapse of the gel network from charge repulsion. It is observed that a stable printing system requires pH away from the isoelectric point of the protein towards the alkaline region (pH −7 to 10). The protein molecules aggregate at the isoelectric point (pI) in the presence of both charges resulting in the decreased efficiency. This affects the gelation property of the ink. However, similar charges increase the efficiency of the inks by repelling each other (Guo *et al.* 2022).

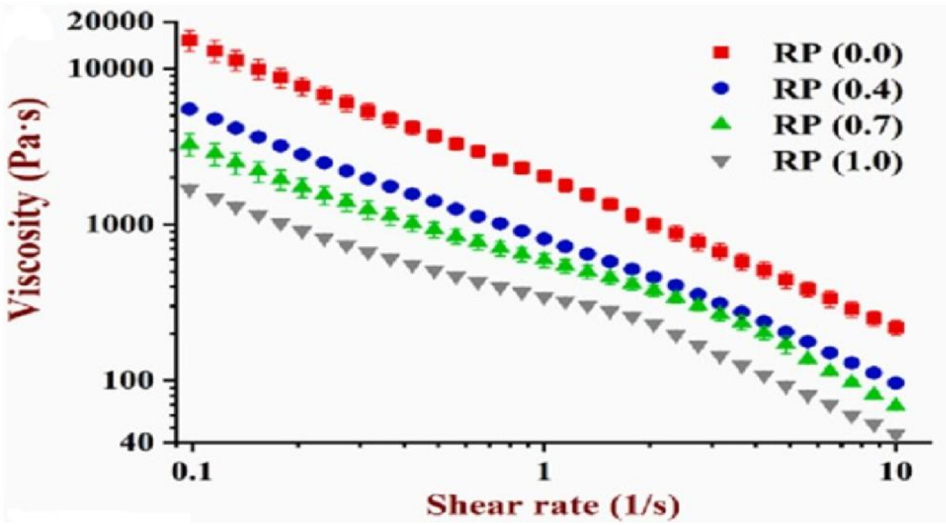

Figure 2.7. Viscosity of soy protein isolate–wheat gluten pastes with different concentrations of RP (rice protein) (Qiu *et al.* 2023).

2.4.2. Filament Fidelity

Filament fidelity is the maintenance of the structure of the extruded material to prevent collapse and sagging. It is related to at least two viscoelastic properties, i.e., yield stress and thixotropy (Mu *et al.* 2021). Insufficient yield stress leads to the collapse of the extruded material under its own weight, so the bulking agents and the thickeners such as food hydrocolloids are added for the stability of the structure. Qiu *et al.* 2023 used different concentrations of rice protein in the SPI-WG ink to check the printing performance and reported that inks having (RP 0.7 and RP 1.0) could be successfully printed into layers. The study also reported RP (0.7) ink with the best print fidelity (Figure 2.8A–D). Also, Chen *et al.* 2022 studied the printing properties of ink formulations containing textured soy protein (TSP) and drawing soy protein (DSP) with different hydrocolloids and reported that TSP with xanthan gum showed the best printing characteristics and maintained the structure during the printing of steak-like foods. Also, a high protein content increases the yield stress efficiency of the printing matrix (Guo *et al.* 2022). Another study by Lille *et al.* 2018 found that the good shape stability of an oat and faba protein isolate was achieved by high yield stress.

Lin *et al*. 2023 reported the effect of the concentration of additives and the printing speed on the fidelity of printed peanut protein. The study showed that a small amount of carrageenan (0.5%) can print objects with high fidelity at the slowest printing speed (12 mm/s speed). It was also reported that the fidelity of the printed product decreases with the increasing printing speed. Similar patterns were seen in the fidelity of the items printed with 0.5% gellan gum at various printing rates (Figure 2.9).

Another property is thixotropy, which is the time-dependent process of rebuilding a molecular structure. It tells us whether the viscosity recovered. High thixotropy requires the highest energy to break down the internal structure, with high resistance to time-dependent flow and high levels of internal viscosity and stability (Mirazimi *et al.* 2022). Mirazimi *et al*. 2022 studied varying shear rates to characterize the effects of soy protein acid hydrolysate (SPAH) and agar and reported that formulation with 6 g SPAH and 0.2 g agar (S6A) exhibited the highest degree of thixotropy (Figure 2.10). According to Clark *et al.* 2019, the addition of collagen and gelatin recovered 75% of the storage modulus within one second whereas, ink with alginate and methylcellulose (MC) showed 56% recovered viscosity after 30 s (Li *et al.* 2017).

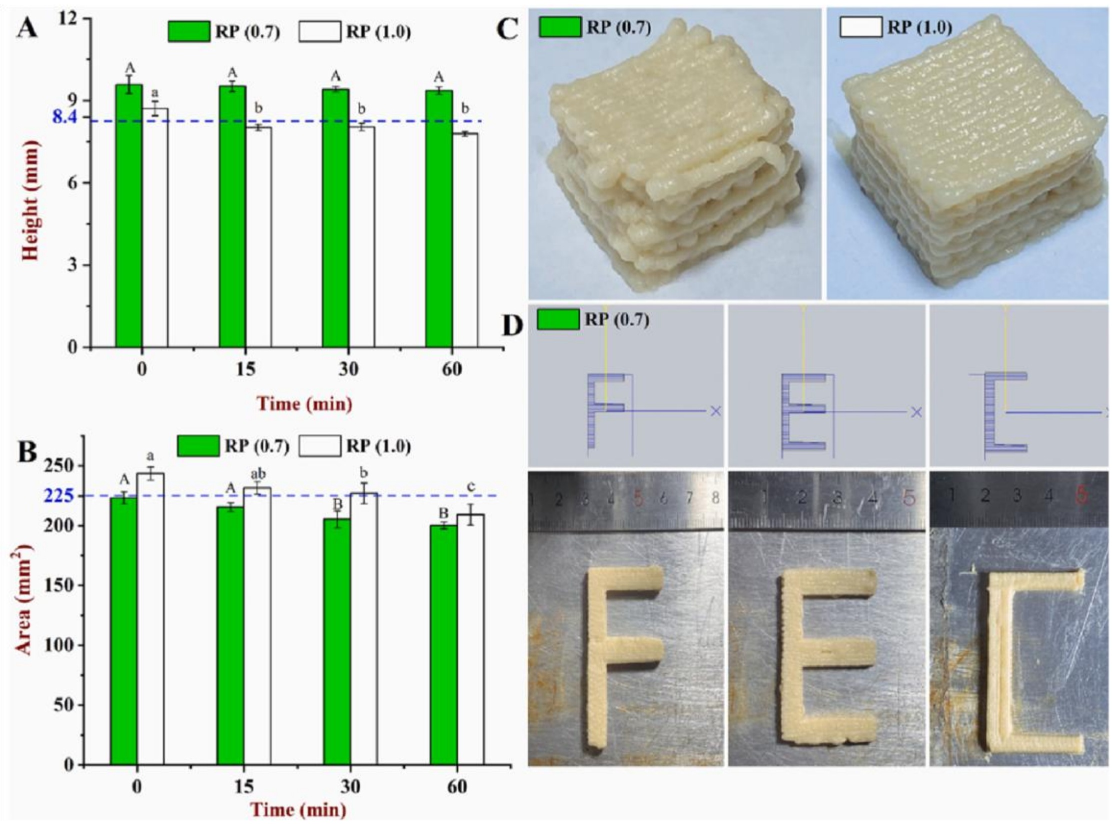

Figure 2.8. Evaluation of printing fidelity. (**A**) Height as a function of time. (**B**) Surface area as a function of time. (**C**) The image of printed cuboid using RP (0.7) and RP (1.0). (**D**) The image of three printed “English Alphabets” (25 mm × 25 mm × 4.2 mm) using RP (0.7) (Qiu *et al.* 2023). Upper-case and Lower-case letters represent significant differences between RP (0.7) and RP (1.0) samples, respectively. Abbreviations used include: RP (Rice protein).

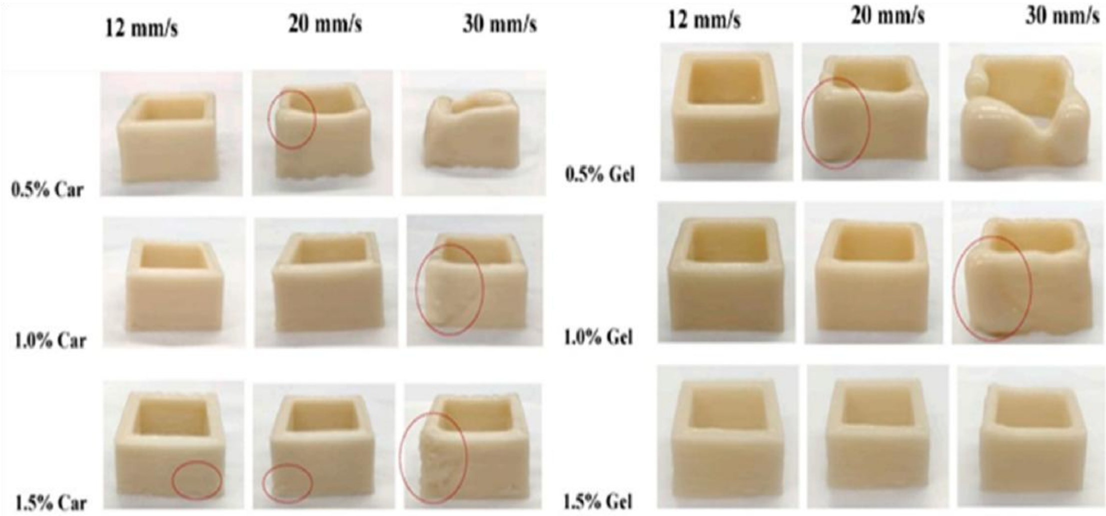

Figure 2.9. Evaluation of print fidelity of peanut protein-based inks as a function of concentration and printing speed (Lin *et al.* 2023).

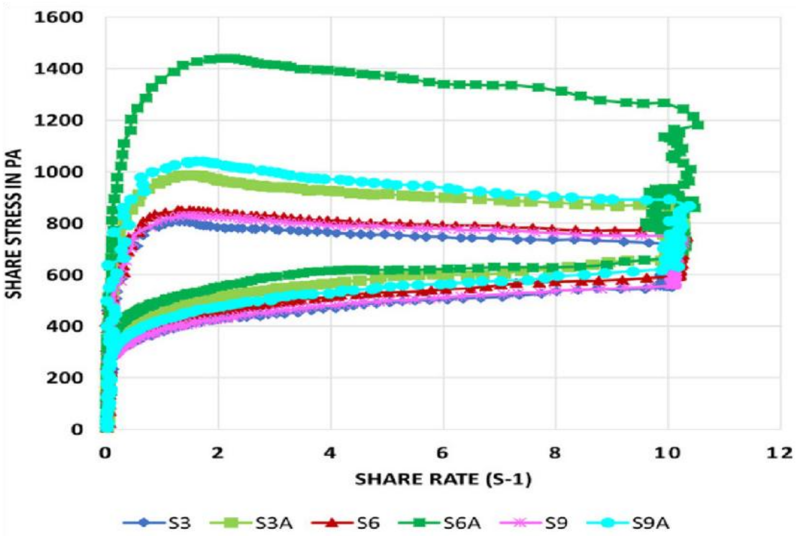

Figure 2.10. Evaluation of thixotropy of SPAH-agar inks for 3D printing. Note: S3 (3 g soy), S6 (6 g soy), S9 (9 g soy), S3A (3 g soy and 0.2 g agar), S6A (6 g soy and 0.2 g agar), and S9A (9 g soy and 0.2 g agar) (Mirazimi *et al.* 2022).

2.4.3. Sol–Gel Transition

Protein molecule crosslinking is frequently linked to the sol–gel transition in 3D printing, which occurs when liquid phases transform into solid phases. This crosslinking is defined by the ratio of storage moduli (G') to loss moduli (G''), where G' and G'' describes the elastic (solid-like) and viscous (liquid-like) properties of the ink, respectively. The sol–gel transition takes place when $G' > G''$ (Mu *et al.* 2021). The sol–gel transition is evaluated using a frequency sweep to give insights into the self-supporting behavior of protein inks after deposition.

The storage modulus is used to measure the solid elastic behavior of the sample, which reflects the mechanical strength of the sample, whereas the loss modulus reflects the liquid behavior of the samples. G' and G'' depend on the frequency. A study reported the effect of the frequency on the storage and loss moduli of SPI-WG-RP-based ink. It was concluded that both G' and G'' values gradually increased with increasing oscillatory frequency, which is consistent with an increase in the internal friction at higher frequencies. It was also seen that $G' > G''$ indicating that the soy protein-based ink exhibited predominantly elastic properties (Figure 2.11) (Qiu *et al.* 2023).

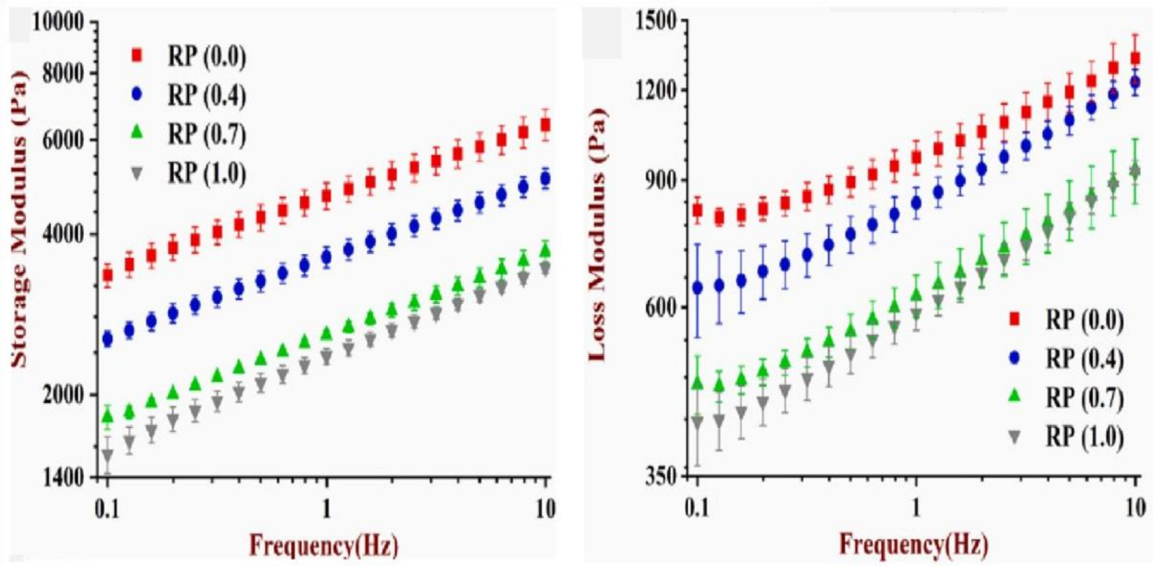

Figure 2.11. G' and G'' of SPI-WG pastes with different concentrations of RP (rice protein) (Qiu *et al.* 2023).

The sol–gel transition is also related to the protein cross-linking which is influenced by the addition of enzymes and heating treatment. Transglutaminase is the widely used enzyme that causes protein-gel formation (Kolpakova *et al.* 2021). For example, L-cysteine hydrochloride breaks the disulfide bonds of protein, thus exposing sites for the action of transglutaminase (T_{Gase}). This leads to the formation of polymers and increased viscosity for optimizing printing ability (Yu *et al.* 2022). Also, adding an alginate solution of 80% to 20% pea protein solution can increase the mechanical strength and consistency of printing (Oyinloye *et al.* 2020). Furthermore, the gel strength and elasticity of the dough can be improved by the addition of fat as it promotes the uniform distribution of fat and gluten protein to obtain a more stable network (Yang *et al.* 2018).

The rheological characteristics of inks are highly influenced by the heating time. Yu *et al.* 2022 reported the G' value increases with an increase in preheating time thus exhibiting sol–gel transition. It is also influenced by the temperature. The temperature has a huge effect on the final printing effect. High-temperature protein denaturation exposes hydrophobic sites for covalent bonding (Cortez-Trejo *et al.* 2021). A study found that the viscosity of SPIs increases with increasing the heating time to 20 min, 25 min, and 30 min, thus increasing the sol–gel transition rate (Yu *et al.* 2022) Also, the 3D printability of protein pastes with different formulations can be improved by adjusting the printing temperature. The printing temperature has a significant impact on the microstructure and texture of printed food. A study revealed that with the increasing printing temperature, the hardness and chewiness of the objects made of S (soy-based), SAG-2 (soy-gelatin-sodium alginate based with 2 g gelatin), and SAG-6 (6 g gelatin) increased significantly (Chen *et al.* 2022).

2.5 Plant-Based Proteins for Extrusion-Based 3D Printing

Extrusion-based 3D printing has been most commonly adapted in the food sector. It involves the extrusion of liquid or semi-solid material from the printing nozzle, moving in the x, y, and z-direction. One benefit of adopting extrusion-based printing is that it is able to print a wide range of materials at the same time to produce a whole meal (Lanaro *et al.* 2017). Materials in 3D printing are broadly classified into three categories (Ramachandraiah *et al.* 2021)—native printable materials, nonnative printable materials, and alternative materials, such as insect-derived 3D structures (Figure 2.12). However, the increasing demand of plant-based proteins as a substitute for animal-based proteins has been a topic of research for a while now due to increasing awareness of the health benefits associated with plant proteins and of environmental concerns, i.e., reducing the environmental footprint, waste, and demand for water and energy (Chao *et al.* 2018). Plant-based proteins are explored commercially to extract isolates because of their unique nutritional (metabolism and growth) and health-promoting attributes such as functionality, sensory characteristics, and labeling. Zhang *et al.* 2021 reported soy as the most common raw material for many plant-based foods possessing all the essential amino acids necessary to meet human nutritional needs; however, more recently, pea was introduced as an alternative protein that is gluten-free and due to its low allergenicity (Lam *et al.* 2018). However, compared to soy, peas can be grown in more moderate climates (Lam *et al.* 2018). Pea protein is a good source of fiber, starch, vitamins, minerals, and phytochemicals. However, its gelling capacity is lower than soy protein, thereby requiring the use of various additives such as hydrocolloids, carbohydrates, and lipid additives. Additives have a long history of application in food, which have the capability of alternating the properties of various natural food gels which alone have poor printing performance which is discussed later in the section.

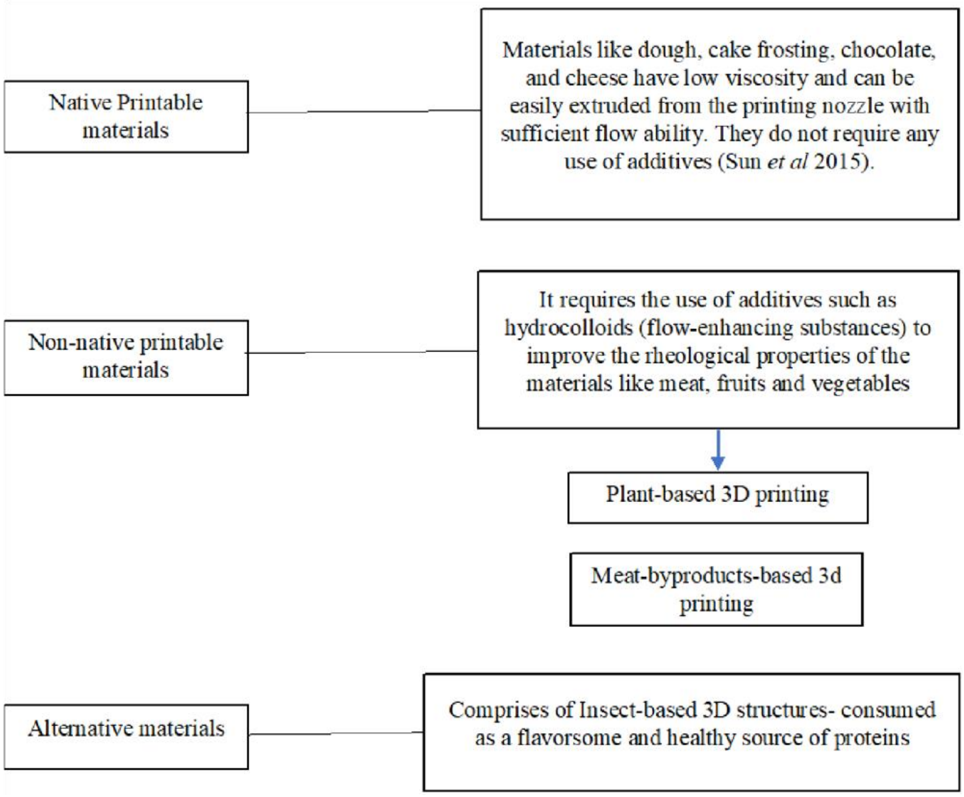

Figure 2.12. Material-based 3D food printing (Ramachandraiah *et al.* 2021).

2.5.1 Role of Plant Protein

There has been considerable research into the use of plant proteins for the formation of 3D printable inks, especially meat analogues (Table 2.3). The formation of protein-based feed focuses on material formation methods in accordance with the final product printed. For instance, the printing of meat analogues requires the careful adjustment of a variety of ingredients that can enhance or limit the desired texture and visual appearance, as well as the overall properties of food. The production of fish and meat analogues comprises careful adjustment of water, flavour, fat, binding agents, proteins, vitamins, minerals, and antioxidants with 50–80% water, which also serves as a plasticizer while processing meat substitutes and gives the finished product the appropriate juiciness (Nowacka *et al.* 2023). Technologies used in the formation of feed are regarded as the major challenge. Processing techniques are classified into two categories: bottom-up and top-down structuring techniques. In the bottom-up approach, the end product is created by assembling individual fibers, whereas the top-down approach involves the development of fibrous structures by blending biopolymers with an external force (Nowacka *et al.* 2023).

Plant-based meat substitutes are made from a variety of ingredients, primarily from oilseeds like cottonseed and rapeseed, legumes like mung beans, common beans, and lentils, and cereals like barley, wheat, corn, oats, and rye. Legumes are a significant source of protein-rich in dietary fiber, vitamins, and minerals with high antioxidant properties (Doss *et al.* 2022).

They are a vital part of the diet known for their effect on inhibiting diseases. Different types of plant-based proteins have been discussed below.

2.5.1.1 Legume-based

Soy Protein

Soy protein isolate (SPI), which contains both essential and non-essential amino acids, is a significant source of protein in the human diet (Shan *et al.* 2015). Being a high-quality vegetable protein, it is successfully used in 3D printing because of its self-supporting ability, water absorption, emulsification, and gelling properties (Yu *et al.* 2022). However, these inherent characteristics of natural soy protein isolate (SPI) pose challenges in catering to diverse food processing requirements. For instance, Yuan *et al.* identified that the dense tertiary and quaternary structures associated with SPI result in poor functional properties of SPI. Opting for an appropriate small biomolecule to form noncovalent bonds with soy protein isolate (SPI) could present an alternative, effective, and environmentally friendly approach to enhancing SPI with improved functional properties (You *et al.* 2021).

Also, soybean is primarily used to create textured vegetable protein and gives a fibrous chewiness, hardness, and mouthfeel to the meat analog (Chiang *et al.* 2018). Chen *et al.* 2021 reported that textured-soy protein (TSP) with xanthan gum showed the best printing characteristics of steak-like foods (Table 2.2). Also, a study showed that the printability of food inks can be improved by adding plant-based hydrocolloids, which are generally used to improve gelatinization. These additives are widely used in 3D printing to improve the printing performance of natural food gels, which is essential for enhancing the fluidity, deposition, and lubricity of the printing material (Voon *et al.* 2019). For instance, the addition of xanthan gum in soy protein isolate resulted in better rheological and textural properties. However, a high concentration of XG (0.5% *w*/*w*) resulted in poor flexibility (Yu *et al.* 2022). Also, the addition of salts (NaCl, KCl, $CaCl_2$, $CaSO_4$) alters the properties of gel, resulting in protein aggregation and gelation. The acquired results revealed that the xanthan gum and NaCl concentration of 0.5 g/30 g and 1 g/100 mL exhibited maximum gel strength and print shape, respectively.

Table 2.2. Printing results of textured-soy protein (TSP) and drawing-soy protein (DSP) using different hydrocolloids (Chen e*t al.* 2021).

Protein	Control	Guar Gum	Sodium Alginate	Hydroxyethyl Cellulose	Xanthan Gum	Sodium Carboxymethyl Cellulose	Konjac Gum
Textured Soybean Protein							
Drawing Soy Protein							

Pea Protein

Pea protein is a hypoallergenic protein source (i.e., with low allergenicity) that is safe for consumption by people with food allergies (Ding *et al.* 2021). Researchers are now focusing on development using pea protein as being a good source of fiber, starch, vitamins, minerals, and phytochemicals; however, its gelling capacity is lower than soy protein, thereby requiring the use of various additives such as hydrocolloids and salts. PPI also has a low water holding capacity and low solubility. The study carried out by Kim *et al.* 2021 investigated the effect of different concentrations of pea protein isolate on the properties of banana-PPI paste ink. The findings of the study revealed that the incorporation of pea protein increased the protein–banana entanglement, resulting in an increase in the storage moduli (G') and loss moduli (G''), thus improving its printability. According to the findings, banana pastes with a 15% PPI concentration could be successfully printed with a well-matched geometry and could maintain their shape after printing (Figure 2.13). However, a 20% PPI-induced protein aggregation in the matrix caused the 3D-printed line to break.

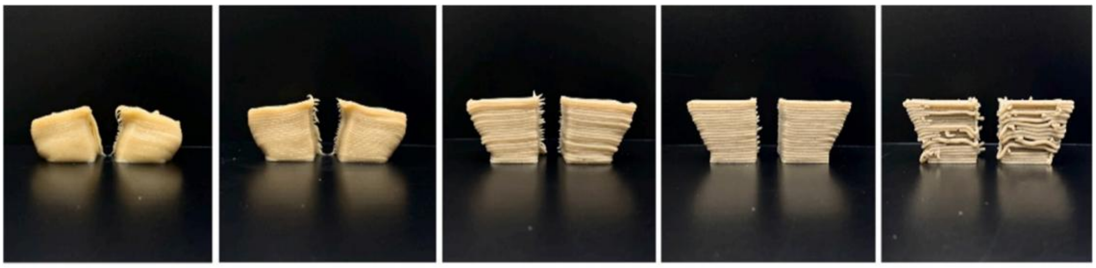

Figure 2.13. Three-dimensional printed PPI-banana pastes with different PPI concentrations (0, 5, 10, 15, 20% (*w*/*w*)) (Kim *et al.* 2021).

Another study determined the optimal alginate and pea protein ratios suitable for printing food with acceptable rheological and textural characteristics (Oyinloye *et al.* 2020). The addition of an appropriate concentration of pea protein can enhance the stability of the structure.

Faba and Mung Bean Protein

Faba bean proteins are known for their good emulsifying and foaming properties, but lesser than soy protein isolates (Fiorentini *et al.* 2020). However, altering the production and processing processes can improve the functionality of faba bean protein.

Mung bean proteins are becoming more and more common as a component of meat substitutes. A plant is known for both its nutritional worth and practical qualities. It has a high protein level (25–28%) and a low fat content (1–2%). A research group at the National University of Singapore produced vegan seafood using microalgae protein and mung bean protein. The team recreated the flaky, chewy, and fatty textures that seafood enthusiasts crave. A study reported optimum processing conditions to produce texturized mung bean protein using response surface methodology. This study showed great potential in mung bean protein as an alternative to meat, acting as a healthier and greener option compared to animal proteins Table 2.3 (Brishti *et al.* 2021).

Table 2.3. Plant proteins and their applications in 3D food printing.

Category	Other Materials	Experimental Conditions	Results	References
Soy protein	Textured-soy protein (TSP), drawing soy protein (DSP,) xanthan gum, Konica gum, sodium alginate, guar gum, sodium carboxymethyl, cellulose	Refrigeration: 4 °C; printing nozzle temperature: 25 °C.	TSP with xanthan gum showed the best printing characteristics.	(Chen *et al.* 2021)
	L-cysteine, Transglutaminase	pH: 7, heating: 90˚C; mixing: 1500 rpm (1 min) and 300 rpm (2 min).	SPI heated for 25 min with l-cysteine had best printability and stability.	(Yu *et al.* 2022)
	K-carrageenan, vanilla powder	Heating: 70 °C; microwave: 50, 80, and 110 W	SPI gel made with 3% carrageenan had the optimal viscosity for 3D printing.	(Phuhongsung *et al.* 2020)
	Guar gum, xanthan gum, soybean oil, NaCl powder	Homogenization: 800 rpm, 5 min; heating: 70 °C, 60 min.	SPI gel with xanthan showed better rheological properties but a high concentration of XG (0.5% *w/w*) resulted in poor flexibility.	(Chen *et al.* 2021)
	Strawberry powder	Microwave: 30, 50 and 70 W	Salt pretreatment improved the printability and shape stability of ink systems. Maximum shape accuracy—70 W.	(Fan *et al.* 2020)
Pea protein	Alginate, calcium chloride, sodium phosphate	Temperature: 45 °C	Alginate solution (80%) and pea protein solution (20%) were most suitable for 3D printing.	(Oyinloye *et al.* 2020)

	Microwave vacuum-dried banana powder, ascorbic acid	Blending: 1 min; sifting: 300 µm; mixing: 2000 rpm, 25 °C, 6 min	Banana pastes with 15% PPI concentration retained their shape and geometry after printing.	(Kim *et al.* 2021)
Mung bean protein	Mung bean flour, hydrochloric acid, sodium hydroxide, Coomassie Blue R250, and bromophenol blue.	Mixing with 100 mL water; blending: pH-9, 2000 rpm, 30 °C, 1h; centrifugation: 8586 g; freeze-drying: 48 h.	Optimized extrusion parameters: feed moisture: 49.33%; screw speed: 80.66 rpm; and barrel temperature: 144.57 °C; fibrous structure, partial protein unfoldment, high retention of amino acids.	(Brishti *et al.* 2021)

2.5.1.2. Cereal-Based

It comprises wheat, corn, oat, and rice, which are known for their high starch content.
Wheat protein, also called gluten, is the most commonly used cereal-based protein, especially in the production of meat analogues, due to its viscoelastic properties (Singh *et al.* 2021). Cereals have been used extensively in extrusion-based 3D printing of pizza, cookies, and dough due to their good shear stability (Feng *et al.* 2019).

Gluten Protein

Wheat is widely consumed around the world, having starch as a primary component followed by proteins and non-protein compounds such as cellulose, hemicelluloses, polyphenols, and minerals. Due to their high nutritional and organoleptic quality, wheat based goods, such as wheat flour (flour with the bran removed) and wheat whole meal (flour with the bran included), are essential dietary components worldwide. Gluten plays a major role in 3D printing a dough and its printability can be improved by the addition of salts such as NaCl. NaCl improves the gluten protein structure stability in the dough by promoting the hydrophobic interaction and polymerization of the gluten proteins (Correa *et al.* 2011).

Oat Protein

Oat protein is known for its good amino acid concentration and has a better nutritional value of 15–20% as compared to other cereal proteins due to its high lysine content. Oat protein has a stable network even at a high denaturation temperature of 110 ˚C, and when mixed with soy protein, it can improve the strength of the gels (Bruckner-Guhmann *et al.* 2021). For instance, 35% oat protein when mixed with 45% fava bean protein isolate printed food of the highest stability (Lille *et al.* 2018). Also, a study reported that oat protein when combined with pea protein produces a good sensory effect (de-Angelis *et al.* 2020).

Rice Protein

Rice, a known low allergenicity raw material and, in particular, promoted as a soy substitute, is a very promising raw material for producing meat analogues. In current studies, rice flour is utilized in meat products to replace fat and benefit from its ability to bind water. A study conducted by Qiu et al. indicated that adding rice protein in soy protein–wheat gluten protein pastes can significantly improve their 3D-printing properties by reducing viscosity and shear modulus.

2.5.2. Role of Additives

In 3D food printing, additives are frequently utilized to improve the printing performance of natural food gels, which is essential for enhancing the fluidity, deposition, and lubricity of printing materials (Voon *et al.* 2019). Various additives like hydrocolloids (xanthan gum, guar gum) were mentioned in the previous sections. These are the most commonly used ones for the 3d printing of plant-based proteins. There are two main functions of additives—improving the stability of final 3D printed products and improving performance in other areas like health and nutrition and sustainability using alternative food sources like meat analogues. For instance, compared to traditional sources of food such as meat (beef) or fish, protein-based meat analogues that mimic traditional meat not only provide high-quality protein but also improve sustainability (reducing the need to rear animals, smaller land requirements, and less greenhouse gas emission). In this regard, the Netherlands Organization for Applied Scientific Research introduced a food that was designed for elderly people to solve their swallowing and chewing problems (Lorenz *et al.* 2022). Patients with dysphagia have varying texture tolerances as described by the International Dysphagia Diet Standardization Initiative (IDDSI). So, in that study, hydrocolloids were added for ink optimization and alteration of texture in 3D-printed dysphagia foods (Lorenz *et al.* 2022). Recently, another class of additives termed polyphenols is gaining interest in 3D printing. Polyphenols such as epigallocatechin function as a bioactive additive that enhances the printability and structural integrity of the material. Its antioxidative properties may contribute to improved stability, while interactions with plant proteins can potentially enhance adhesion and overall printing performance (You *et al.* 2021). Previously, some studies have studied the effect of EGCG on protein emulsions and reported that EGCG when combined with proteins can stabilize emulsions (Zhang *et al.* 2023). Additives currently used in 3D food printing are shown in Table 2.4.

Table 2.4. Recent applications of additives in 3D printing of plant-based proteins and main changes in printing characteristics.

Types	Additives	Materials	Finding		References
Hydrocolloids	Alginate	Pea protein powder (PP), calcium chloride	Increased gel strength.	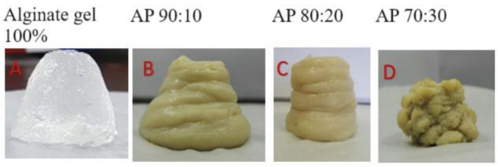	(Oyinloye *et al.* 2020)
	Agar	Soy protein acid hydrolysate (SPAH)	Improved mechanical strength and increased self-supporting capacity of 3D printed structures.	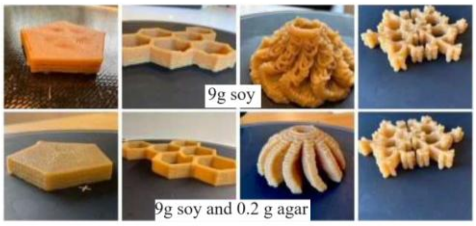	(Mirazimi *et al.* 2022)
	Kappa-carrageenan	Soy protein isolate (SPI), vanilla powder (for flavor)	3D printed structures with smooth surfaces and denser gel network structures.	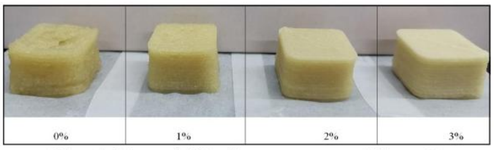 Printed objects of SPI with carrageenan at different %	(Phuhongsung *et al.* 2020)
	Xanthan gum (XG)	Pea protein isolate (PPI)	A small amount of XG improved mechanical strength and chewing and swallowing easiness.	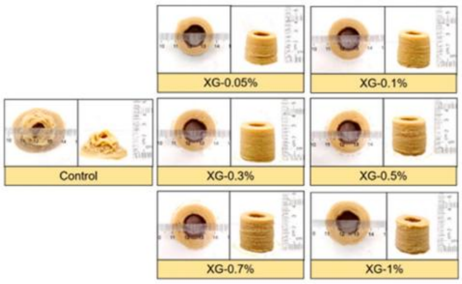	(Liu *et al.* 2023)

Others	Transglutaminase (T_{Gase}) powder	Mung bean protein isolate (MBPI), methylcellulose (MC)	Smooth printed surface, improved mechanical strength, increased hardness. Optimal TG: 4 U/g of MBPI.	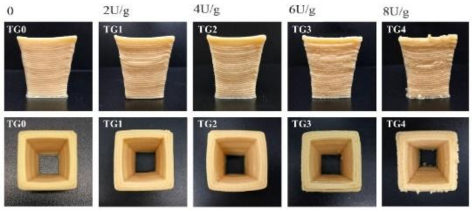	(Wen *et al.* 2022)
Polyphenols	Epigallocatechin gallate (EGCG)	Sea bass protein (SBP), H_2O_2, ascorbic acid, astaxanthin, algal oil	SBP-EGCG complex showed excellent thixotropic recovery, mechanical strength, and shape fidelity.	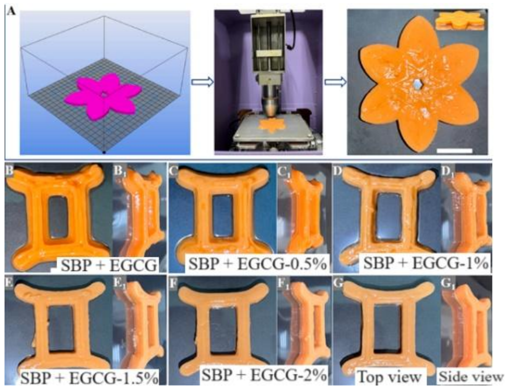	(Zhang *et al.* 2023)

2.6. Post-Printing Treatments

Post-processing refers to the steps carried out after the actual printing of the food item to enhance the final product's quality, appearance, and taste. Typically, food inks suitable for printing are either pre-processed to ensure the desired taste upon printing or pre-processed, necessitating post-treatments after deposition to guarantee edibility (Kewuyemi *et al.* 2022).

Only a small fraction of 3D-printed products do not require post-processing treatments, while most of the 3D-printed food products need post-processing, including baking, steaming, and frying, which can induce favorable alterations in the texture—an essential sensory characteristic influencing product quality and attractiveness (Demei *et al.* 2022). Drying is a frequently employed post-processing approach in the field of food printing (Demei *et al.* 2022). At present, various drying techniques such as freeze drying, oven drying, vacuum microwave drying, and other recently innovated methods are employed to manipulate the characteristics of 3D-printed foods (Demei *et al.* 2022). Various researchers have studied the influence of different drying methods on the shape stability of 3D food products. A study reported the effect of oven drying and freeze drying on protein–cellulose based ink with different dry matter. Experimental findings indicated that the freeze-drying process of printing characterized by a low dry matter content (35%) results in a stable structure. One potential explanation for this observation is that, with an initial low dry matter content of 35%, the water content is elevated, leading to increased structural strength (Lille *et al.* 2018). Another study investigated the effect of microwave drying (MD), catalytic infrared drying (CID), and hot air drying (HAD) on the color of curcumin–whey protein isolate nanoparticle (C-WPI-NP) printed samples. It was reported that CID showed a consistent and obvious red color shift, with a 92.35% retention rate in the size of the dried product (Shen *et al.* 2023) as shown in Figure 2.14.

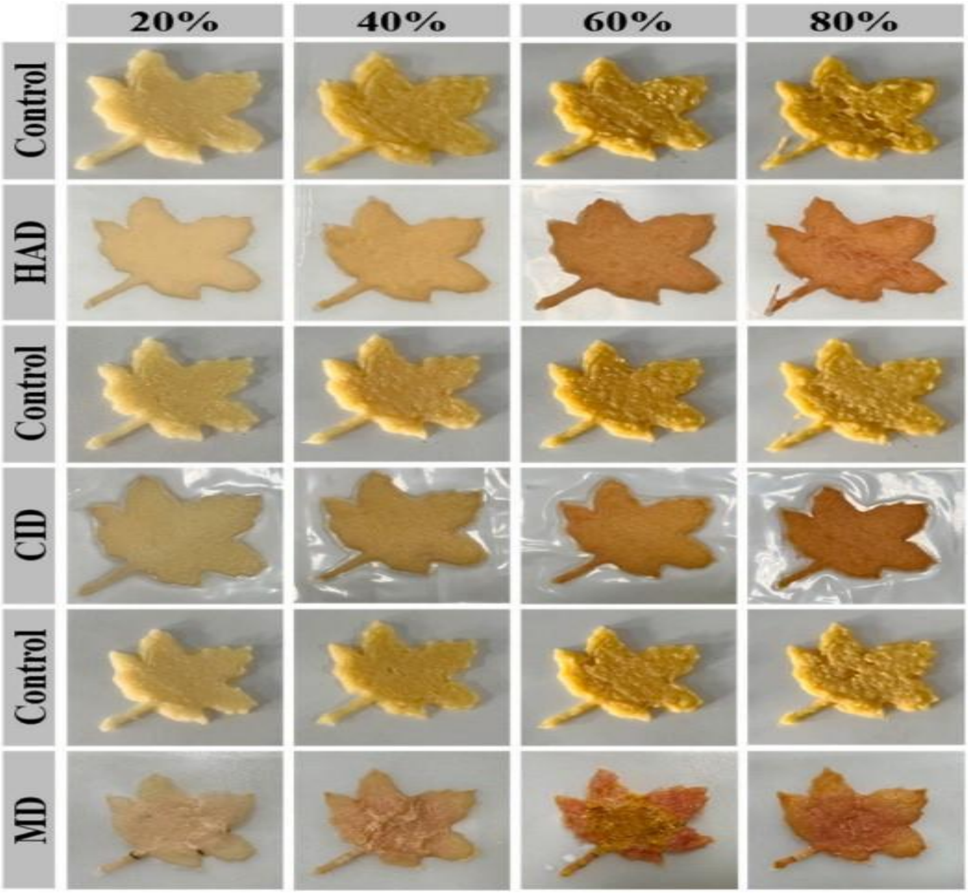

Figure 2.14. Effect of different drying methods on 3D printed C-WPI-NPs Shen *et al.* 2023).

Also, in order to facilitate the widespread adoption and approval of 3D printed foods among consumers, it is essential for 3D printing technology to integrate seamlessly with conventional food processing methods such as baking, steaming, frying, and other cooking techniques. Nevertheless, a significant challenge in achieving this lies in preserving the structural stability of 3D-printed foods throughout the cooking process, which can be improved by the use of additives (He *et al.* 2020). A study evaluated the effect of transglutaminase (TG) on the cooking loss and shrinkage of mung bean protein isolate–methylcellulose complexes (MBPI-MC). It was concluded that when comparing different cooking methods, the cooking loss and shrinkage of TG meat analogues were lower after steaming than after baking, frying, and microwaving (Figure 2.15) (Wen *et al.* 2022). This may have been due to the high water-retention ability of the meat analogue during steaming and the formation of soluble protein aggregates (Wen *et al.* 2022).

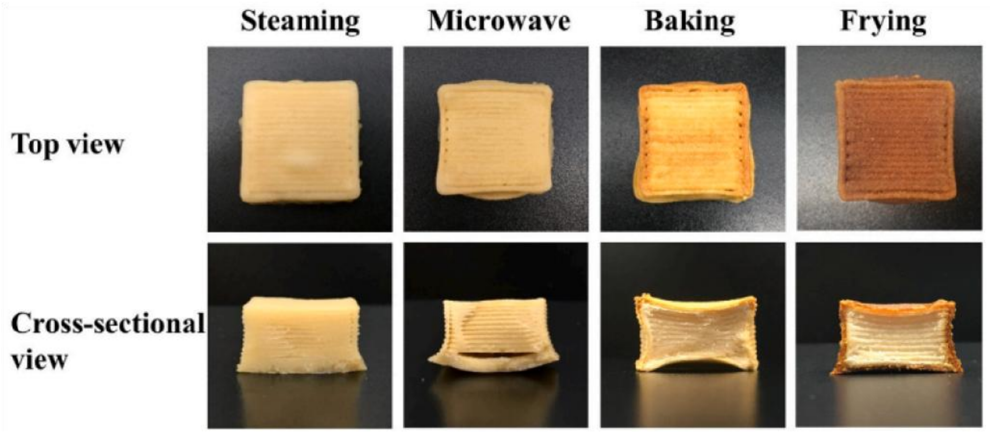

Figure 2.15. Effect of TG on different post-treatment methods of MBPI-MC meat analogues (Wen *et al.* 2022).

2.7 Challenges and Future Perspectives

Realizing nutrition's comprehensiveness and customization is the primary goal of 3D-printed food. These duties enable us to ensure strict product quality and accurate nutrition control to cater to the needs of people like athletes, sick, elderly, children, and pregnant women who require high-quality and readily digestible protein. The researchers should pay attention to the quality and concentration of the materials used to make 3D printing inks as they directly affect the health of humans.

The current development trend is towards developing foods for vegetarians. For that, it is important to note that various sources of plant protein such as pea, soy, and oat can be mixed together in an optimal quantity so as to be used as a potential substitute to meat protein. Animal protein does not have the same health benefits as plant protein, which in return has a longer shelf life and has plenty of nutrients, fiber, and antioxidants. Additionally, plant proteins meet the dietary requirements of vegetarians and have the potential to be used as a substitute to produce meat analogues. For instance, soy protein due to its self-supporting structure and gel-forming properties is termed as an essential plant protein to produce meat products.

Although plant protein materials show promise for 3D-printing applications, the following points need to be better understood for their use in this application.

- Printing precision and shape stability are the biggest challenges to overcome. The development of future 3D-printing inks still depends on the concentration, type, and the environmental and operating conditions which need to be controlled in accordance with the rheological properties of the food. A superior finished product is made by controlling printing parameters such as pH, temperature, speed of nozzle, nozzle diameter, and the material quality and quantity. The printability and self-supporting property of the ink is improved by incorporating various additives to the ink such as hydrocolloids, carbohydrates, lipid additives, phenolic compounds, enzymes, starches, and hydrogels. Lately, there has been a demonstration of cellulose's potential to enhance the characteristics of emulsions based on proteins. Cellulose materials are attracting attention due to their status as the main constituent in plants. Cellulose, as a sustainable and inexhaustible polymeric raw material, has the capacity to fulfill the growing need for eco-friendly products (Dai *et al.* 2018). Also, it might be effective to combine 3D food printing with other cutting-edge technology. For instance, microwave and ultrasonic technologies are applied during pre- or post-processing to enhance the printing accuracy and shape stability (Fan *et al.* 2020).
- Preserving the textural and sensory attributes of the printed food. Sensory attributes such as mouthfeel are influenced by product texture and its ability to bind water. The sensory and textural characteristics of food are impacted by the presence of fats. However, the prolonged excessive intake of saturated fats heightens the susceptibility to numerous chronic conditions, including obesity, cardiovascular disease, and metabolic syndrome. In recent times, nutritional awareness has grown and there is an increased focus on low-fat products. Emulsions are the potential fat replacers, and incorporating cellulose into protein emulsion-based fat replacers enhances the nutritional, textural, and sensory attributes. This improvement is attributed to cellulose's ability to effectively retain water, stabilize interfaces/networks, and thickening effects in addition to its nutritional value as dietary fiber (Dai *et al.* 223).
- Meat products are characterized by a red or pink color that is obviously hard to obtain without the application of colorants. Unfortunately, the issue still exists since many consumers who choose vegetarian goods also avoid additives, which makes the matter more technologically challenging. However, the growing use of 4D printing has encouraged a more thorough investigation into product appearance, which includes color and shape.
- Production efficiency. The size and speed of 3D food printing prevent its usage in industrial-scale food production. Although the printing speed or nozzle diameter can be increased, doing so frequently leads to a loss of printing resolution. Researchers have suggested speeding up

printing by using adaptive algorithms, which might change the printing settings to balance the printing quality and time (Voon *et al.* 2019). Using multi nozzle printers to print multiple 3D objects at once is another possible strategy. Future studies should look into the incorporation of phenolic compounds such as flavonoids, as they are closely related to the sensory and nutritional quality of the food. Future research must examine these issues and opportunities for plant-protein-based inks.

- Consumer acceptance: Acceptability and pleasantness of 3D-printed food is one of the major challenges. A study conducted by Lupton *et al.* 2016 reported the concerns of many participants that the food created using a printer might be inedible, unsafe, or nutritionally deficient. Additionally, the term 'printer,' typically linked with non-food industries, appeared to negatively influence participants' willingness to accept such technology. Ross *et al.* 2022 conducted a study on Irish people and reported that the attitudes of consumers towards the use of 3D food printing technologies might differ depending on the consumer's country of residence. A study revealed that consumer acceptance to 3D-printed food depends on (1) the initial information provided, i.e., the first impression consumers receive, and that (2) well-designed communication has the potential to positively shape consumers' attitudes toward 3D-printed food (Brunner *et al.* 2018).

2.8 Conclusion

This review article entails the virtually new concept of personalized nutrition called 3D food printing. This is a new and innovative field having the potential to customize the design, nutrition, and composition of food products. A focus was placed on plant-protein based inks given their wider usage in research, as compared to animal proteins. One of the most diverse applications of plant proteins is to produce meat analogs. Consumers are becoming vegetarians or seeking out goods that are not made from animal products at an increasing rate today. The majority of meat substitutes contain soy and wheat derived proteins, such as gluten. Although plant-based beef burgers and sausages have been used successfully, most of these recipes use minced meat instead of whole-cut meat fillets, which lack their distinctive appearance. This might be as a result of the extrusion processing methods used for the current plant-based meat substitutes that create a product having a consistent appearance. Although plant proteins are frequently acknowledged as a sustainable substitute for animal proteins, care must also be taken to minimize their harmful effects on the environment during their extraction. Additionally, it was also discovered that hydrocolloids and other additives had significant roles in the production of plant-protein-based printable gels. As we explore new sources of protein to fulfill the needs of a growing population, the demand for plant-based protein will undoubtedly rise in the coming years. Despite the breakthroughs in 3D food printing technology, the issues of providing comprehensive nutrition and personalization, rational protein extraction techniques, improving printing precision and accuracy, and paying attention to the appearance and texture of the finished product still exist.

References

1. Brishti, F.H.; Chay, S.Y.; Muhammad, K.; Ismail-Fitry, M.R.; Zarei, M.; Saari, N. Texturized mung bean protein as a sustainable food source: Effects of extrusion on its physical, textural and protein quality. *Innov. Food Sci. Emerg. Technol.* **2021**, *67*, 102591.
2. Brückner-Gühmann, M.; Kratzsch, A.; Sozer, N.; Drusch, S. Oat protein as plant-derived gelling agent: Properties and potential of modification. Futur. *Foods* **2021**, *4*, 100053.
3. Brunner, T.A.; Delley, M.; Denkel, C. Consumer's attitudes and chane in attitude toward 3D-printed food. *Food Qual. Prefer.* **2018**, *68*, 389–396.
4. Carranza, T.; Guerrero, P.; de la Caba, K.; Etxabide, A. Texture-modified soy protein foods: 3D printing design and red cabbage effect. *Food Hydrocoll.* **2023**, *145*, 109141.
5. Chao, D.; Aluko, R.E. Modification of the structural, emulsifying, and foaming properties of an isolated pea protein by thermal pretreatment. *CYTA-J. Food* **2018**, *16*, 357–366.
6. Chen, J.; Sun, H.; Mu, T.; Blecker, C.; Richel, A.; Richard, G.; Jacquet, N.; Haubruge, E.; Goffin, D. Effect of temperature on rheological, structural, and textural properties of soy protein isolate pastes for 3D food printing. *J. Food Eng.* **2022**, *323*, 110917.
7. Chen, Y.; Zhang, M.; Bhandari, B. 3D Printing of Steak-like Foods Based on Textured Soybean Protein. *Foods* **2021**, *10*, 2011.
8. Chiang, J.H.; Loveday, S.M.; Hardacre, A.K.; Parker, M.E. Effects of soy protein to wheat gluten ratio on the physicochemical properties of extruded meat analogues. *Food Struct.* **2018**, *19*, 100102.
9. Clark, C.C.; Aleman, J.; Mutkus, L.; Skardal, A. A mechanically robust thixotropic collagen and hyaluronic acid bioink supplemented with gelatin nanoparticles. *Bioprinting* **2019**, *16*, e00058.
10. Correa, M.J.; Pérez, G.T.; Ferrero, C. Pectins as Breadmaking Additives: Effect on Dough Rheology and Bread Quality. *Food Bioprocess Technol.* **2011**, *5*, 2889–2898.
11. Cortez-Trejo, M.C.; Gaytán-Martínez, M.; Reyes-Vega, M.; Mendoza, S. Protein-gum-based gels: Effect of gum addition on microstructure, rheological properties, and water retention capacity. *Trends Food Sci. Technol.* **2021**, *116*, 303–317.
12. Dai, H.; Luo, Y.; Huang, Y.; Ma, L.; Chen, H.; Fu, Y.; Yu, Y.; Zhu, H.; Wang, H.; Zhang, Y. Recent advances in protein-based emulsions: The key role of cellulose. *Food Hydrocoll.* **2023**, *136*, 108260.

13. Dai, L.; Cheng, T.; Duan, C.; Zhao, W.; Zhang, W.; Zou, X.; Aspler, J.; Ni, Y. 3D printing using plant-derived cellulose and its derivatives: A review. *Carbohydr. Polym.* **2018**, *203*, 71–86.
14. de Angelis, D.; Kaleda, A.; Pasqualone, A.; Vaikma, H.; Tamm, M.; Tammik, M.-L.; Squeo, G.; Summo, C. Physicochemical and sensorial evaluation of meat analogues produced from dry-fractionated pea and oat proteins. *Foods* **2020**, *9*, 1754.
15. Demei, K.; Zhang, M.; Phuhongsung, P.; Mujumdar, A.S. 3D food printing: Controlling characteristics and improving technological effect during food processing. *Food Res. Int.* **2022**, *156*, 111120.
16. Derossi, A.; Caporizzi, R.; Azzollini, D.; Severini, C. Application of 3D printing for customized food. A case on the development of a fruit-based snack for children. *J. Food Eng.* **2018**, *220*, 65–75.
17. Dick, A.; Bhandari, B.; Prakash, S. 3D printing of meat. *Meat Sci.* **2019**, *153*, 35–44.
18. Ding, J.; Ju, H.; Zhong, L.; Qi, L.; Sun, N.; Lin, S. Reducing the allergenicity of pea protein based on the enzyme action of alcalase. *Food Funct.* **2021**, *12*, 5940–5948.
19. Doss, A.; Esther, A.; Rajalakshmi, R. Influence of UV-B treatment on the accumulation of free phenols and tannins in the legumes of *Abrus precatorius* L. and *Vigna mungo* (L.) Hepper. *Phytomedicine Plus* **2022**, *2*, 100189.
20. Fan, H.; Zhang, M.; Liu, Z.; Ye, Y. Effect of microwave-salt synergetic pre-treatment on the 3D printing performance of SPI-strawberry ink system. *LWT* **2020**, *122*, 109004.
21. Feng, C.; Zhang, M.; Bhandari, B. Materials Properties of Printable Edible Inks and Printing Parameters Optimization during 3D Printing: A review. *Crit. Rev. Food Sci. Nutr.* **2019**, *59*, 3074–3081.
22. Fiorentini, M.; Kinchla, A.J.; Nolden, A.A. Role of sensory evaluation in consumer acceptance of plant-based meat analogs and meat extenders: A scoping review. *Foods* **2020**, *9*, 1334.
23. Gao, T.; Gillispie, G.J.; Copus, J.S.; Pr, A.K.; Seol, Y.-J.; Atala, A.; Yoo, J.-J.; Lee, S.-J. Optimization of gelatin–alginate composite bioink printability using rheological parameters: A systematic approach. *Biofabrication* **2018**, *10*, 034106.
24. Godoi, F.C.; Prakash, S.; Bhandari, B.R. 3d printing technologies applied for food design: Status and prospects. *J. Food Eng.* **2016**, *179*, 44–54.
25. Guo, Z.; Arslan, M.; Li, Z.; Cen, S.; Shi, J.; Huang, X.; Xiao, J.; Zou, X. Application of Protein in Extrusion-Based 3D Food Printing: Current Status and Prospectus. *Foods* **2022**, *11*, 1902.

26. He, C.; Zhang, M.; Fang, Z. 3D printing of food: Pretreatment and post-treatment of materials. *Crit. Rev. Food Sci. Nutr.* **2020**, *60*, 2379–2392.
27. Huang, M.S.; Zhang, M.; Bhandari, B. Assessing the 3D Printing Precision and Texture Properties of Brown Rice Induced by Infill Levels and Printing Variables. *Food Bioprocess Technol.* **2019**, *12*, 1185–1196.
28. Kewuyemi, Y.O.; Kesa, H.; Adebo, O.A. Trends in functional food development with three-dimensional (3D) food printing technology: Prospects for value-added traditionally processed food products. *Crit. Rev. Food Sci. Nutr.* **2022**, *62*, 7866–7904.
29. Kim, H.W.; Lee, J.H.; Park, S.M.; Lee, M.H.; Lee, I.W.; Doh, H.S.; Park, H.J. Effect of Hydrocolloids on Rheological Properties and Printability of Vegetable Inks for 3D Food Printing. *J. Food Sci.* **2018**, *83*, 2923–2932.
30. Kim, Y.; Kim, H.W.; Park, H.J. Effect of pea protein isolate incorporation on 3D printing performance and tailing effect of banana paste. *LWT-Food Sci. Technol.* **2021**, *150*, 111916.
31. Kolpakova, V.V.; Gaivoronskaya, I.S.; Kovalenok, V.A.; Slozhenkina, M.I.; Mosolov, A.A. Protein plant-based composites synthesized with transglutaminase. *IOP Conf. Ser. Earth Environ. Sci* **2021**, *677*, 032046.
32. Lam, A.C.Y.; Can Karaca, A.; Tyler, R.T.; Nickerson, M.T. Pea protein isolates: Structure, extraction, and functionality. *Food Rev. Int.* **2018**, *34*, 126–147.
33. Lanaro, M.; Forrestal, D.P.; Scheurer, S.; Slinger, D.J.; Liao, S.; Powell, S.K.; Woodruff, M.A. 3D printing complex chocolate objects: Platform design, optimization and evaluation. *J. Food Eng.* **2017**, *215*, 13–22.
34. Li, H.; Tan, Y.J.; Leong, K.F.; Li, L. 3D Bioprinting of Highly Thixotropic Alginate/Methylcellulose Hydrogel with Strong Interface Bonding. *ACS Appl. Mater. Interfaces* **2017**, *9*, 20086–20097.
35. Lille, M.; Nurmela, A.; Nordlund, E.; Metsä-Kortelainen, S.; Sozer, N. Applicability of protein and fiber-rich food materials in extrusion-based 3D printing. *J. Food Eng.* **2018**, *220*, 20–27.
36. Lin, Q.; Hu, Y.; Qiu, C.; Li, X.; Sang, S.; McClements, D.J.; Chen, L.; Long, J.; Xu, X.; Wang, J.; et al. Peanut protein-polysaccharide hydrogels based on semi-interpenetrating networks used for 3D/4D printing. *Food Hydrocoll.* **2023**, *137*, 108332.
37. Liu, L.; Ciftci, O.N. Effects of high oil compositions and printing parameters on food paste properties and printability in a 3D printing food processing model. *J. Food Eng.* **2020**, *288*, 110135.

38. Liu, Z.; Bhandari, B.; Prakash, S.; Mantihal, S.; Zhang, M. Linking rheology and printability of a multicomponent gel system of carrageenan-xanthan-starch in extrusion based additive manufacturing. *Food Hydrocoll.* **2019**, *87*, 413–424.
39. Liu, Z.; Bhandari, B.; Zhang, M. Incorporation of probiotics (*Bifidobacterium animalis* subsp. *Lactis*) into 3D printed mashed potatoes: Effects of variables on the viability. *Food Res. Int.* **2019**, *128*, 108795.
40. Liu, Z.; Chen, X.; Dai, Q.; Xu, D.; Hu, L.; Li, H.; Hati, S.; Chitrakar, B.; Yao, L.; Mo, H. Pea protein-xanthan gum interaction driving the development of 3D printed dysphagia diet. *Food Hydrocoll.* **2023**, *139*, 108497.
41. Lorenz, T.; Iskandar, M.M.; Baeghbali, V.; Ngadi, M.O.; Kubow, S. 3D Food Printing Applications Related to Dysphagia: A Narrative Review. *Foods* **2022**, *11*, 1789.
42. Lupton, D.; Turner, B. 'Both Fascinating and Disturbing': Consumer Responses to 3D FoodPrinting and Implications for Food Activism. In *Digital Food Activism*; Schneider, T., Eli, K., Dolan, C., Ulijaszek, S., Eds.; Routledge: London, UK, 2016; Available online: https://ssrn.com/abstract=2799191 (accessed on 26 November 2023).
43. Malda, J.; Visser, J.; Melchels, F.P.; Jüngst, T.; Hennink, W.E.; Dhert, W.J.A.; Groll, J.; Hutmacher, D.W. 25th anniversary article: Engineering hydrogels for biofabrication. *Adv. Mater.* **2013**, *25*, 5011–5028.
44. Mantihal, S.; Kobun, R.; Lee, B.B. 3D food printing of as the new way of preparing food: A review. *Int. J. Gastron. Food Sci.* **2020**, *22*, 100260.
45. Mirazimi, F.; Saldo, J.; Sepulcre, F.; Gràcia, A.; Pujola, M. Enriched puree potato with soy protein for dysphagia patients by using 3D printing. *Food Front.* **2022**, *3*, 706–715.
46. Mu, X.; Agostinacchio, F.; Xiang, N.; Pei, Y.; Khan, Y.; Guo, C.; Cebe, P.; Motta, A.; Kaplan, D.L. Recent advances in 3D printing with protein-based inks. *Prog. Polym. Sci.* **2021**, *115*, 101375.
47. Natural Machines, Advanced User Settings Explained, Knowl. Base. 2021. Available online: https://support.naturalmachines.com/portal/en/kb/articles/advanced-settings-explained (accessed on 7 September 2023).
48. Nowacka, M.; Trusinska, M.; Chraniuk, P.; Drudi, F.; Lukasiewicz, J.; Nguyen, N.P.; Przybyszewska, A.; Pobiega, K.; Tappi, S.; Tylewicz, U.; et al. Developments in Plant Proteins Production for Meat and Fish Analogues. *Molecules* **2023**, *28*, 2966.
49. Oyinloye, T.M.; Yoon, W.B. Stability of 3D printing using a mixture of pea protein and alginate: Precision and application of additive layer manufacturing simulation approach for stress distribution. *J. Food Eng.* **2020**, *288*, 110127.

50. Pérez, B.; Nykvist, H.; Brøgger, A.F.; Larsen, M.B.; Falkeborg, M.F. Impact of macronutrients printability and 3D-printer parameters on 3D-food printing: A review. *Food Chem.* **2019**, *287*, 249–257.
51. Phuhongsung, P.; Zhang, M.; Bhandari, B. 4D printing of products based on soy protein isolate via microwave heating for flavor development. *Food Res. Int.* **2020**, *137*, 109605.
52. Qiu, Y.; McClements, D.J.; Chen, J.; Li, C.; Liu, C.; Dai, T. Construction of 3D printed meat analogs from plant-based proteins: Improving the printing performance of soy protein- and gluten-based pastes facilitated by rice protein. *Food Res. Int.* **2023**, *167*, 112635.
53. Ramachandraiah, K. Potential development of sustainable 3d-printed meat analogues: A review. *Sustainability* **2021**, *13*, 938.
54. Ross, M.M.; Collins, A.M.; McCarthy, M.B.; Kelly, A.L. Overcoming barriers to consumer acceptance of 3D-printed foods in the food service sector. *Food Qual. Prefer.* **2022**, *100*, 1004615.
55. Severini, C.; Derossi, A.; Azzollini, D. Variables affecting the printability of foods: Preliminary tests on cereal-based products. *Innov. Food Sci. Emerg. Technol.* **2016**, *38*, 281–291.
56. Shan, H.; Lu, S.W.; Jiang, L.Z.; Wang, L.K.; Liao, H.; Zhang, R.Y.; Dai, C.J.; Yao, X.M.; Zhang, Y.L.; Su, P.; et al. Gelation property of alcohol-extracted soy protein isolate and effects of various reagents on the firmness of heat-induced gels. *Int. J. Food Prop.* **2015**, *18*, 627–637.
57. Shen, C.; Chen, W.; Li, C.; Chen, X.; Cui, H.; Lin, L. 4D printing system stimulated by curcumin/whey protein isolate nanoparticles: A comparative study of sensitive color change and post-processing. *J. Food Eng.* **2023**, *342*, 111357.
58. Shi, H.; Li, J.; Xu, E.; Yang, H.; Liu, D.; Yin, J. Microscale 3D printing of fish analogues using soy protein food ink. *J. Food Eng.* **2023**, *347*, 111436.
59. Singh, M.; Trivedi, N.; Enamala, M.K.; Kuppam, C.; Parikh, P.; Nikolova, M.P.; Chavali, M. Plant-based meat analogue (PBMA) as a sustainable food: A concise review. *Eur. Food Res. Technol.* **2021**, *247*, 2499–2526.
60. Sun, J.; Zhou, W.; Huang, D.; Fuh, J.Y.H.; Hong, G.S. An Overview of 3D Printing Technologies for Food Fabrication. *Food Bioprocess Technol.* **2015**, *8*, 1605–1615.
61. Voon, S.L.; An, J.; Wong, G.; Zhang, Y.; Chua, C.K. 3D food printing: A categorised review of inks and their development. *Virtual Phys. Prototyp.* **2019**, *14*, 203–218.
62. Wang, L.; Zhang, M.; Bhandari, B.; Yang, C. Investigation on FishSurimi Gel as Promising Food Material for 3D Printing. *J. Food Eng.* **2018**, *220*, 101–108.

63. Wang, T.; Kaur, L.; Furuhata, Y.; Aoyama, H.; Singh, J. 3D Printing of Textured Soft Hybrid Meat Analogues. *Foods* **2022**, *11*, 478.
64. Wen, Y.; Chao, C.; Che, Q.T.; Kim, H.W.; Park, H.J. Development of plant-based meat analogs using 3D printing: Status and opportunities. *Trends Food Sci. Technol.* **2023**, *132*, 76–92.
65. Wen, Y.; Kim, H.W.; Park, H.J. Effects of transglutaminase and cooking method on the physicochemical characteristics of 3D-printable meat analogs. *Innov. Food Sci. Emerg. Technol.* **2022**, *81*, 103114.
66. Xu, K.; Wu, C.; Fan, G.; Kou, X.; Li, X.; Li, T.; Dou, J.; Zhou, Y. Rheological properties, gel properties and 3D printing performance of soy protein isolate gel inks added with different types of apricot polysaccharides. *Int. J. Biol. Macromol.* **2023**, *242*, 124624.
67. Yang, F.; Zhang, M.; Prakash, S.; Liu, Y. Physical properties of 3D printed baking dough as affected by different compositions. *Innov. Food Sci. Emerg. Technol.* **2018**, *49*, 202–210.
68. You, Y., Yang, L., Chen, H., Xiong, L., & Yang, F. Effects of (-)-Epigallocatechin-3-gallate on the functional and structural properties of soybean protein isolate. *J. Agric. Food Chem.* **2021**, 69, 2306-2315, doi: https://dx.doi.org/10.1021/acs.jafc.0c07337?ref=pdf
69. Yu, X.; Zhao, Z.; Zhang, N.; Yan, B.; Gao, W.; Huang, J.; Zhao, J.; Zhang, H.; Chen, W.; Fan, D. Effects of preheating-induced denaturation treatments on the printability and instant curing property of soy protein during microwave 3D printing. *Food Chem.* **2022**, *397*, 133682.
70. Zhang, L., Zhou, C., Xing, S., Chen, Y., Su, W., Wang, H., & Tang, M. Sea bass protein-polyphenol complex stabilized high internal phase of algal oil Pickering emulsions to stabilize astaxanthin for 3d food printing. *Food Chemistry*, **2023**, 417, 135824, doi: https://doi.org/10.1016/j.foodchem.2023.135824.
71. Zhang, T.; Dou, W.; Zhang, X.; Zhao, Y.; Zhang, Y.; Jiang, L.; Sui, X. The development history and recent updates on soy protein-based meat alternatives. *Trends Food Sci. Technol.* **2021**, *109*, 702–710.

CONNECTING TEXT

The review of literature showed the potential for 3D printing of plant-based proteins, relationships between various 3D printing parameters and their collective impact on printability, and the need for additives.

The chapter highlights that there has been extensive research conducted on the impact of printing parameters on the printability of plant-based proteins. However, there is limited information available on the influence of EGCG-based ink on the printing properties of soy protein products.

In the following section (Chapter III), we delve into the comprehensive understanding of the impact of 3D printing parameters on the printability of SPI-WG-EGCG complexes. Adjusting for nozzle diameter, nozzle height, and printing speed, this chapter aims to understand their individual and combined effects on the 3D printability of ink.

III. Assessment of 3D printability of SPI-WG-EGCG complexes

3.1 Abstract

Protein gels, particularly those derived from plant sources like soy, are gaining attention in the food industry due to their nutritional and environmental advantages. Soy protein offers a rich array of fiber, starch, vitamins, and minerals, along with phytochemicals such as galactosides, saponins, phytates, and phenols associated with various health benefits. However, leveraging these benefits in 3D printing with plant protein-based materials presents notable challenges. Natural plant proteins often exhibit poor printability and stability, leading to suboptimal print quality during the printing process.

To address these challenges, additives play a crucial role. One potential additive, epigallocatechin-3-gallate (EGCG), a polyphenol found in green tea, shows promising results in modifying the surface hydrophobicity of soy protein isolate (SPI) and improving its gelation properties. While polyphenols have been known to strengthen protein gels in animal-based materials, their role in altering plant protein gels remains ambiguous. In this study, we investigate the impact of varying EGCG concentration on the printing performance of edible inks formulated from soy protein, wheat gluten, water, and oil in a specific ratio of 5:3:33.33:2. Through systematic experimentation varying nozzle diameter, nozzle height, printing speed, and material composition, we aim to assess printability and accuracy. This research endeavors to bridge the gap between the inherent challenges of 3D printing with plant proteins and the potential for innovation in additive-based solutions, ultimately advancing the efficiency and sustainability of this emerging technology in the food industry.

3.2 Introduction

3D food printing is a promising innovation in the food industry, with evolving applications in gastronomy, personalized nutrition, and ingredient creation (Sun *et al.* 2015). Despite enormous potential, its impact has been limited due to critical pre-processing and post-processing constraints. Key constraints include the complex rheological requirements of food inks, which must balance flowability and structural integrity (Liu *et al.* 2017), and precise temperature control during printing to prevent deformation and ensure product stability (Keerthana *et al.* 2020).

Important processing factors include the printing mechanism (extrusion-based, selective sintering, binder jetting, inkjeting.), ink material properties (rheological, mechanical and textural), equipment parameters (nozzle height and diameter, printing speed, infill percentage) and post-processing requirements (cooking/baking, drying, frying, freezing, fermentation) (Liu *et al.* 2017). Considerable work has been done on 3D printing of carbohydrate-based products (Jagadiswaran *et al.* 2021; Montoya *et al.* 2021; Keerthana *et al.* 2020). However, there has been recent and increasing interest in printing protein-based products (Yu *et al.* 2022; Chen *et al.* 2021; Oyinloye *et al.* 2020).

The case for printing protein-based products include the need to transition towards sustainable food systems. Soy protein is a candidate for 3D printing due to its exceptional emulsifying, gelation and foaming properties (Yu *et al.* 2022). The yield and quality of soy protein isolate (SPI) gels are largely due to their gelation rate and network structure formation capacity (Xu *et al.* 2020). The natural state of soy protein poses challenges for printability due to the difficulty in controlling its gelation rate and network structure. Consequently, current research efforts focus on improving its rheological properties by incorporating various additives.

Polyphenols can bind to proteins via hydrophobic interactions, hydrogen bonds, and electrostatic interactions, that can modify surface hydrophobicity and structure of the proteins, consequently altering their functional properties (Sun *et al.* 2022). Epigallocathechin Gallate (EGCG), a prominent and highly effective polyphenol found in green tea, possesses numerous biological properties, including antioxidative, antibacterial, free-radical scavenging, and anticancer effects (Lorenzo *et al.* 2013). EGCG could potentially change the surface hydrophobicity of SPI, improve its gelation rate, and help create a more uniform network structure. Thus, addition of EGCG could improve material properties and holds promise for advancing both the precision and reliability of 3D printing of protein-based products. There has been no study on the effectiveness of EGCG in modifying SPI properties with respect to modulating its printability.

Achieving precision and reliability in 3D printing the product requires a multidimensional approach that integrates advancements in material science, gel formulation and adjustment of printing technology. Printability refers to a material's capacity to be consistently extruded in accordance with a predefined shape and to maintain dimensional stability post-printing. Evaluating printability involves assessing (a) dimensional stability (b) extrudability, and (c) stability (Kadival *et al.* 2023). However, assessing 3D printability of food products remains a significant challenge. There is need for precise evaluation methods that can quantitatively assess resultant geometric accuracy of 3D printed objects. Current evaluation methods predominantly rely on subjective visual inspections or rudimentary dimensional measurements (Lille *et al*. 2018). These methods often provide qualitative assessments rather than precise quantitative data, making it difficult to evaluate how well printed objects match their intended geometries accurately. Advanced techniques, such as using image processing software like ImageJ, offer a more sophisticated approach to analyzing the correlation between printed outcomes and original designs (Derossi *et al.* 2020). Improving printability also necessitates optimizing the physicochemical, rheological, structural, and mechanical properties of printing gels, enabling 3D-printed structures to endure subsequent processing stages (Barrios-Rodriguez *et al.* 2024). However, achieving more effective printing requires careful assessment and analysis of both the food's characteristics and other external elements interacting with the printing gels. Selecting the appropriate formulation for the gel and fine-tuning its printing parameters are pivotal for its printing, serving as the primary determinant of 3D printing accuracy (Feng *et al.* 2019). Specifically, adjustment of printing parameters such as nozzle diameter, nozzle height, nozzle speed, printing temperature, and extrusion rate significantly influence the process's outcome (Hao *et al*. 2010). Wang *et al.* (2018) reported that a smaller nozzle diameter produces higher-resolution printed objects, whereas a larger nozzle diameter results in lower resolution. However, excessively small nozzles can lead to inconsistent printing lines. The distance between the nozzle tip and the top of the last deposited layer is known as nozzle height or layer height. Various studies theoretically reported the use of equal nozzle height and nozzle diameter. Yang *et al.* (2018) suggested that the layer height should be smaller than the nozzle diameter for better adhesion. Combination of precise evaluation methods, such as advanced image processing techniques, with optimized gel formulations and meticulous adjustment of printing parameters (like nozzle specifications and extrusion rates), is essential for enhancing printability and ensuring the structural integrity of printed food products (Hao *et al*. 2010). This study aims to investigate the impact of formulation and process variables such as nozzle height-to-diameter ratio, nozzle diameter, and nozzle speed on 3D printability of SPI-WG-EGCG complexes. The study would enhance and provide crucial pathways for production of printed SPI based products.

3.3 Materials and Method

3.3.1 Materials

Soy protein isolate was procured from Fisher Scientific (Ottawa, Ontario, Canada). Wheat gluten was obtained from Sigma-Adrich (St. Louis, Missouri, USA). Epigallocatechin-3-gallate (purity >=98.0% HPLC) was purchased from MilliporeSigma (Oakville, Ontario, Canada). The all other reagents were of analytical grade.

3.3.2 Preparation of SPI-polyphenol complexes

SPI, WG, oil and water were combined in the ratio of 5:3:2:33.3, respectively. Following this, varying concentrations of EGCG were incorporated into the mixture. The EGCG concentrations used were 0, 0.25, 0.5, and 1%. The resulting mixtures were labelled as SPI-E1, SPI-E2, SPI-E3, and SPI-E4, corresponding to the concentrations of 0, 0.25, 0.5, and 1% EGCG.

3.3.3 3D Printing of Products

The SPI-WG-EGCG complexes were printed using a commercial 3D printer Foodini (Natural Machines, Barcelona, Spain). The printing system operated with a nozzle connected to a piston and prints food using a precision control system. Printing took place at room temperature, maintained at 23 ± 0.3◦C throughout the process. To study printing characteristics, cylinder models were designed using FreeCAD software (open-source, version 0.20.2), with dimensions tailored to the printer nozzle diameters. For the 4 mm printer nozzle, the cylinder model was designed with diameter of 3 cm and height of 2 cm to ensure sufficient surface area for material flow, maintaining stability and reducing clogging risks. For the 1.5 mm nozzle, a 2.5 cm diameter and 3 cm height cylinder were chosen to maintain a balance between stability and material flow. Subsequently, the cylinders were printed at the different printer parameter settings.

3.3.4 Dimensional Stability of Printed Products

Design schematic and dimensions of the model cylinders are shown in Figure 3.1. The shape and stability of the printed cylinders were assessed. Images of the top and side views of each printed cylinder were captured using a Canon EOS Rebel T3i Digital SLR camera (Canon Inc., Japan). The camera was mounted on a tripod and positioned at a fixed distance from the printed product for consistent imaging. The captured images were processed in ImageJ software to determine shape parameters. The base diameter was measured from the top-view images. Calibration of dimensions was achieved using a printed object with known accurate dimensions, verified with vernier callipers. These measurements served as the standard reference for the remaining printed cylinders in ImageJ, ensuring consistent and precise assessments. Following calibration, two diameter measurements were made from each image of the printed cylinders to account for any non-uniform diameters. The percent variation between the designed and printed cylinder dimensions was calculated using Equation 1 (Maldonado-Rosas *et al.* 2022):

$$\%\text{error} = \frac{D_{designed} - D_{calculated}}{D_{designed}} \text{ x } 100 \quad (1)$$

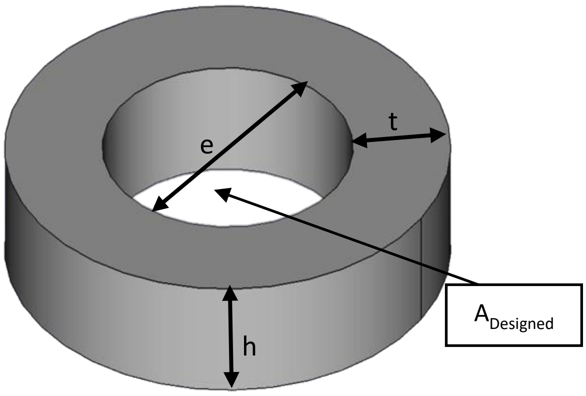

Figure 3.1 Isometric view of the hollow cylinders with 4 mm nozzle diameter, t=25 mm, $A_{Designed}$= 3298.67 mm^2, e=30 mm, h=20 mm and 1.5 mm nozzle diameter, $A_{Designed}$= 3337.94 mm^2, e=25 mm, h=30 mm

3.3.5 Experimental Design

A fractional factorial experimental design was applied in the study. The design included 4 key experimental factors namely: i) EGCG concentration (0, 0.25, 0.5 and 1%), ii) nozzle diameter (1.5 and 4 mm), iii) H/D ratio (0.85, 1, and 1.25), and iv) nozzle speed (50, 58, 65, 228, 235, and 245 mm/sec). The nozzle height represented the layer thickness. The nozzle speed represented the speed at which the print head moved along the X and Y axes during printing. The nozzle diameter marked the width of the extruded material line, which influenced the thickness of deposited layers when combined with layer height settings. The experimental treatments were duplicated resulting in a total of 72 runs.

3.3.6 Statistical Analysis

Analysis of variance (ANOVA) was conducted on the experimental data using the SAS (Version 9.4, SAS Institute Inc., Cary, NC, USA) software. Statistical significance was determined at the 5% level.

Percent error was used to indicate the accuracy of the printing. Regression analysis was used to quantify the effect the experimental factors (independent variables) on print percent error. A stepwise regression analysis was applied to elucidate the relationships between various factors and their interactions. This approach was selected due to its superior explanatory power and to ensure that the model's complexity was balanced with its factor's performance.

3.4 Results and Discussion

3.4.1 Visual Appeal and Dimensional Integrity

There were notable variabilities in printing errors across different nozzle diameters, nozzle H/D ratios, and nozzle speeds (Figure 3.2). Analysis of variance showed that nozzle speed did not significantly affect ($p > 0.05$) the dimensional stability of the printed samples. However, other factors namely nozzle diameter, nozzle H/D ratio, and EGCG concentration showed significant effect ($p < 0.05$) on variations in diameter obtained from the printed cylinder.

EGCG concentrations significantly affected diameter changes. Specifically, at the nozzle height-to-diameter (H/D) ratio of 0.85, the printing error decreased from $11.71 \pm 8.87\%$ to $4.60 \pm 3.98\%$ as EGCG concentration increased from 0 (control) to 1%. This suggests that higher EGCG concentrations enhance the material's flow properties and improve layer adhesion. Apparently, EGCG modified the surface hydrophobicity of soy protein isolate (SPI), which facilitated better gelation and a more uniform network structure, leading to more consistent diameter measurements (Xu *et al*. 2020). In contrast, using a 1.5 mm nozzle diameter and a H/D ratio of 1.25, printing errors remained high and reached up to 100% at the nozzle speeds of 50, 58, and 65 mm/sec for control samples. The result demonstrates the difficulty of controlling gelation rate of the SPI network without EGCG, and it underscores the role of EGCG as a cross-linking agent. The instability of control samples, exacerbated by higher nozzle speeds that increased turbulence and shear forces, further disrupted the already weak gel network, leading to higher printing errors and collapse of the structure (Xu *et al.* 2020). According to Khan *et al.* (2024) and Liu *et al*. (2020), such high speeds can introduce flow instability and excessive material shear, undermining the structural integrity and buildability of the printed object.

The 4 mm nozzle diameter exhibited significantly lower printing errors, particularly at the higher nozzle speeds of 228 and 245 mm/sec. This suggests that larger nozzle diameters are better suited for handling increased extrusion rates with fewer errors, likely due to their ability to reduce shear forces and improve material flow (Khan *et al.* 2024). However, variabilities within each category, such as nozzle speeds or height-to-diameter (H/D) ratios, were often substantial, indicating inconsistent performance across various printing conditions. Similar to the 1.5 mm nozzle diameter, increasing the EGCG concentration also led to decreased printing errors, with errors dropping from 8.82 ± 5.46% at control levels to 5.81 ± 4.56% at a 1% EGCG concentration. Also, nozzle speeds of 228 mm/sec or less resulted in low feed pressure and low flow rate, leading to line breakage for both 1.5 mm and 4 mm nozzle diameters. This result agrees with the findings of Feng *et al. (*2019) who reported that a decrease in the nozzle diameter not only increases the printing time but also raises the feed pressure. With nozzle diameters of 0.8 mm and 1.5 mm, a discontinuous deposition phenomenon occurs when the surimi gel is extruded. Furthermore, low speeds result in insufficient feed pressure and flow rate, which can lead to wire breakage.

Visual inspection showed that the structural integrity and surface smoothness of the products varied with the different printing parameters, particularly the nozzle H/D ratio and the concentration of EGCG (Table 3.1). Particularly, as the H/D ratio increased to 1.25, the samples tended to collapse, indicating that a higher H/D ratio may result in instability of the printed structures. This instability could be attributed to the insufficient support provided by the higher nozzle height relative to the diameter, causing the printed layers to sag or collapse under their own weight.

In terms of surface texture, samples printed at lower EGCG concentrations appeared rougher. This roughness can be attributed to the lower viscosity and weaker intermolecular interactions in the solution, which may result in less cohesive layer formation and increased surface irregularities. Conversely, as the concentration of EGCG increased, the appearance and stability of the printed samples improved. The higher polyphenol content enhanced the gluten network in WG by promoting protein cross-linking, which increased the elasticity and cohesiveness of the sample. Elasticity was critical for maintaining the stability of printed layers leading to smoother surfaces and more structurally stable prints.

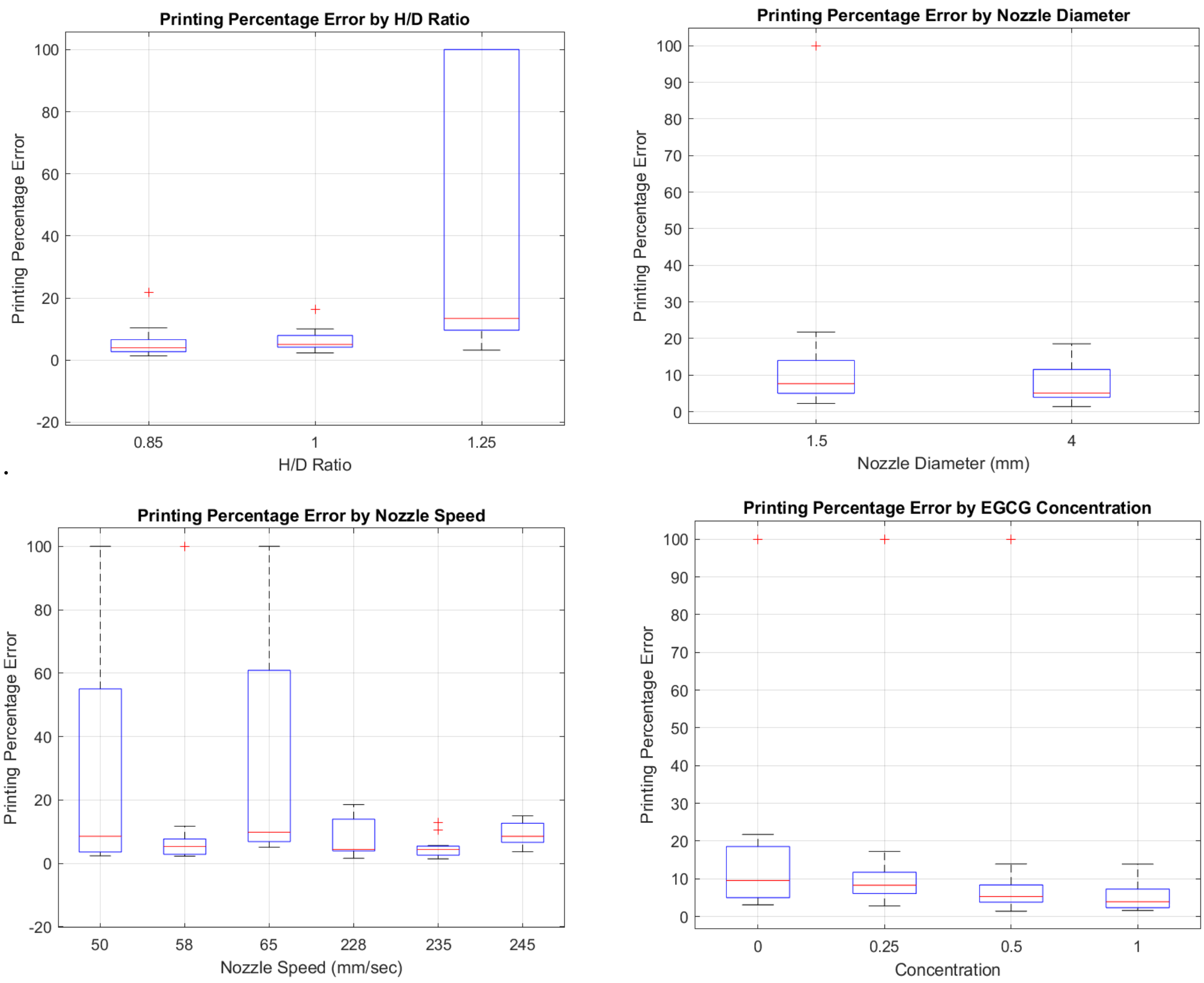

Figure 3.2 Box Plot Analysis of Printing Percentage Error Across Different Parameters i) H/D ratio ii) nozzle diameter (mm) iii) nozzle speed (mm/sec) iv) EGCG concentration

Table 3.1 Effect of printing parameters on printability of SPI-WG-EGCG complexes

EGCG concentration	Nozzle diameter	H/D ratio	Nozzle speed	Replicate 1	Replicate 2
0	1.5	0.85	58		
0	1.5	1	50	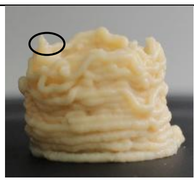	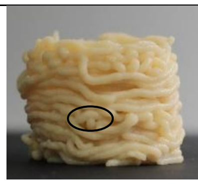

0.25	1.5	0.85	58		
0.25	1.5	1.25	65		
0.5	1.5	1	50		
0.5	1.5	0.85	58		
1	1.5	0.85	58		
1	1.5	1.25	58		
0	4	0.85	228		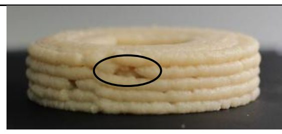
0	4	1.25	245		
0.25	4	0.85	235		
0.25	4	1	228		

0.5	4	0.85	235		
0.5	4	1	245		
1	4	1	228		
1	4	0.85	235		

3.4.2 Effects of Printing Parameters

Figure 3.3 presents a Pareto chart illustrating the impact of the independent variables: nozzle speed, nozzle diameter, EGCG concentration, and H/D ratio on printing percentage error of 3D printed samples. Among these variables, the H/D ratio exhibited the most substantial effect, with an estimated influence of 83.71. This was followed by the effects of EGCG concentration, nozzle diameter, and nozzle speed, which were -18.77, -14.80, and 0.11, respectively. Notably, the H/D ratio demonstrated a positive correlation with printing error, indicating that an increase in the H/D ratio corresponded to a higher printing error. Conversely, both the EGCG concentration and nozzle diameter exhibited negative correlations, suggesting that higher EGCG concentrations and larger nozzle diameters resulted in a decrease in printing error.

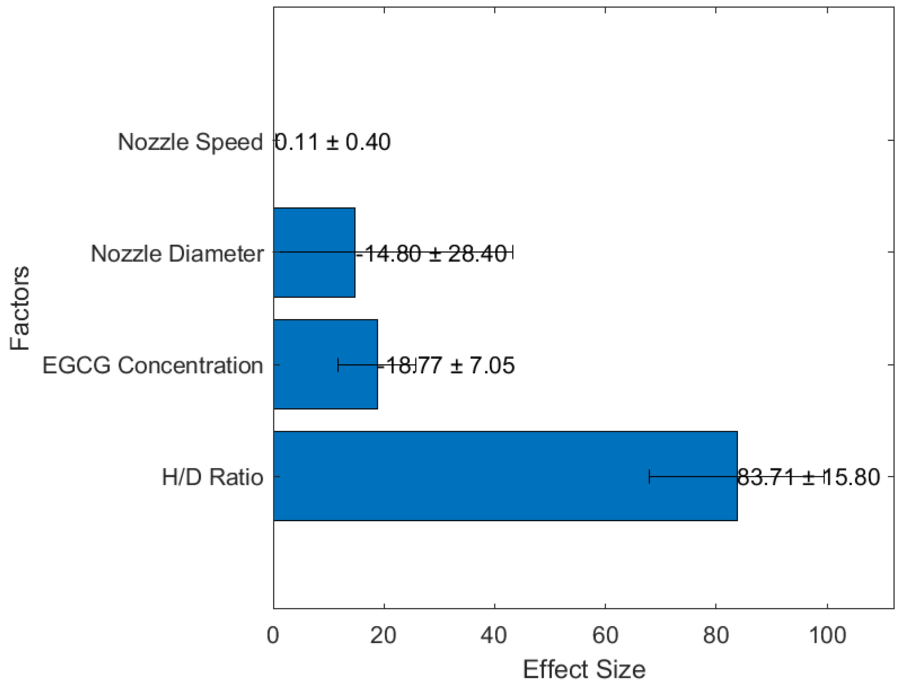

Figure 3.3 Pareto chart describing the effects of nozzle speed, nozzle diameter, EGCG concentration, and H/D ratio on the printing percentage error of SPI-WG-EGCG printed samples.

Figure 3.4 illustrates a 3-dimensional surface plot for Nozzle Diameter versus Nozzle Speed, revealing the relationship between these parameters and their impact on printing percentage error. Despite the clear visualization of changes in printing error as both nozzle diameter and nozzle speed were varied, statistical analysis revealed that nozzle speed did not significantly impact printing percentage error ($p > 0.05$). The 3D surface plot demonstrates that nozzle diameter did not significantly impact printing percentage error with respect to changes in nozzle speed. Across the tested range of speeds (58 mm/sec to 235 mm/sec) and both nozzle diameters (1.5 mm and 4 mm), the surface remained relatively flat. This flatness suggests that changing the nozzle speed within the tested range across changing nozzle diameters does not lead to substantial variations in error, aligning with the statistical conclusion of non-significance.

To further understand the result, a 80 mm line was printed with the sample solutions. The result shows that nozzle speeds led to three distinct scenarios: slow speed resulted in line breakage due to insufficient material flow and weak adhesion (Case A), while high speed caused slurry accumulation and larger diameter wavy lines (Case C). At an intermediate speed of 58 mm/sec (Case B), the printed line achieved optimal consistency, with a smooth and continuous filament flow, resulting in uniform dimensions and stable adhesion (Figure 3.5). This speed facilitated balanced extrusion, producing a high-quality line print without the issues observed at lower or higher speeds. These findings align with the report of Yang *et al.* (2018). Despite these observable trends, the effect of nozzle speed on overall printing error remained non-significant. This can be attributed to the complex interplay of other variables, such as the nozzle height-to-diameter (H/D) ratio and EGCG concentration, which overshadowed the influence of nozzle speed. The impact of these factors likely masked any potential effects of speed variations, leading to the observed lack of significance. Consequently, while nozzle speed affects specific aspects of print quality, its overall contribution to printing errors was not statistically substantial when considered alongside other parameters.

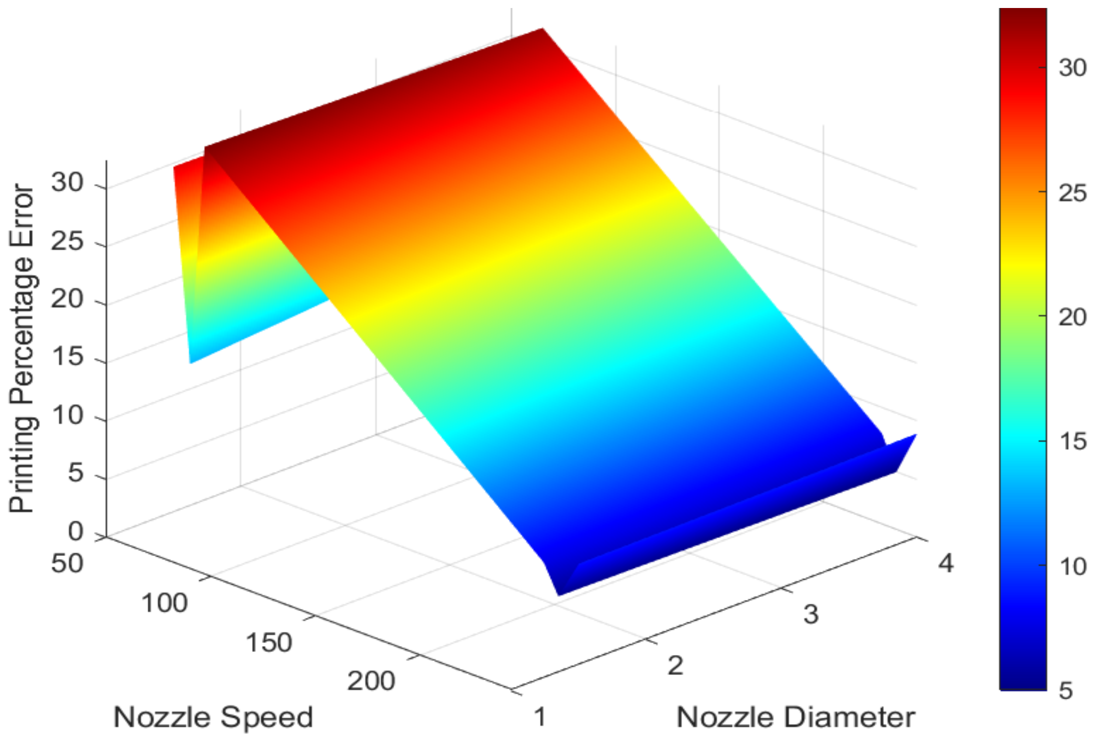

Figure 3.4 3D Surface plots showing the effect of Nozzle Diameter vs. Nozzle Speed on printing percentage error across different variables.

Figure 3.5 Scenarios obtained during 3D printing with different Nozzle speeds: Case A (nozzle speed = 50 mm/sec), Case B (nozzle speed = 58 mm/sec), Case C (nozzle speed = 65 mm/sec).

The effect of the nozzle H/D ratio is illustrated in Figure 3.6. The surface plot demonstrates a steep decline in printing percentage error from a maximum of 100 to 21.76% as the H/D ratio decreases from 1.25 to 0.85 across different nozzle diameters. The most notable reduction in error occurs when the H/D ratio is lowered to 0.85, where printing errors drop significantly, indicating that a smaller height-to-diameter ratio is crucial for ensuring better dimensional accuracy and print quality. A lower H/D ratio (e.g., 0.85) corresponds to a nozzle height smaller than the diameter, which is consistent with optimal layer deposition. As the plot suggests, maintaining a smaller nozzle height relative to its diameter ensures that newly deposited layers bond more effectively, enhancing adhesion between layers and reducing the likelihood of print defects, such as collapse or uneven structures. This phenomenon is evident from the steep slope of the surface plot as the H/D ratio decreases, reflecting a corresponding decrease in printing error.

For nozzle diameters of 1.5 mm and 4 mm, line prints revealed that a H/D ratio of 0.85 and 1 produced fine prints, whereas higher H/D ratios resulted in wavy lines (Figure 3.7). From the 3D printed structures, it was found that the best prints were achieved with an H/D ratio of 0.85, corresponding to nozzle heights of 1.3 mm for a 1.5 mm diameter nozzle and 3.4 mm for a 4 mm diameter nozzle. As mentioned by Yang *et al.* (2018), various theoretical studies suggest using equal nozzle height and diameter; however, in practice, the layer height should be smaller than the nozzle diameter for better adhesion, which aligns with our results showing that a smaller nozzle height provided the best outcomes.

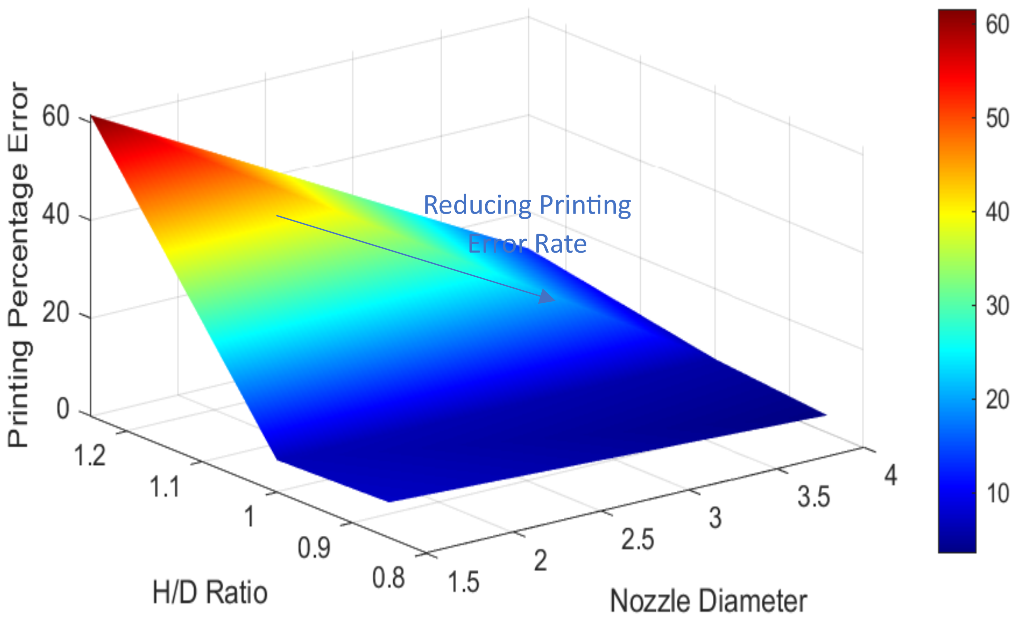

Figure 3.6 3D Surface plots showing the effect of Nozzle Diameter vs. Nozzle H/D ratio on printing percentage error across different variables.

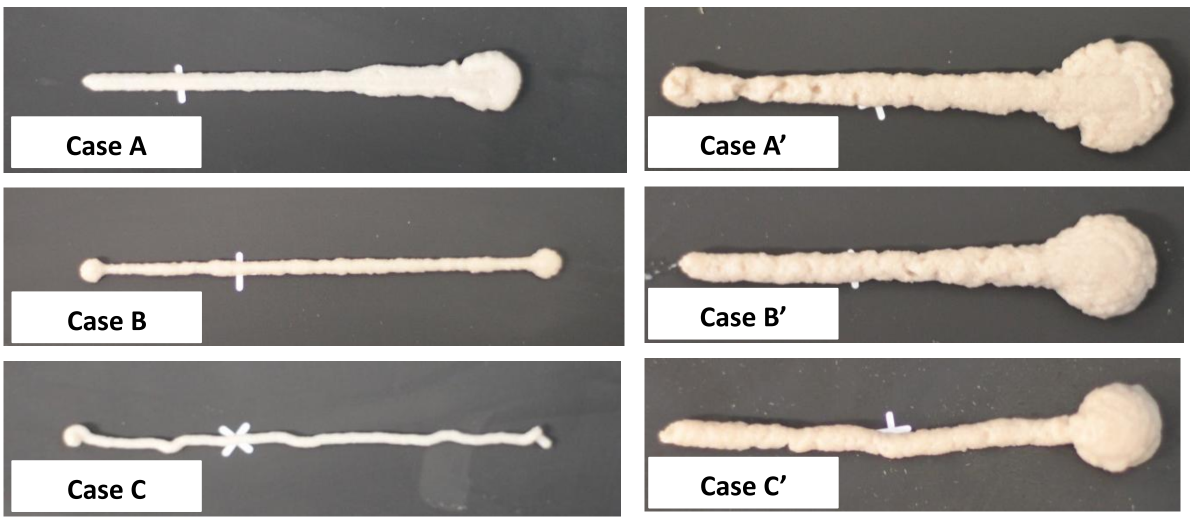

Figure 3.7 Scenarios obtained during 3D printing with different Nozzle H/D ratios for nozzle diameters 1.5 and 4 mm respectively: Case A and A' (nozzle H/D ratio = 0.85), Case B and B' (nozzle H/D ratio = 1), Case C and C' (nozzle H/D ratio = 1.25)

The influence of EGCG concentration on printing percentage error is illustrated through a surface plot shown in Figure 3.8. The result demonstrates a steady decrease in printing percentage error as the concentration of Epigallocatechin Gallate (EGCG) increased from 0 to 1%. This trend highlights EGCG's critical role in improving print performance through key biochemical interactions, particularly hydrophobic interactions and hydrogen bonding. EGCG, as a polyphenol, interacts with the hydrophobic regions of soy protein isolate (SPI) and wheat gluten (WG) during the mixing process at room temperature. These interactions occur as the proteins alter their surface exposure to water, reducing water interaction and leading to changes in surface hydrophobicity and protein conformation, ultimately enhancing the mixture's gelation properties. This strengthened protein network is crucial for maintaining structural integrity during 3D printing. Additionally, the hydroxyl groups of EGCG form hydrogen bonds with the polar amino and carboxyl groups of SPI and WG, further stabilizing the protein matrix and promoting a cohesive network structure. These bonds improve viscoelasticity, giving better control over material flow during extrusion. The formation of this stable and cross-linked network ensures consistency during extrusion and layer formation, resulting in precise print quality and improved shape retention of the printed structures.

The surface plot reveals a clear downward trend, indicating a significant reduction in printing percentage error as EGCG concentration increases across both nozzle diameters (1.5 mm and 4 mm). This effect is most noticeable at higher EGCG concentrations (0.5 and 1%), where the error decreases markedly, suggesting that the material's printability improves with EGCG addition. For the 1.5 mm nozzle, the error drops from 40.724 ± 44.049 at 0% EGCG to 5.218 ± 3.146 at 1% EGCG, while for the 4 mm nozzle, it decreases from 9.977 ± 7.758 to 7.563 ± 5.945. These results show that increasing EGCG concentration significantly enhances the stability and precision of printed structures, producing prints closer to the intended design specifications.

The surface plot also suggests that EGCG's effect on printing error is more pronounced for the 1.5 mm nozzle than for the 4 mm nozzle. While both nozzles benefit from increased EGCG concentrations, the greater reduction in printing errors for the smaller nozzle can be linked to improved material properties and bonding. Higher EGCG concentrations enhance the rheological properties of the printing material, resulting in more consistent extrusion and stronger interlayer adhesion. This leads to more structurally stable prints with fewer defects and better dimensional accuracy. Conversely, at lower EGCG concentrations, the material may exhibit poorer flow and bonding properties, causing more defects and reduced print precision.

These results align with previous studies, such as Yang *et al.* (2018), which highlighted the importance of optimizing material properties for achieving high-quality 3D prints. Additionally, the study by Xu *et al.* (2020) on the gel properties of transglutaminase-induced soy protein isolate–polyphenol complex demonstrated that the addition of EGCG significantly improved the stability of SPI, supporting our findings that higher EGCG concentrations enhance the structural stability and dimensional accuracy of 3D printed structures.

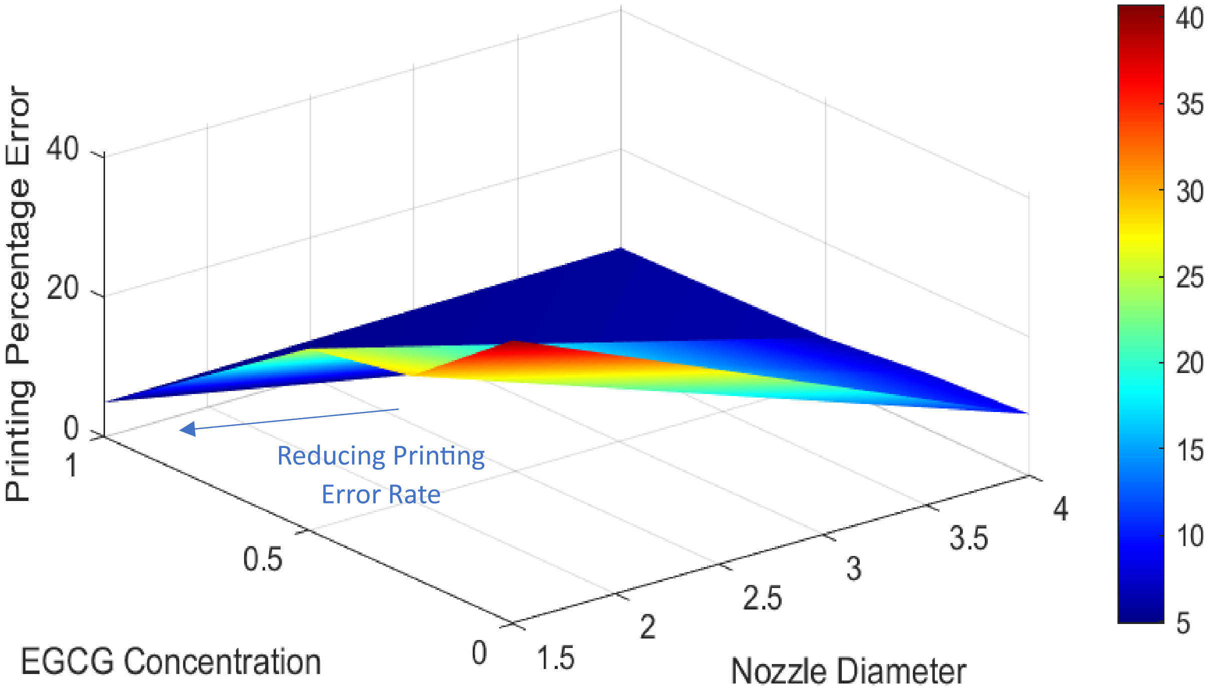

Figure 3.8 3D Surface plots showing the effect of nozzle diameter on printing percentage error across different variables. (a) Nozzle Diameter vs. Nozzle Speed, (b) Nozzle Diameter vs. H/D Ratio, (c) Nozzle Diameter vs. EGCG Concentration.

3.5 Conclusion

3D printing has successfully enabled the fabrication of 3D-designed SPI-WG-EGCG-based complexes, demonstrating the feasibility of utilizing polyphenol-based inks for intricate geometries and functional structures. The H/D ratio, EGCG concentration, and nozzle diameter significantly affected the accuracy and consistency of the printed components. Specifically, the H/D ratio emerged as a critical factor, influencing the dimensional stability of the prints, while EGCG concentration and nozzle diameter further fine-tuned the quality of the output. Surprisingly, nozzle speed did not exhibit a significant effect on printing errors, challenging the initial hypothesis that it would be a key determinant in printability. This finding highlights the complex interactions between printing parameters and material properties, suggesting that other factors may overshadow the influence of speed.

The optimized parameters derived from this study—58 mm/sec speed, 0.85 H/D ratio, and 1% EGCG concentration for the 1.5 mm nozzle diameter, and 235 mm/sec speed, 0.85 H/D ratio, and 1% EGCG concentration for the 4 mm nozzle diameter—demonstrate a practical approach for enhancing print quality. These settings not only improved the dimensional accuracy and stability of the prints but also contributed to a more efficient 3D printing process. The ability to identify and implement these optimal parameters underscores the importance of detailed parameter analysis in achieving high-quality results in polyphenol-based 3D printing. This optimization framework provides valuable insights for future applications, paving the way for advanced and precise manufacturing of polyphenol-based products.

References

1. Barrios-Rodríguez, Y. F., Igual, M., Martínez-Monzó, J., & García-Segovia, P. Multivariate evaluation of the printing process on 3D printing of rice protein. *Food Research International,* **2024**, 176, 113838, doi: https://doi.org/10.1016/j.foodres.2023.113838.
2. Derossi, A., Paolillo, M., Caporizzi, R., Severini, C. Extending the 3D food printing tests at high speed. Material deposition and effect of non-printing movements on the final quality of printed structures. Journal of Food Engineering, **2020**, vol. 275:109865, doi: https://doi.org/10.1016/j.jfoodeng.2019.109865.
3. Feng, C., Zhang, M., & Bhandari, B. Materials properties of printable edible inks and printing parameters optimization during 3D printing: a review. *Critical Reviews in Food Sci. & Nutr.,* **2019**, vol. 59(19), pg. 3074-3081, doi: https://doi.org/10.1080/10408398.2018.1481823.
4. Hao, L., Mellor, S., Seaman, O., Henderson, J., Sewell, N., & Sloan, M. Material characterization and process development for chocolate additive layer manufacturing. Virtual and Physical Prototyping, **2010**, vol. 5(2), pg. 57–64, doi: https://doi.org/ 10.1080/17452751003753212.
5. Kadival, A., Kour, M., Meena, S., Mitra, J. Extrusion-based 3d food printing: Printability assessment and improvement techniques. *Food and Bioprocess technology,* **2023,** 16:987-1008, doi: https://doi.org/10.1007/s11947-022-02931-z.
6. Khan, S.A., Ilcan, H., Imran, R., Aminipour, E., Sahin, O., Rashid, A.A., Sahmaran, M., & Koc, M. The impact of nozzle diameter and printing speed on geopolymer-based 3D-Printed concrete structures: Numerical modeling and experimental validation. *Results in Engineering,* **2024**, vol. 21, 101864, doi: https://doi.org/10.1016/j.rineng.2024.101864.
7. Lille, A., Nurmela, M., Nordlund, E., Kortelainen, S.M., Sozer, N. Applicability of protein and fiber-rich food materials in extrusion-based 3D printing. *Journal of Food Engineering,* **2018**, 220(20-27), doi: https://doi.org/10.1016/j.jfoodeng.2017.04.034.
8. Liu, L.; Ciftci, O.N. Effects of high oil compositions and printing parameters on food paste properties and printability in a 3D printing food processing model. *J. Food Eng.* **2020**, *288*, 110135, doi: https://doi.org/10.1016/j.jfoodeng.2020.110135
9. Liu, Z., Zhang, M., Bhandari, B., Wang, Y. 3D printing: Printing precision and application in food sector. *Trends in Food Sci. & Tech.,* **2017**, 69, pg. 83-94, doi: http://dx.doi.org/10.1016/j.tifs.2017.08.018.
10. Lorenzo, C.D., Agli, M.D., Sangiovanni, E., Santos, A.D., Uberti, F., Moro, E., Bosisio, E., & Restani, P. Correlation between catechin content and NF-Kb inhibition by infusions of green

and black tea. *Plant Foods Hum Nutr,* **2013**, vol 68, pg. 149-154, doi: 10.1007/s11130-013-0354-0.

11. Maldonado-Rosas, R., Tejada-Ortigoza, V., Cuan-Urquizo, E., Mendoza-Cachú, D., Morales-de la Peña, M., Alvarado-Orozco, J. M., & Campanella, O. H. Evaluation of rheology and printability of 3D printing nutritious food with complex formulations. *Additive Manufacturing,* **2022**, 58, 103030, doi: https://doi.org/10.1016/j.addma.2022.103030
12. Sun, X., Sarteshnizi, R.A., & Udenigwe, C.C. Recent advances in protein-polyphenol interactions focusing on structural properties related to antioxidant activities. *Functional Foods & Nutrition,* **2022**, 45:100840, doi: https://doi.org/10.1016/j.cofs.2022.100840.
13. Wang, L., Zhang, M., Bhandari, B., & Yang, C. Investigation on fish surimi gel as promising food material for 3D printing. *Journal of Food Engineering*, **2018**, 220 (101–108), doi: https://doi.org/10. 1016/j.jfoodeng.2017.02.029.
14. Xu, J., Guo, S., Li, X., Jiang, S., Zhong, X., & Zheng, Z. Gel properties of transglutaminase-induced soy protein isolate–polyphenol complex: influence of epigallocatechin-3-gallate. *Journal of the Sci. of Food and Agri.,* **2020**, vol. 101 (9), pg. 3870-79, doi: https://doi.org/10.1002/jsfa.11025.
15. Yang, F., Zhang, M., Bhandari, B., & Liu, Y. Investigation on lemon juice gel as food material for 3D printing and optimization of printing parameters. *Lwt*, **2018**, 87(67–76), doi: https://doi.org/10. 1016/j.lwt.2017.08.054.
16. Yu, X., Zhao, Z., Zhang, N., Yan, B., Gao, W., Huang, J., Zhao, J., Zhang, H., Chen, W., & Fan, D. Effects of pre-heating induced denaturation treatments on the printability and instant curing property of soy protein during microwave 3D printing. *Food Chem.,* **2022**, 397, 133682, doi: https://doi.org/10.1016/j.foodchem.2022.133682.

CONNECTING TEXT

Chapter III investigated the effect of printing parameters (nozzle diameter, nozzle height, and nozzle speed) and varying concentrations of epigallocatechin (EGCG) on the printability of 3D-printed SPI-WG-EGCG structures. In the following section, Chapter IV, we delve into the image analysis used to measure the line filament extrusion of SPI-WG-EGCG complexes. Subsequently, we developed predictive models to estimate material extrudability based on polyphenol concentration and printing parameters. This data-driven approach to predicting material extrudability aims to reduce the need for excessive trial-and-error experiments in future research.

IV. Predicting the Printability of SPI-WG-EGCG line filaments

4.1 Abstract

Predicting the printability of SPI-WG-EGCG complexes during 3D printing is crucial for enhancing precision and customization in the food industry, especially for achieving personalized nutrition. Material printability, which comprises the smooth and consistent flow of printing materials, directly impacts the quality, structural integrity, and accuracy of printed food products. Ensuring optimal extruding ability is essential for creating high-precision food items that meet specific dietary requirements and preferences.

This study investigates the printability of SPI-WG-EGCG line filaments by varying concentrations of epigallocatechin (EGCG) and key printing parameters, including nozzle diameter, nozzle H/D ratio, and nozzle speed. The research aims to optimize these factors to achieve superior print quality and material performance. A comprehensive dataset of 72 unique combinations of material concentrations and printing parameters was generated. To quantify extrudability, image analysis techniques were employed, focusing on the target digital design dimensions (line width, line thickness, and cross-sectional area) of the printed filaments. This approach allows for rapid and accurate assessment of printability, facilitating the development of predictive models.

The results highlight the importance of precise control over material properties and printing parameters to improve 3D-printed food performance. Adjusting EGCG concentration and fine-tuning printing settings can optimize printability, enhancing the quality and customization of printed food products. This data-driven approach reduces trial-and-error and enables efficient production of personalized nutrition solutions in the food industry.

4.2 Introduction

3D printing, also known as additive manufacturing, is a process of creating three-dimensional objects by layering materials based on digital models. This technology has revolutionized various industries, including aerospace, automotive, healthcare and more recently, the food industry (Sun *et al.* 2015). 3D food printing, a subset of this technology, involves the precise deposition of food-grade materials to create intricate and customized food products. This innovation is significant for the food industry as it opens new areas for personalized nutrition, culinary creativity, and sustainable food production (Lipton *et al*. 2015). Thus, the development of 3D food printing has allowed the opportunity to address the needs of diverse consumers including children, athletes, the elderly, and pregnant women who are increasingly interested in foods that are customized to their preferences or tailored to their nutritional needs (Derossi *et al.* 2018; Dick *et al.* 2019). A critical aspect of 3D food printing is the printability of a printing medium, which refers to the ability of the material to be successfully printed into a specific shape (Liu *et al.* 2017). Evaluating and ensuring good printability is essential because it affects the quality, accuracy and consistency of the final printed product (Godoi *et al.* 2016). A material is deemed suitable for printing when it meets several criteria: it must be capable of being extruded smoothly, maintain its intended shape post-extrusion, ensure continuous extrusion of filaments, and result in a stable final structure (Duty *et al.* 2018). In previous studies, "printability" has been described as the ratio between the actual height achieved by the printed object and its intended height (In *et al.* 2021). Other printability evaluation metrics includes the assessment of extrudability, dimensional accuracy and stability of the 3D printed structure (Kadival *et al.* 2023). Extrudability is the ease of extruding, a critical step toward achieving other aspects of 3D printability, such as shape fidelity and retention over time (Ma *et al.* 2021). The current definitions of printability typically focus on factors such as the material's ability to flow through the nozzle, its viscosity, and its final appearance, but they often overlook the ink's ability to be extruded and maintain its shape. Extrudability is a primary criterion of extrusion-based 3D printing and can be directly measured using line extrusion tests. An extruded line can be analysed either by manual inspection or image processing (Huang *et al.* 2020; Ma *et al.* 2021). Previous studies reported by Liu *et al.* (2019) investigated the extrudability of carrageenan-xanthan-starch gels across various temperatures, primarily through manual inspection of extruded lines. Building upon this research, Ma *et al.* (2021) advanced the methodology by employing image processing techniques. They used classification models to evaluate extrudability based on criteria such as line width, mode width, width consistency, and line height. This approach allowed for more precise quantification and assessment of the printing quality, distinguishing between acceptable and unacceptable extrusion limits. Also, previous studies have often indirectly measured extrudability by focusing on the rheological characterization of food ink (Liu *et al.* 2017; Godoi *et al.* 2016). The rheological characteristics of food materials used in 3D printing play a crucial role in achieving optimal extrudability, ensuring effective bonding between different printed layers, and maintaining structural integrity without deformation under compression (Liu *et al.* 2017). Numerous studies have explored the impact of variations in formulations and printing conditions on the extrusion behavior and stability of printed food structures. Besides rheological parameters, studies have identified that the key printing parameters including nozzle diameter, nozzle height, and nozzle speed are crucial in determining the extrudability and printability of alginate/gelatin hydrogels as they directly impact the extrusion process (He *et al.* 2016). Recent studies have investigated how parameters such as nozzle diameter, layer height, printing speed, extrusion rate, and extrusion temperature affect the quality and performance of printed structures. A smaller nozzle diameter produces printed objects with higher resolution, whereas a larger nozzle diameter results in lower resolution. However, using an excessively small nozzle can lead to inconsistencies in the printed lines (Wang *et al*. 2018). The extrusion rate denotes the volume of material extruded per unit of time, while print speed refers to the speed at which the nozzle moves. Extruded material may not have sufficient time to settle on the bed during high speed printing whereas there may be discontinuous filament deposition at low printing speeds (Feng *et al.* 2019).

Creating new ingredients for 3D food printing require automated, quick, and quantitative assessments of the new material extrudability. Several techniques have been developed to evaluate the extrudability of food printing materials. For instance, microscopic and optical pictures are widely used to measure the size of extruded lines. Image analysis programs like ImageJ were used to quantify line dimensions from optical pictures manually (Nijdam *et al.* 2021 and Lanaro *et al.* 2017). Fahmy *et al.* (2020) introduced a camera-based system that automates the assessment of cereal-based printing materials. Their advanced method employed algorithms to analyse parameters such as line width distribution, end-line extrusion, and consistency, offering a more sophisticated approach to extrudability evaluation. Paxton *et al.* (2017) presented a method involving visual inspection of continuous filament formation and structure using manual syringe pressure during dispensing. While effective as an initial qualitative screening tool, this approach does not account for other important printing characteristics.

In recent years, the integration of data-driven modeling approach has revolutionized predictive modeling in various fields, including 3D printing. Machine learning enables the extraction of complex patterns and relationships from large datasets, enhancing the accuracy and robustness of predictive models (Solle *et al.* 2017). For instance, in non-food 3D printing, researchers have successfully applied machine learning algorithms to predict material properties, printing parameters, and printing outcomes (Goh *et al.* 2021). Elbadawi *et al.* (2020) demonstrated the application of machine learning algorithms to predict the printability of pharmaceutical tablet materials. Their study integrated rheological properties with printing parameters to model the intricate relationships governing tablet production. By collecting variables that represent tablet rheology in pharmaceutical manufacturing, they employed a hybrid modeling approach known as "gray-box modeling." This method combines mechanistic insights from white box models with the data-driven capabilities of black box models, thereby enhancing predictability of complex relationships between printing parameters and material properties (Roupas, 2008 and Raja *et al.* 2023). These approaches not only improve prediction accuracy but also facilitate real-time optimization of printing processes based on continuous feedback from data analysis. In that context, machine learning will play a pivotal role in developing predictive models for SPI-WG-EGCG extrudability, allowing for valuable insights into how different compositional and operational factors influence printing performance.

This study aims to fill this gap by developing predictive models to estimate key extrudability parameters such as key line width, thickness and cross-sectional area of printed filaments of SPI-WG-EGCG complexes using advanced image analysis techniques.

4.3 Materials and Method

4.3.1 Materials

Epigallocatechin-3-gallate (purity ≥ 98.0% HPLC) was purchased from MilliporeSigma (Oakville, Ontario, Canada). The soy protein isolate (SPI) was procured from Fisher Scientific (Ottawa, Ontario, Canada). Wheat gluten was obtained from Sigma-Adrich (St. Louis, Missouri, USA). All other reagents are of analytical grade.

4.3.2 Preparation of SPI-polyphenol complexes

SPI (Soy Protein Isolate), wheat gluten, oil, and water were combined in a specific ratio of 5:3:2:33.3, respectively. Following this, varying concentrations of EGCG (Epigallocatechin Gallate) were incorporated into the mixture at the levels of 0, 0.25, 0.5, and 1%. The resulting solutions were labelled as SPI-E1, SPI-E2, SPI-E3, and SPI-E4, sequentially denoting the ascending order of catechin concentration.

4.3.3 Evaluating Printability of SPI-WPI-EGCG Line filaments

4.3.3.1 3D printing experiment

The 3D printability of SPI-WPI-EGCG line prints was evaluated through a structured experimental workflow as shown in Figure 4.1. Extrusion-based 3D printing was carried out using a commercial 3D printer Foodini (Natural Machines, Barcelona, Spain) which features two primary components: creations and fillings. The samples were carefully loaded into a printing syringe, and the syringe was closed off with a pressure cap. Printing took place at room temperature, maintained at 23 ± 0.3°C throughout the process. To facilitate printing, line filaments were designed using FreeCAD software with line length (L) of 80 mm. Other design parameters, including line width (XX) and thickness (YY), were determined, and the cross-sectional area (ZZ) was calculated accordingly.

These models were then exported as .stl files and imported into the Foodini software. The printing system performed a point extrusion at different printer parameters, including nozzle diameter, nozzle height, and nozzle speed. It was ensured that the location of the extrusion nozzle was fixed such that each printed line initiated at the same location on the printing platform. The nozzle diameters used in the study were 1.5 and 4 mm. Nozzle heights were adjusted at achieve nozzle height-to-diameter (H/D) ratios of 0.85, 1, and 1.25. Six nozzle speeds namely 50, 58, 65, 228, 235 and 245 mm/s were studied. A full factorial design was applied in the study resulting in a total of 144 experimental units. The experiments were conducted in duplicate.

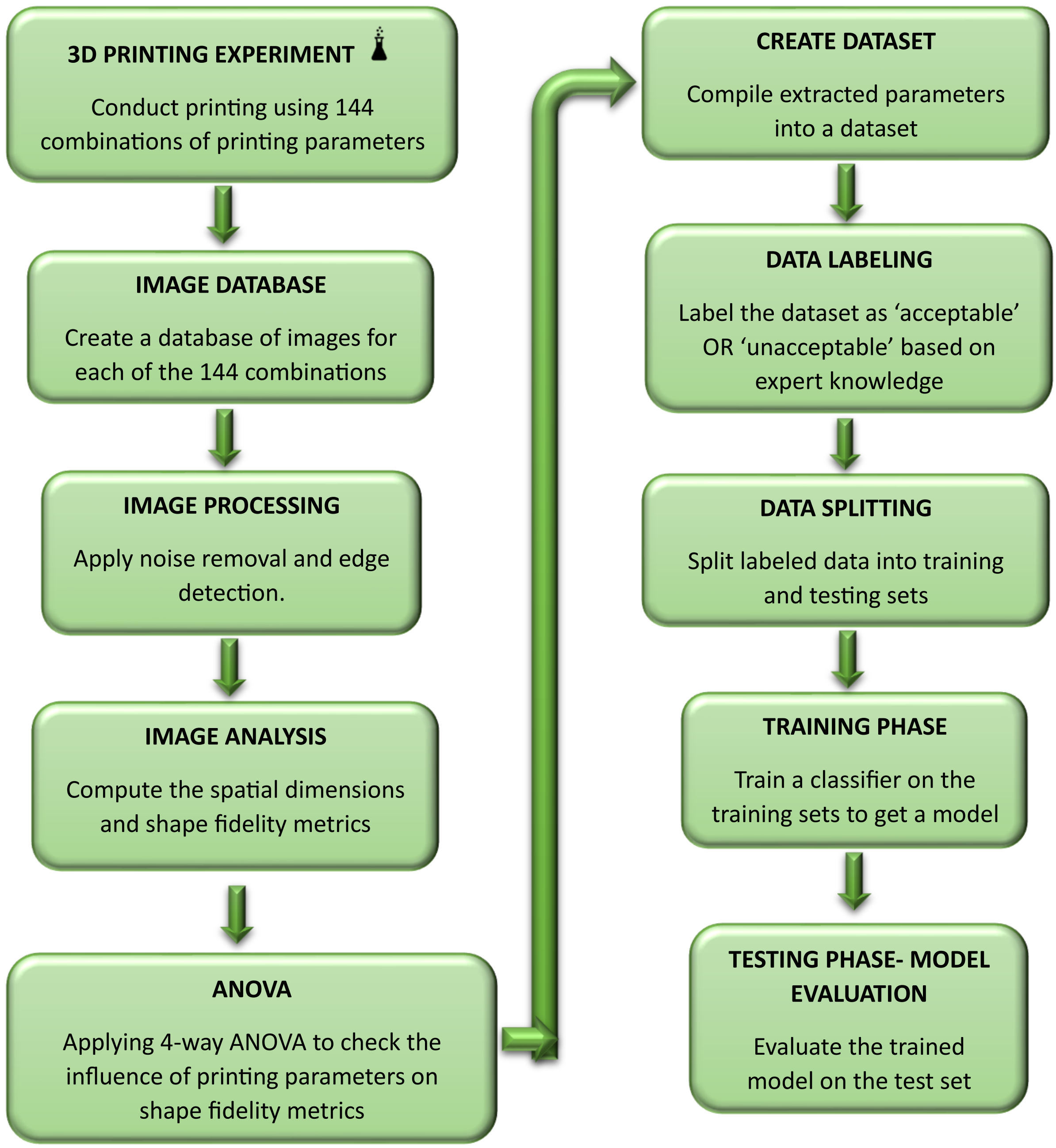

Fig 4.1. Implementation Steps for predicting extrusion-based printability of SPI-WG-EGCG line filaments.

4.3.3.2 Image Database

A Canon EOS Rebel T3i Digital SLR camera (Canon Inc., Japan) was positioned at a fixed distance with a tripod for top-view and front-view shots of printed samples. A black silicon sheet was placed as the background for maximum contrast to the image and the pictures were taken within 15 s after extrusion (Figure 4.2). This setup ensured consistent image capture conditions, critical for subsequent image processing and analysis. Each image corresponded to one of the 144 unique combinations of printing parameters, creating a comprehensive database of extruded sample images.

4.3.3.3 Image Processing

Image preprocessing steps were taken to remove noise and detect edges to make the images ready for further image analysis.

The raw images of line extrusion were denoised using a median filter, which effectively preserves edges while filtering out noise. These smoothed RGB images were then converted to grayscale using MATLAB (Version R2024a Update 6 (24.1.0.2689473), The Mathworks, Inc., Natik, Massachusetts, United States). Building upon the methodology of Fahmy *et al.* (2020), the RGB format was further transformed to HSV to leverage the saturation channel for suppressing extraneous images (such as the cross on the silicon mat of the printer platform). MATLAB was subsequently utilized to identify connected components in a binary image, enabling the analysis of target design dimensions such as line width, line thickness, and cross-sectional area across the length of the line prints. The shape fidelity parameters—line width, line thickness, and cross-sectional area depend on four evaluation metrics encompassing mode, consistency, arithmetic mean deviation and root mean square deviation. This comprehensive approach ensures a detailed assessment of print quality.

4.3.3.4 Image analysis

Image analysis involved extraction of meaningful information, such as identifying printing patterns, measuring dimensions, and detecting objects. For each unique combination of printing parameters, metrics related to shape fidelity parameters such as mode, consistency, arithmetic mean deviation, and root mean square deviation were extracted from the images of the extruded samples. These metrics were then used to assess how closely the extruded samples matched the target design dimensions (namely length, width, thickness, and cross-sectional area). The line length was fixed at 80 mm, representing its maximum extent along the longitudinal axis. Line thickness denotes the vertical dimension of the line when viewed frontally, measured as the perpendicular distance between its highest and lowest points in the front view image. This measurement offers critical insights into the thickness (height) of the printed line, essential for evaluating its dimensional accuracy and uniformity. Line width refers to the line's horizontal dimension when viewed from above, determined as the distance between its widest points along the horizontal axis. This parameter provides valuable information about the line's lateral spread across its longitudinal axis. The cross-sectional area of the extruded lines was determined by conceptualizing it as a flattened tube, resembling a rectangle with two semicircular edges (Equation 1) (Ma *et al.* 2021).

$$A = (w-t) \times t + \pi (t/2)^2 \quad (1)$$

Where A is the cross-sectional area (mm^2), W is the width-consistency (mm), t is the line thickness (mm), Figure 4.2 illustrates the parameters of printed line.

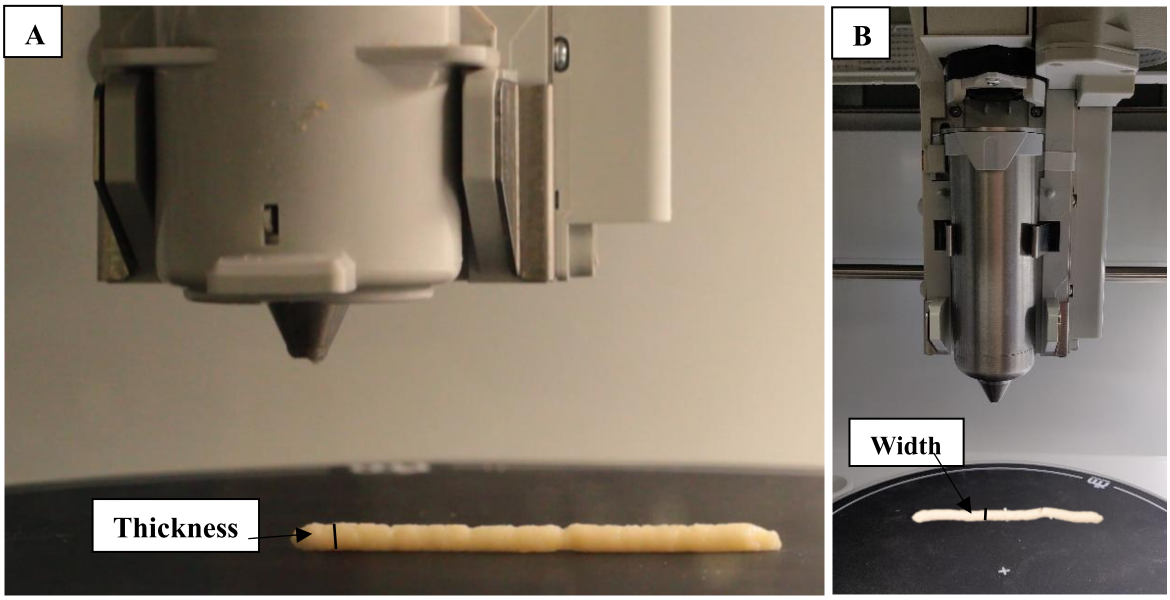

Fig 4.2 Representation of thickness and width of printed line. A. Schematic representation of thickness (t) of line filament from front-view B. Schematic representation of width consistency (w) of line filament from top-view.

4.3.3.5 Shape fidelity dataset

The printed sample shape fidelity metrics included dimension mode, consistency, arithmetic mean deviation, and root mean square deviation. These were compiled into a structured dataset. Each parameter was meticulously recorded to reflect the characteristics of the extruded samples across the various printing conditions.

Mode captures the most frequent occurrence in the distribution of the dimensions (width, cross-sectional area, and height) of the extruded sample (Ma *et al.* 2021). Consistency measures how uniformly the extruded sample dimensions adhere to the mode. It is calculated as the ratio of the number of samples $n\ddot{S}$ within 10% of the mode $-0.1M < \ddot{S} < 1.1M$ to the total number of sample points nS (Ma *et al.* 2021) (Equation 2). This parameter assesses the distribution's uniformity in terms of width, height, or cross-sectional area.

$$C = \frac{n\ddot{S}}{nS} \tag{2}$$

Where M is the mode value for the given dimension (such as width, height, or cross-sectional area), $\ddot{S}$ is the number of sample points (in mm) that fall within 10% of the mode, S is the measurement of the sample dimension (in mm), such as width, cross-sectional area, or height, used for comparison against the mode and n is the total number of sample points.

Arithmetic mean (Ra) deviation measures the roughness of the surface of the extruded sample. It calculates the average deviation of each dimension profile point $|Z(x)|$ from the target dimension profile (H) along the longitudinal axis (L) (Equation 3). This measure provides insight into how consistently the extruded dimensions align with the intended profile.

$$R_a = \frac{1}{L}\int_0^L |Z(x)|\,dx \tag{3}$$

Where L is 80 mm, $|Z(x)| = Z(x) - H$ represents the absolute deviation of each point from the target dimension profile H.

Root mean square (RMS) deviation quantifies the roughness of the surface but does so by computing the root mean square average deviation (R_q) (James *et al.* 2013) (Equation 4). It provides a measure of the surface roughness by evaluating the deviation of the dimension profile Z(x) from the target profile H along the longitudinal axis L.

$$R_q = \left[\frac{1}{L}\int_0^L Z(x)^2\,dx\right]^{1/2} \tag{4}$$

These parameters were aggregated into a comprehensive dataset that encompasses all unique combinations of printing parameters used in the experiments. This dataset was essential for the next stages of the analysis, including data labeling, model training, and performance evaluation.

4.3.3.6 Extrusion Modeling for line-filaments

Predictive extrusion modeling involves the application of mathematical and computational techniques to simulate and predict the extrusion process of materials (Elbadawi *et al.* 2020). This approach aims to understand and predict how different factors such as material properties, processing conditions, and equipment parameters influence the extrudability of substances. The printability of line filaments was investigated by systematically varying polyphenol concentration and printer parameters for 72 unique combinations. The approach involved generating graphical representations illustrating the variability of line thickness, width, and cross-sectional area along the filament length, providing essential visual insights into material behaviour under varying conditions.

Statistical analyses were conducted on the dataset to assess the consistency and variability of extrusion outcomes. Specifically, the mode, consistency, arithmetic mean deviation, and root mean square deviation for thickness, width, and cross-sectional area were calculated across all 144 possible combinations (including duplicates). These statistical measures served as indicators of filament dimensional uniformity and predictability, crucial for maintaining high-quality standards in extruded products. The statistical analysis (4-way) revealed the significant values affecting mode, consistency, arithmetic mean, and root mean square.

4.3.3.6.1 Data Labeling

The dataset was categorized into two distinct classes: "Acceptable" and "Unacceptable." This classification was based on expert judgment and predefined criteria, which considered specific ranges of the measured parameters (Table 4.1). For each data entry, the label was determined by comparing the extracted dimensions of the extruded samples against the acceptable limits established for each parameter. Notably, the criteria for width mode and thickness mode were based on the Slic3r software manual (Hodgson *et al.* 2021*)*, while most of the other parameters were defined arbitrarily. If the measurements fell within these predefined acceptable ranges, the sample was labeled as "Acceptable." Conversely, if the measurements deviated from these limits, the sample was labeled as "Not Acceptable." This systematic approach ensured that each sample was categorized based on its compliance with quality standards, facilitating effective analysis and modeling in subsequent phases of the study.

Table 4.1 Sample Line shape fidelity parameter classification, evaluation metrics, acceptable, unacceptable error thresholds, number of positive (acceptable) and negative (unacceptable) samples

Shape Fidelity Parameters	Acceptable Error Threshold	Unacceptable Error Threshold	Number of Positive Samples	Number of Negative Samples	Test sample size
Area					
Consistency	< 50%	≥ 50%	16	56	72
Mode	< 25%	≥ 25%	55	17	72
Arithmetic Deviation	< 0.25 * Nozzle Diameter	≥ 0.25 * Nozzle Diameter	28	44	72
RMS	< 0.25 * Nozzle Diameter	≥ 0.25 * Nozzle Diameter	18	54	72
Thickness					
Consistency	< 25%	≥ 25%	16	56	72
Mode	< 15%	≥ 15%	37	35	72
Arithmetic Deviation	< 0.15 * Nozzle Diameter	≥ 0.15 * Nozzle Diameter	25	47	72
RMS	< 0.20 * Nozzle Diameter	≥ 0.15 * Nozzle Diameter	28	44	72
Width					
Consistency	< 40%	≥ 40%	24	48	72
Mode	< 10%	≥ 10%	32	40	72
Arithmetic Deviation	< 0.20 * Nozzle Diameter	≥ 0.20 * Nozzle Diameter	16	56	72
RMS	< 0.25 * Nozzle Diameter	≥ 0.25 * Nozzle Diameter	18	54	72

4.3.3.6.2 Training and Testing

The dataset was divided into two parts namely 90% for training and 10% for testing to facilitate the development and evaluation of predictive models. K-fold cross-validation was employed by dividing the data set into ten equal parts or folds as outlined by Ma *et al.* (2021). In each iteration, one fold was reserved as the test set while the remaining nine folds were used as the training set. This rotation ensured that each data point was included in both the training and testing phases at different times, providing a comprehensive assessment of the model's performance. Linear Discriminant Analysis (LDA) was used to develop predictive models for the various printing parameters.

The performance of the model was assessed through the calculation of total accuracy, True positive rate (TPR), true negative rate (TNR), precision accept rate (PAR), and precision reject rate (PRR) which indicated the model's effectiveness in correctly identifying labels for the test samples. By determining the average accuracy, insights into the model's generalizability and effectiveness were gained. This assessment is crucial for understanding the model's reliability and its potential applicability to real-world scenarios.

4.3.4 Software packages

Image analysis was achieved using MATLAB and ANOVA and predictive modelling was done using MATLAB and SAS programming packages.

4.4 Results and Discussion

4.4.1 Shape Fidelity of Printed Samples

ANOVA results indicate that nozzle speed significantly ($p < 0.05$) influenced the mode, consistency, arithmetic mean, and root mean square deviation of width, thickness, and area of printed samples. EGCG concentration also had significant impact, particularly on thickness metrics. Nozzle diameter and H/D ratio affected thickness and area, with notable interactions between factors, especially between nozzle speed and other parameters. The highest R-square values were observed for models involving width and thickness metrics, indicating strong explanatory power of the factors studied.

Fig. 4.3 illustrates the impact of EGCG and nozzle speed on the thickness and width modes for the acceptable and unacceptable ranges. As EGCG concentration increases, the thickness mode values converge towards the target dimensions. This improvement is indicative of better material flow and adherence to design specifications, which enhances the overall quality and precision of the printed samples. Regarding nozzle speed, speeds of 58 mm/s and 235 mm/s resulted in more samples with width modes near the target dimensions, indicating better precision and dimensional accuracy. In contrast, lower speeds of 50 mm/s and 228 mm/s and higher speeds of 65 mm/sec and 245 mm/sec produced fewer acceptable samples, suggesting that moderate nozzle speeds are more favorable for achieving consistent extrusion and higher-quality prints.

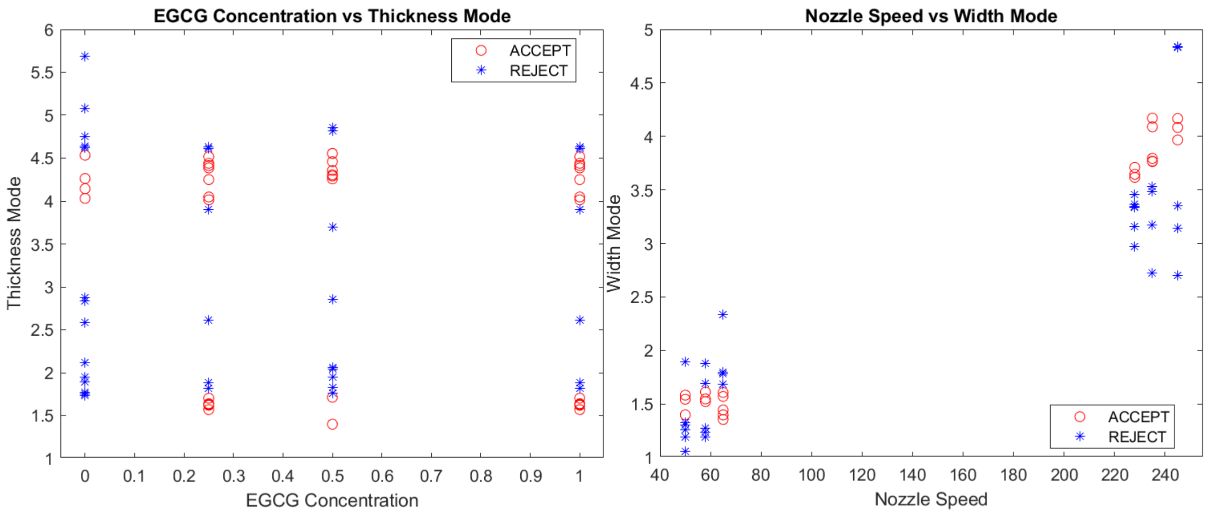

Figure 4.3 Scatter plot for (A) ECCG Concentration vs Thickness Mode and (B) Nozzle vs Width Mode

4.4.2 Model Performance

Given the printing parameters, the average performance over 10-fold cross-validation of the linear discriminant analysis (LDA), in predicting the shape fidelity of extruded line filaments are displayed in Tables 4.2. Analysis of the results showed that the LDA successfully predicted the shape fidelity parameters with overall accuracy ranging from 67 to 100%.

4.4.2.1 Area

The model's total accuracy for area consistency was close to 95% with TPR and TNR of 94 and 93%, respectively. Both PAR and the PRR were 93%.

For area mode, the total accuracy was close to 85% with TPR, TNR, PAR and PRR of 92, 89, 45 and 90%, respectively.

The model performance for area arithmetic deviation was 89% with the related prediction metrics of 83, 98, 97 and 85% for TPR, TNR, PAR and PRR, respectively.

4.4.2.2 Thickness

The model achieved a high total accuracy of 94.6% in predicting the consistency of thickness for extruded line filaments. The model performed strongly with a TPR of 95% and a TNR of 93.6%. Both PAR and PRR were similarly high at 93 and 96.7%, respectively.

In predicting the mode of thickness, the model showed a moderate total accuracy of 80.7%, with a TPR of 80.3% and a TNR of 88.8%. The precision values for PAR and PRR were 87.5 and 73.3%, respectively.

For the arithmetic mean deviation of thickness, the model recorded a total accuracy of 85.4%. It achieved a TPR of 100%, though the TNR was slightly lower at 75.9%. Both precision metrics were strong, with PAR at 78% and PRR at 100%.

For the root mean square deviation of thickness, the model demonstrated a robust total accuracy of 88.8%, with a TPR of 94.2% and a TNR of 85.2%. The precision values were similarly strong, with PAR at 86% and PRR at 95.5%.

4.4.2.3 Width

The model showed the lowest total accuracy in predicting the mode width and consistency of the extruded line compared to their performance in predicting area and thickness. Specifically, the model demonstrated moderate performance with a total accuracy of 90.1%, achieving a TPR of 67.2% and a TNR of 77.7%. PAR and PRR were 72.5 and 64.2%, respectively.

For the prediction of mode width, the model recorded a lower total accuracy of 69.2%, though it maintained balanced TPR and TNR values of 89.2% and 88.8%, respectively. Precision for PAR and PRR were 89% and 93.5%.

For the arithmetic mean deviation of width, the model achieved an impressive total accuracy of 97.1%, with a remarkable TPR of 96.7% and a TNR of 100%. Precision values for PAR and PRR were also at 100% and 90%, respectively. The LDA model's performance for the arithmetic mean deviation was the highest among all fidelity parameters, including area and thickness.

A total accuracy of 100% was achieved for predicting the root mean square deviation of width. It exhibited a TPR of 96.1% and a TNR of 100%, with precision values for PAR at 93.6% and a PRR of 100%. These metrics suggest that the model effectively identified variations in the root mean square deviation.

Table 4.2 Average 10-fold cross-validation results for linear discriminant analysis technique (LDA) in predicting filament printability.

Shape Fidelity Parameters	**True Positive Rate (TPR)**	**True Negative Rate (TNR)**	**Precision Accept Rate (PAR)**	**Precision Reject Rate (PRA)**	**Total Accuracy**
Area					
Consistency	0.936	0.933	0.933	0.933	0.945
Mode	0.921	0.889	0.45	0.900	0.846
Arithmetic Deviation	0.975	0.843	0.830	0.975	0.883
RMD	0.690	0.660	0.640	0.790	0.7702
Thickness					
Consistency	0.950	0.936	0.930	0.967	0.946
Mode	0.803	0.888	0.875	0.733	0.807
Arithmetic Deviation	1	0.759	0.7800	1	0.854
RMD	0.942	0.852	0.8600	0.9550	0.888
Width					
Consistency	0.672	0.777	0.725	0.6417	0.901
Mode	0.892	0.888	0.89	0.9350	0.692
Arithmetic Deviation	0.967	1	1	0.9000	0.971
RMD	0.961	1	0.936	0.8833	1

In this study, the effectiveness of predicting the consistency of extruded filaments in 3D food printing by using the LDA classifier was assessed. The findings revealed that the LDA model consistently performed well. The success of the model is particularly significant given the nature of 3D food printing, where the shape fidelity of the final product is crucial. The consistency in the spatial dimensions of the extruded filament directly impacts the final product's appearance and texture. The model's high accuracy in predicting this consistency indicates its potential to better ensure that the printed food matches the target digital design, which is a critical factor for consumer satisfaction. Additionally, the findings highlight the practical implications of using LDA in 3D food printing. For instance, the model's predictive capabilities can be leveraged to automate the adjustment of printing parameters, ensuring consistent quality across different production batches. This automation is particularly important as 3D food printing scales up to meet growing global demands for customized, nutrient-rich food. Also, the model's ability to handle different concentrations of food materials with high accuracy supports the integration of various ingredients into the printing process. This is crucial for producing complex meals that replicate traditional recipes while offering the customization needed for specific dietary requirements, such as those for patients with special nutritional needs.

4.5 Conclusion

This chapter proposes the application of machine learning to predict the shape fidelity of extruded filaments before 3D printing food materials. The predictive model, leveraging Linear Discriminant Analysis (LDA), demonstrates that artificial intelligence (AI) can enhance cost-effectiveness in 3D printing by ensuring consistent quality and reducing trial-and-error processes. By focusing on four key parameters—EGCG concentration, nozzle speed, nozzle diameter, and H/D ratio—the LDA model can identify optimal settings by predicting whether a particular combination is acceptable for producing high-quality filaments, the fundamental building blocks of 3D structures. Although the study was limited by a small sample size and a constrained dataset, these challenges were mitigated by utilizing robust image analysis and machine learning techniques. The LDA model, with its superior accuracy, offers a valuable tool for predicting the acceptability of future parameter combinations, laying the groundwork for more precise and efficient 3D food printing.

4.6 Data Availability

The data supporting the findings of this study can be found in the appendices of the manuscript. This includes:

- MATLAB code for Linear Discriminant Analysis (LDA) used to predict printability.
- Data labeling tables detailing the categorization and parameters used in the analysis.

References

1. Derossi, A., Caporizzi, R., Azzollini, D., & Severini, C. Application of 3D printing for customized food. A case on the development of a fruit-based snack for children. *Journal of Food Engineering*, **2018**, 220, 65–75, doi: https://doi.org/10.1016/j.jfoodeng.2017.05.015.
2. Dick, A., Bhandari, B., & Prakash, S. Post-processing feasibility of composite-layer 3D printed beef. *Meat Science*, **2019**, 153, 9–18, doi: https://doi.org/10.1016/j.meatsci.2019.02.024.
3. Duty, C., Ajinjeru, C., Kishore, V., Compton, B., Hmeidat, N., Chen, X., Liu, P., Hassen, A.A., Lindahl, J., & Kunc, V. What makes a material printable? A viscoelastic model for extrusion-based 3D printing of polymers. *Journal of Manufacturing Processes,* **2018**, 35(526-537), doi: https://doi.org/10.1016/j.jmapro.2018.08.008.
4. Elbadawi, M., Castro, B. M., Gavins, F. K., Ong, J. J., Gaisford, S., P´erez, G., Basit, A.W., Cabalar, P., & Goyanes, A. M3DISEEN: A novel machine learning approach for predicting the 3D printability of medicines. *International Journal of Pharmaceutics,* **2020**, 590, 119837, doi: https://doi.org/10.1016/j.ijpharm.2020.119837.
5. Fahmy, A. R., Becker, T., & Jekle, M. 3D printing and additive manufacturing of cereal-based materials: Quality analysis of starch-based systems using a camera-based morphological approach. *Innovative Food Science & Emerging Technologies,* **2020**, 63, 102384, doi: https://doi.org/10.1016/j.ifset.2020.102384.
6. Feng, C., Zhang, M., & Bhandari, B. Material properties of printable edible inks and printing parameters optimization during 3D printing: a review. *Critical Reviews in Food Science and Nutrition*, **2019**, vol. 59, 19(3074-3081), doi: https://doi.org/10.1080/10408398.2018.1481823.
7. Godoi, F.C., Prakash, S., Bhandari, B.R., & de Melo, A.C. 3D printing technologies applied for food design: Status and prospects. *Journal of Food Engineering*, **2016**, 179, 44-54, doi: https://doi.org/10.1016/j.jfoodeng.2016.01.026.
8. Goh, G.D., Sing, S.K., Yeong, W.Y. A review on machine learning in 3D printing: applications, potential, and challenges. *Artificial Intelligence Review,* **2021,** 54(1), 63-94, doi: https://doi.org/10.1007/s10462-020-09876-9.
9. He, Y., Yang, F., Zhao, H., Gao, Q., Xia, B., & Fu, J. Research on the printability of hydrogels in 3D bioprinting. *Scientific Reports,* **2016**, *6*(1), 1–13, doi: https://doi.org/10.1038/ srep29977.
10. Hodgson, G., Ranellucci, A., & Moe, J. (2021). Slic3r Manual – Flow Math (Accessed 5 Jan 2021) http://manual.slic3r.org/advanced/flow-math.

11. Huang, M., Zhang, M., & Guo, C. F. 3D printability of brown rice gel modified by some food hydrocolloids. *Journal of Food Processing and Preservation*, **2020**, 44(7), 1–9, doi: https://doi.org/10.1111/ jfpp.14502.
12. In, J., Jeong, H., Song, S., & Min, S.C. Determination of material requirements for 3D gel food printing using a fused deposition modeling 3D printer. *Foods*, **2021**, 10(10), 2272, doi: https://doi.org/10.3390/foods10102272.
13. James, G., Witten, D., Hastie, T., Tibshirani, R., Taylor, J. *An Introduction to Statistical Learning: with Applications in Python*. *Springer Texts in Statistics*, **2013**, doi: https://doi.org/10.1007/978-3-031-38747-0.
14. Kadival, A., Kour, M., Meena, D., & Mitra, J. Extrusion-Based 3D Food Printing: Printability Assessment and Improvement Techniques. *Food and Bioprocess Technology*, **2023**, 16, 987-1008, doi: https://doi.org/10.1007/s11947-022-02931-z.
15. Lanaro, M., Forrestal, D. P., Scheurer, S., Slinger, D. J., Liao, S., Powell, S. K., & Woodruff, M. A. 3D printing complex chocolate objects: Platform design, optimization and evaluation. *Journal of Food Engineering,* **2017,** 215, 13–22, doi: https://doi. org/10.1016/j.jfoodeng.2017.06.029.
16. Lipton, J. I., Cutler, M., Nigl, F., Cohen, D., & Lipson, H. Additive manufacturing for the food industry. *Trends in Food Science & Technology*, **2015**, 43(1), 114-123, doi: https://doi.org/10.1016/j.tifs.2015.02.004.
17. Liu, Z., Zhang, M., Bhandari, B., & Wang, Y. 3D printing: Printing precision and application in food sector. *Trends in Food Science and Technology*, **2017**, 69, 83-94, doi: https://doi.org/10.1016/j.tifs.2017.08.018.
18. Ma, Y., Schutyser, M.A.I., Boom, R.M., & Zhang, L. Predicting the extrudability of complex food materials during 3D printing based on image analysis and gray-box data-driven modeling. *Innovative Food Science and Emerging Technologies*, **2021**, 73, 102764, doi: https://doi.org/10.1016/j.ifset.2021.102764.
19. Nijdam, J. J., Agarwal, D., & Schon, B. S. Assessment of a novel window of dimensional stability for screening food inks for 3D printing. *Journal of Food Engineering,* **2021**, 292, 110349, doi: https://doi.org/10.1016/j.jfoodeng.2020.110349.
20. Paxton, N., Smolan, W., B¨ock, T., Melchels, F., Groll, J., & Jungst, T. Proposal to assess printability of bioinks for extrusion-based bioprinting and evaluation of rheological properties governing bioprintability. *Biofabrication,* **2017,** 9(4), 044107, doi: https://doi.org/10.1088/1758-5090/aa8dd8.

21. Putri, L.A., Rahman, I., Puspita, M., Hidayat, S.N., Dharmawan, A.B., Rianjanu, A., Wibirama, S., Roto, R., Triyana, K., & Wasisto, H.S. Rapid analysis of meat floss origin using a supervised machine learning-based electronic nose towards food authentication. *Science of Food,* **2023**, 7, 31, doi: https://doi.org/10.1038/s41538-023-00205-2.
22. Raja, V., Nimbkar, S., Moses, J.A., Nair, S.V.R., & Anandharamakrishnan, C. Modeling and Simulation of 3D Printing Systems- Scope, Advances, and Challenges. *Foods*, **2023**, 12(18), 3412, doi: https://doi.org/10.3390/foods12183412.
23. Roupas, P. Predictive modelling of dairy manufacturing processes. *International Dairy Journal,* **2018***,* 18(7*),* 741–753, doi: https://doi.org/10.1016/j.idairyj.2008.03.009.
24. Solle, D.; Hitzmann, B.; Herwig, C.; Pereira Remelhe, M.; Ulonska, S.; Wuerth, L.; Prata, A.; Steckenreiter, T. Between the Poles of Data-Driven and Mechanistic Modeling for Process Operation. *Chemie Ing. Tech.* **2017**, *89*, 542–561, doi: https://doi.org/10.1002/cite.201600175.
25. Sun, J., Zhou, W., Huang, D., Fuh, J. Y. H., & Hong, G. S. An overview of 3D printing technologies for food fabrication. *Food and Bioprocess Technology*, **2015**, 8(8), 1605-1615, doi: https://doi.org/10.1007/s11947-015-1528-6.
26. Wang, L., Zhang, M., Bhandari, B., & Yang, C. Investigation on fish surimi gel as promising food material for 3D printing. *Journal of Food Engineering*, **2018**, 220 (101–108), doi: https://doi.org/10. 1016/j.jfoodeng.2017.02.029.
27. Xue J.H., and Titterington, D.M. Do unbalanced data have a negative effect on LDA? *Pattern Recognition,* **2008**, 41, (5): 1558-1571, doi: https://doi.org/10.1016/j.patcog.2007.11.008.
28. Zhao, Y. R and data mining: Examples and case studies. *Academic Press,* **2012**.

V. General summary, Conclusion, Limitations, Challenges and Future Research

5.1 Summary and Conclusions

This study comprehensively assessed the impact of various 3D printing parameters on the printability of SPI-WG-EGCG complexes and developed predictive models to enhance the precision and customization of 3D-printed food products. The research focused on addressing the challenges inherent in using plant-based protein gels, particularly soy protein isolate (SPI), for 3D printing, where printability and dimensional accuracy are often compromised. Through systematic experimentation and the application of machine learning models, this study has advanced the understanding of how specific printing parameters influence the quality of 3D-printed food products and provided a framework for optimizing these parameters to achieve high-quality results.

Key findings of this research demonstrated that the height-to-diameter (H/D) ratio, EGCG concentration, and nozzle diameter significantly impact the accuracy and consistency of printed structures. Notably, the H/D ratio emerged as a critical factor influencing dimensional stability, with higher concentrations of EGCG further enhancing the quality of the printed products. The study also revealed that nozzle speed, contrary to initial expectations, did not significantly affect printing errors, suggesting that other factors, such as material composition and nozzle dimensions, play a more crucial role in determining print quality.

Machine learning played a pivotal role in this study, particularly through the application of the Linear Discriminant Analysis (LDA) classifier model in predicting the consistency of the extruded filaments. The LDA model's success highlights its potential for ensuring that printed food products closely match the target digital designs, a critical factor for consumer satisfaction. The model's predictive capabilities can be leveraged to automate the adjustment of printing parameters, ensuring consistent quality across different production batches, which is essential as 3D food printing scales up to meet global demands.

The practical implications of this study are significant, especially in the context of producing personalized nutrition solutions in the food industry. The optimized printing parameters identified in this research—such as specific combinations of nozzle speed, H/D ratio, and EGCG concentration—provide a valuable reference for improving the dimensional accuracy and stability of 3D-printed food products. Moreover, the integration of machine learning into the optimization process reduces trial and error, making the production process more efficient and scalable.

The following key conclusions were drawn from this research:

- The H/D ratio, EGCG concentration, and nozzle diameter are critical factors significantly influencing the dimensional accuracy and stability of 3D-printed SPI-WG-EGCG-based products.
- The optimal printing parameters derived from this study—58 mm/sec speed, 0.85 H/D ratio, and 1% EGCG concentration for the 1.5 mm nozzle diameter, and 235 mm/sec speed, 0.85 H/D ratio, and 1% EGCG concentration for the 4 mm nozzle diameter—enhanced print quality and efficiency.
- Nozzle speed did not exhibit a significant effect on printing errors, indicating the complexity of interactions between material properties and printing parameters.
- The LDA classifier provided high accuracy in predicting the consistency of extruded filaments demonstrating its potential for ensuring shape fidelity in 3D food printing.
- The successful application of machine learning in this study underscores its importance in optimizing 3D printing processes and ensuring consistent quality in food production.

5.2 Limitations and Challenges

- The experiments were limited to a controlled laboratory environment, presenting challenges for scaling the process to industrial production. Variability in equipment, environmental conditions, and raw materials could affect reproducibility at a larger scale. Process standardization and automation require further investigation.
- The study focused on soy protein isolate (SPI) and wheat gluten (WG), limiting the generalizability of the findings. Different plant-based proteins may behave differently in terms of extrudability and printability.
- This study did not include sensory evaluations such as taste, texture, or visual appeal, which are essential for consumer acceptance.
- The study assumed uniformity in the quality of SPI, WG, and EGCG. However, natural variations in these ingredients could affect printability and product performance. Future research should account for these variables.

- The environmental impact of using SPI and WG on a large scale, particularly in terms of energy use and waste management, was not evaluated. Sustainability concerns are critical for the long-term feasibility of 3D food printing.

5.3 Recommendations for Future Studies

1. Future research should explore the influence of other potential additives and their interactions with SPI to further enhance printability and stability in 3D-printed food products.
2. Future studies should incorporate sensory evaluation, such as flavor, mouthfeel, and visual aesthetics, to gain insights into consumer preferences. Sensory analysis would provide a more consumer-oriented perspective, enabling a deeper understanding of how 3D-printed food products are perceived, particularly regarding their appeal and acceptance in real-world markets.
3. Investigations into the long-term stability and consumer acceptability of 3D-printed foods with optimized parameters could provide valuable insights for commercial applications.
4. Future studies could expand the work on predicting printability by incorporating the rheological properties of the materials, which play a crucial role in determining the flow behavior. Additionally, exploring various printer parameters, such as infill percentage and others specific to different 3D printers, could provide a more comprehensive understanding of how these factors influence the quality and precision of 3D-printed structures.
5. The development of more sophisticated machine learning models that can handle non-linear relationships and complex interactions within 3D printing datasets may lead to even better predictions and optimizations.
6. Expanding the scope of this research to include a broader range of plant-based proteins such as pea, lentil, or chickpea would help enhance the versatility of 3D food printing technologies. These proteins offer unique functional properties, and their incorporation could cater to specific dietary requirements or intolerances, such as gluten-free diets.

7. Further studies should focus on scaling up the 3D printing process for industrial applications, addressing the challenges associated with large-scale production while maintaining high precision and quality.

Appendix-A

Table A.1: Area Mode Results with Parameter Combinations

Concentration	Nozzle_Speed	Nozzle_Diameter	H_D_Ratio	Area_Mode	Label
0	228	16	0.85	16.7720597	ACCEPT
0	228	16	1	13.4643469	ACCEPT
0	228	16	1.25	15.4151479	ACCEPT
0	235	16	0.85	15.9776624	ACCEPT
0	235	16	1	16.8144656	ACCEPT
0	235	16	1.25	16.6191796	ACCEPT
0	245	16	0.85	12.9902893	ACCEPT
0	245	16	1	25.6881248	REJECT
0	245	16	1.25	23.1365931	REJECT
0	50	2.25	0.85	2.29837304	ACCEPT
0	50	2.25	1	1.84888218	ACCEPT
0	50	2.25	1.25	4.06772647	REJECT
0	58	2.25	0.85	2.17441567	ACCEPT
0	58	2.25	1	2.8415597	REJECT
0	58	2.25	1.25	1.99494317	ACCEPT
0	65	2.25	0.85	5.65251277	REJECT
0	65	2.25	1	2.6390237	ACCEPT
0	65	2.25	1.25	2.96099434	REJECT
0.25	228	16	0.85	12.5497362	ACCEPT
0.25	228	16	1	11.7464158	REJECT
0.25	228	16	1.25	15.3586304	ACCEPT
0.25	235	16	0.85	17.6505094	ACCEPT
0.25	235	16	1	18.6462311	ACCEPT
0.25	235	16	1.25	17.7357003	ACCEPT
0.25	245	16	0.85	22.0626689	REJECT
0.25	245	16	1	18.6076559	ACCEPT
0.25	245	16	1.25	17.0801763	ACCEPT
0.25	50	2.25	0.85	2.29106955	ACCEPT
0.25	50	2.25	1	2.02343497	ACCEPT
0.25	50	2.25	1.25	2.12948439	ACCEPT
0.25	58	2.25	0.85	1.94649559	ACCEPT
0.25	58	2.25	1	1.99963149	ACCEPT
0.25	58	2.25	1.25	4.84383968	REJECT
0.25	65	2.25	0.85	1.8368911	ACCEPT
0.25	65	2.25	1	2.46326403	ACCEPT
0.25	65	2.25	1.25	3.83777585	REJECT
0.5	228	16	0.85	17.4822136	ACCEPT
0.5	228	16	1	15.0650743	ACCEPT
0.5	228	16	1.25	14.8560324	ACCEPT
0.5	235	16	0.85	12.4142965	ACCEPT
0.5	235	16	1	17.5325494	ACCEPT

0.5	235	16	1.25	12.5060282	ACCEPT
0.5	245	16	0.85	10.8027146	REJECT
0.5	245	16	1	16.5930369	ACCEPT
0.5	245	16	1.25	12.92412	ACCEPT
0.5	50	2.25	0.85	2.68708098	ACCEPT
0.5	50	2.25	1	2.27887818	ACCEPT
0.5	50	2.25	1.25	2.21251731	ACCEPT
0.5	58	2.25	0.85	4.66238438	REJECT
0.5	58	2.25	1	2.61834597	ACCEPT
0.5	58	2.25	1.25	2.03423743	ACCEPT
0.5	65	2.25	0.85	6.69574558	REJECT
0.5	65	2.25	1	2.05862172	ACCEPT
0.5	65	2.25	1.25	2.16579712	ACCEPT
1	228	16	0.85	12.5497362	ACCEPT
1	228	16	1	11.7464158	REJECT
1	228	16	1.25	15.3586304	ACCEPT
1	235	16	0.85	17.6505094	ACCEPT
1	235	16	1	18.6462311	ACCEPT
1	235	16	1.25	17.7357003	ACCEPT
1	245	16	0.85	22.0626689	REJECT
1	245	16	1	18.6076559	ACCEPT
1	245	16	1.25	17.0801763	ACCEPT
1	50	2.25	0.85	2.29106955	ACCEPT
1	50	2.25	1	2.02343497	ACCEPT
1	50	2.25	1.25	2.12948439	ACCEPT
1	58	2.25	0.85	1.94649559	ACCEPT
1	58	2.25	1	1.99963149	ACCEPT
1	58	2.25	1.25	4.84383968	REJECT
1	65	2.25	0.85	1.8368911	ACCEPT
1	65	2.25	1	2.46326403	ACCEPT
1	65	2.25	1.25	3.83777585	REJECT

Table A.2: Area Consistency Results with Parameter Combinations

Conc.	Nozzle_Speed	Nozzle_Diameter	H_D_Ratio	Area_Consistency	Label
0	228	16	0.85	0.668	ACCEPT
0	228	16	1	0.459	REJECT
0	228	16	1.25	0.579	ACCEPT
0	235	16	0.85	0.533	ACCEPT
0	235	16	1	0.633	ACCEPT
0	235	16	1.25	0.585	ACCEPT
0	245	16	0.85	0.247	REJECT
0	245	16	1	0.543	ACCEPT
0	245	16	1.25	0.533	ACCEPT
0	50	2.25	0.85	0.364	REJECT

0	50	2.25	1	0.327	REJECT
0	50	2.25	1.25	0.175	REJECT
0	58	2.25	0.85	0.278	REJECT
0	58	2.25	1	0.244	REJECT
0	58	2.25	1.25	0.048	REJECT
0	65	2.25	0.85	0.162	REJECT
0	65	2.25	1	0.132	REJECT
0	65	2.25	1.25	0.098	REJECT
0.25	228	16	0.85	0.329	REJECT
0.25	228	16	1	0.218	REJECT
0.25	228	16	1.25	0.349	REJECT
0.25	235	16	0.85	0.452	REJECT
0.25	235	16	1	0.391	REJECT
0.25	235	16	1.25	0.313	REJECT
0.25	245	16	0.85	0.36	REJECT
0.25	245	16	1	0.51	ACCEPT
0.25	245	16	1.25	0.433	REJECT
0.25	50	2.25	0.85	0.46	REJECT
0.25	50	2.25	1	0.366	REJECT
0.25	50	2.25	1.25	0.314	REJECT
0.25	58	2.25	0.85	0.518	ACCEPT
0.25	58	2.25	1	0.523	ACCEPT
0.25	58	2.25	1.25	0.304	REJECT
0.25	65	2.25	0.85	0.025	REJECT
0.25	65	2.25	1	0.396	REJECT
0.25	65	2.25	1.25	0.141	REJECT
0.5	228	16	0.85	0.549	ACCEPT
0.5	228	16	1	0.557	ACCEPT
0.5	228	16	1.25	0.476	REJECT
0.5	235	16	0.85	0.287	REJECT
0.5	235	16	1	0.337	REJECT
0.5	235	16	1.25	0.348	REJECT
0.5	245	16	0.85	0.178	REJECT
0.5	245	16	1	0.291	REJECT
0.5	245	16	1.25	0.527	ACCEPT
0.5	50	2.25	0.85	0.455	REJECT
0.5	50	2.25	1	0.202	REJECT
0.5	50	2.25	1.25	0.476	REJECT
0.5	58	2.25	0.85	0.285	REJECT
0.5	58	2.25	1	0.28	REJECT
0.5	58	2.25	1.25	0.426	REJECT
0.5	65	2.25	0.85	0.222	REJECT
0.5	65	2.25	1	0.208	REJECT
0.5	65	2.25	1.25	0.179	REJECT
1	228	16	0.85	0.329	REJECT
1	228	16	1	0.218	REJECT

1	228	16	1.25	0.349	REJECT
1	235	16	0.85	0.452	REJECT
1	235	16	1	0.391	REJECT
1	235	16	1.25	0.313	REJECT
1	245	16	0.85	0.36	REJECT
1	245	16	1	0.51	ACCEPT
1	245	16	1.25	0.433	REJECT
1	50	2.25	0.85	0.46	REJECT
1	50	2.25	1	0.366	REJECT
1	50	2.25	1.25	0.314	REJECT
1	58	2.25	0.85	0.518	ACCEPT
1	58	2.25	1	0.523	ACCEPT
1	58	2.25	1.25	0.304	REJECT
1	65	2.25	0.85	0.025	REJECT
1	65	2.25	1	0.396	REJECT
1	65	2.25	1.25	0.141	REJECT

Table A.3 Area Arithmetic Mean Results with Parameter Combinations

Conc.	Nozzle_Speed	Nozzle_Diameter	H_D_Ratio	Area_Arithmentic_ Mean_Deviation	Label
0	228	16	0.85	0.216504588	ACCEPT
0	228	16	1	0.498575211	ACCEPT
0	228	16	1.25	0.341186755	ACCEPT
0	235	16	0.85	0.2061028	ACCEPT
0	235	16	1	0.247851458	ACCEPT
0	235	16	1.25	0.266683577	ACCEPT
0	245	16	0.85	0.428623561	ACCEPT
0	245	16	1	0.16936668	ACCEPT
0	245	16	1.25	0.168877443	ACCEPT
0	50	2.25	0.85	13.93420802	REJECT
0	50	2.25	1	13.39035524	REJECT
0	50	2.25	1.25	13.61778941	REJECT
0	58	2.25	0.85	13.31281586	REJECT
0	58	2.25	1	13.65295385	REJECT
0	58	2.25	1.25	12.72982755	REJECT
0	65	2.25	0.85	13.75018721	REJECT
0	65	2.25	1	13.62808854	REJECT
0	65	2.25	1.25	13.79303281	REJECT
0.25	228	16	0.85	3.858806042	ACCEPT
0.25	228	16	1	4.697664696	REJECT
0.25	228	16	1.25	4.373419698	REJECT
0.25	235	16	0.85	4.292486938	REJECT
0.25	235	16	1	4.593168564	REJECT
0.25	235	16	1.25	3.279707334	ACCEPT
0.25	245	16	0.85	2.349895753	ACCEPT

0.25	245	16	1	2.23818042	ACCEPT
0.25	245	16	1.25	3.702655243	ACCEPT
0.25	50	2.25	0.85	21.70711836	REJECT
0.25	50	2.25	1	15.30193298	REJECT
0.25	50	2.25	1.25	19.51987684	REJECT
0.25	58	2.25	0.85	19.40075311	REJECT
0.25	58	2.25	1	13.39066702	REJECT
0.25	58	2.25	1.25	15.43858855	REJECT
0.25	65	2.25	0.85	5.280419174	REJECT
0.25	65	2.25	1	21.18391023	REJECT
0.25	65	2.25	1.25	17.34394867	REJECT
0.5	228	16	0.85	0.608918287	ACCEPT
0.5	228	16	1	0.572881461	ACCEPT
0.5	228	16	1.25	0.096656256	ACCEPT
0.5	235	16	0.85	1.337685371	ACCEPT
0.5	235	16	1	1.084935417	ACCEPT
0.5	235	16	1.25	0.554662262	ACCEPT
0.5	245	16	0.85	1.285873632	ACCEPT
0.5	245	16	1	1.541981657	ACCEPT
0.5	245	16	1.25	0.715864017	ACCEPT
0.5	50	2.25	0.85	13.17951705	REJECT
0.5	50	2.25	1	12.41782851	REJECT
0.5	50	2.25	1.25	13.37313397	REJECT
0.5	58	2.25	0.85	12.94798546	REJECT
0.5	58	2.25	1	13.58803176	REJECT
0.5	58	2.25	1.25	13.19590811	REJECT
0.5	65	2.25	0.85	13.44322727	REJECT
0.5	65	2.25	1	13.30178744	REJECT
0.5	65	2.25	1.25	13.53267062	REJECT
1	228	16	0.85	3.858806042	ACCEPT
1	228	16	1	4.697664696	REJECT
1	228	16	1.25	4.373419698	REJECT
1	235	16	0.85	4.292486938	REJECT
1	235	16	1	4.593168564	REJECT
1	235	16	1.25	3.279707334	ACCEPT
1	245	16	0.85	2.349895753	ACCEPT
1	245	16	1	2.23818042	ACCEPT
1	245	16	1.25	3.702655243	ACCEPT
1	50	2.25	0.85	21.70711836	REJECT
1	50	2.25	1	15.30193298	REJECT
1	50	2.25	1.25	19.51987684	REJECT
1	58	2.25	0.85	19.40075311	REJECT
1	58	2.25	1	13.39066702	REJECT
1	58	2.25	1.25	15.43858855	REJECT
1	65	2.25	0.85	5.280419174	REJECT
1	65	2.25	1	21.18391023	REJECT

1	65	2.25	1.25	17.34394867	REJECT

Table A.4 Area Root Mean Square Results with Parameter Combinations

Conc.	Nozzle_Speed	Nozzle_Diameter	H_D_Ratio	Area_Root_Mean_Square_Deviation	Label
0	228	16	0.85	1.162804538	ACCEPT
0	228	16	1	1.534795958	ACCEPT
0	228	16	1.25	1.440218671	ACCEPT
0	235	16	0.85	1.605601442	ACCEPT
0	235	16	1	1.466563813	ACCEPT
0	235	16	1.25	1.603017912	ACCEPT
0	245	16	0.85	1.581670213	ACCEPT
0	245	16	1	1.191189459	ACCEPT
0	245	16	1.25	1.62936395	ACCEPT
0	50	2.25	0.85	14.03033212	REJECT
0	50	2.25	1	13.57774909	REJECT
0	50	2.25	1.25	13.7782437	REJECT
0	58	2.25	0.85	13.48872096	REJECT
0	58	2.25	1	13.74553376	REJECT
0	58	2.25	1.25	13.23292029	REJECT
0	65	2.25	0.85	13.80057884	REJECT
0	65	2.25	1	13.72520814	REJECT
0	65	2.25	1.25	13.90807198	REJECT
0.25	228	16	0.85	4.024239689	REJECT
0.25	228	16	1	4.949880237	REJECT
0.25	228	16	1.25	4.656285401	REJECT
0.25	235	16	0.85	4.903856961	REJECT
0.25	235	16	1	4.817519329	REJECT
0.25	235	16	1.25	4.352341431	REJECT
0.25	245	16	0.85	4.381402704	REJECT
0.25	245	16	1	4.683745371	REJECT
0.25	245	16	1.25	4.818654549	REJECT
0.25	50	2.25	0.85	35.81318722	REJECT
0.25	50	2.25	1	22.28212046	REJECT
0.25	50	2.25	1.25	33.40623884	REJECT
0.25	58	2.25	0.85	30.40446866	REJECT
0.25	58	2.25	1	19.92844991	REJECT
0.25	58	2.25	1.25	23.40394283	REJECT
0.25	65	2.25	0.85	5.477712547	REJECT
0.25	65	2.25	1	32.18495959	REJECT
0.25	65	2.25	1.25	22.79338868	REJECT
0.5	228	16	0.85	1.584876991	ACCEPT
0.5	228	16	1	1.790581292	ACCEPT
0.5	228	16	1.25	2.136016011	ACCEPT
0.5	235	16	0.85	2.173231461	ACCEPT

0.5	235	16	1	2.346931988	ACCEPT
0.5	235	16	1.25	2.148394156	ACCEPT
0.5	245	16	0.85	2.962000945	ACCEPT
0.5	245	16	1	2.335095286	ACCEPT
0.5	245	16	1.25	1.937861357	ACCEPT
0.5	50	2.25	0.85	13.35281235	REJECT
0.5	50	2.25	1	12.6051293	REJECT
0.5	50	2.25	1.25	13.5323201	REJECT
0.5	58	2.25	0.85	13.11479833	REJECT
0.5	58	2.25	1	13.77958119	REJECT
0.5	58	2.25	1.25	13.32807719	REJECT
0.5	65	2.25	0.85	13.56432832	REJECT
0.5	65	2.25	1	13.52310022	REJECT
0.5	65	2.25	1.25	13.70540007	REJECT
1	228	16	0.85	4.024239689	REJECT
1	228	16	1	4.949880237	REJECT
1	228	16	1.25	4.656285401	REJECT
1	235	16	0.85	4.903856961	REJECT
1	235	16	1	4.817519329	REJECT
1	235	16	1.25	4.352341431	REJECT
1	245	16	0.85	4.381402704	REJECT
1	245	16	1	4.683745371	REJECT
1	245	16	1.25	4.818654549	REJECT
1	50	2.25	0.85	35.81318722	REJECT
1	50	2.25	1	22.28212046	REJECT
1	50	2.25	1.25	33.40623884	REJECT
1	58	2.25	0.85	30.40446866	REJECT
1	58	2.25	1	19.92844991	REJECT
1	58	2.25	1.25	23.40394283	REJECT
1	65	2.25	0.85	5.477712547	REJECT
1	65	2.25	1	32.18495959	REJECT
1	65	2.25	1.25	22.79338868	REJECT

Table A.5 Width Mode Results with Parameter Combinations

Concentration	Nozzle_Speed	Nozzle_Diameter	H_D_Ratio	Width_Mode	Label
0	228	4	0.85	3.61584602	ACCEPT
0	228	4	1	3.34368769	REJECT
0	228	4	1.25	3.71009314	ACCEPT
0	235	4	0.85	3.52998102	REJECT
0	235	4	1	3.76423926	ACCEPT
0	235	4	1.25	3.79415914	ACCEPT
0	245	4	0.85	3.14239049	REJECT
0	245	4	1	4.84111491	REJECT
0	245	4	1.25	4.8306075	REJECT

0	50	1.5	0.85	1.19365522	REJECT
0	50	1.5	1	1.05977039	REJECT
0	50	1.5	1.25	1.89065407	REJECT
0	58	1.5	0.85	1.23832322	REJECT
0	58	1.5	1	1.52110862	ACCEPT
0	58	1.5	1.25	1.69187593	REJECT
0	65	1.5	0.85	1.79926539	REJECT
0	65	1.5	1	1.78494441	REJECT
0	65	1.5	1.25	1.68620573	REJECT
0.25	228	4	0.85	2.96993108	REJECT
0.25	228	4	1	3.15871894	REJECT
0.25	228	4	1.25	3.64536185	ACCEPT
0.25	235	4	0.85	4.1697205	ACCEPT
0.25	235	4	1	4.08968422	ACCEPT
0.25	235	4	1.25	3.76830057	ACCEPT
0.25	245	4	0.85	4.16670633	ACCEPT
0.25	245	4	1	4.08381618	ACCEPT
0.25	245	4	1.25	3.96696103	ACCEPT
0.25	50	1.5	0.85	1.30335035	REJECT
0.25	50	1.5	1	1.25911263	REJECT
0.25	50	1.5	1.25	1.39764932	ACCEPT
0.25	58	1.5	0.85	1.1932497	REJECT
0.25	58	1.5	1	1.23579588	REJECT
0.25	58	1.5	1.25	1.87968612	REJECT
0.25	65	1.5	0.85	2.33257624	REJECT
0.25	65	1.5	1	1.35447579	ACCEPT
0.25	65	1.5	1.25	1.60718226	ACCEPT
0.5	228	4	0.85	3.36611468	REJECT
0.5	228	4	1	3.45785446	REJECT
0.5	228	4	1.25	3.33403717	REJECT
0.5	235	4	0.85	2.71978089	REJECT
0.5	235	4	1	3.48302751	REJECT
0.5	235	4	1.25	3.16892624	REJECT
0.5	245	4	0.85	2.69771343	REJECT
0.5	245	4	1	3.35098787	REJECT
0.5	245	4	1.25	3.14335927	REJECT
0.5	50	1.5	0.85	1.58214926	ACCEPT
0.5	50	1.5	1	1.32895341	REJECT
0.5	50	1.5	1.25	1.54337084	ACCEPT
0.5	58	1.5	0.85	1.61150221	ACCEPT
0.5	58	1.5	1	1.54638099	ACCEPT
0.5	58	1.5	1.25	1.27621283	REJECT
0.5	65	1.5	0.85	1.5696605	ACCEPT
0.5	65	1.5	1	1.39750072	ACCEPT
0.5	65	1.5	1.25	1.44316299	ACCEPT
1	228	4	0.85	2.96993108	REJECT

1	228	4	1	3.15871894	REJECT
1	228	4	1.25	3.64536185	ACCEPT
1	235	4	0.85	4.1697205	ACCEPT
1	235	4	1	4.08968422	ACCEPT
1	235	4	1.25	3.76830057	ACCEPT
1	245	4	0.85	4.16670633	ACCEPT
1	245	4	1	4.08381618	ACCEPT
1	245	4	1.25	3.96696103	ACCEPT
1	50	1.5	0.85	1.30335035	REJECT
1	50	1.5	1	1.25911263	REJECT
1	50	1.5	1.25	1.39764932	ACCEPT
1	58	1.5	0.85	1.1932497	REJECT
1	58	1.5	1	1.23579588	REJECT
1	58	1.5	1.25	1.87968612	REJECT
1	65	1.5	0.85	2.33257624	REJECT
1	65	1.5	1	1.35447579	ACCEPT
1	65	1.5	1.25	1.60718226	ACCEPT

Table A.6 Width Consistency Results with Parameter Combinations

Concentration	Nozzle_Speed	Nozzle_Diameter	H_D_Ratio	Width_Consistency	Label
0	228	4	0.85	0.823	ACCEPT
0	228	4	1	0.618	ACCEPT
0	228	4	1.25	0.687	ACCEPT
0	235	4	0.85	0.652	ACCEPT
0	235	4	1	0.737	ACCEPT
0	235	4	1.25	0.69	ACCEPT
0	245	4	0.85	0.531	REJECT
0	245	4	1	0.661	ACCEPT
0	245	4	1.25	0.699	ACCEPT
0	50	1.5	0.85	0.446	REJECT
0	50	1.5	1	0.418	REJECT
0	50	1.5	1.25	0.378	REJECT
0	58	1.5	0.85	0.398	REJECT
0	58	1.5	1	0.374	REJECT
0	58	1.5	1.25	0.182	REJECT
0	65	1.5	0.85	0.239	REJECT
0	65	1.5	1	0.238	REJECT
0	65	1.5	1.25	0.246	REJECT
0.25	228	4	0.85	0.473	REJECT
0.25	228	4	1	0.4	REJECT
0.25	228	4	1.25	0.433	REJECT
0.25	235	4	0.85	0.514	REJECT
0.25	235	4	1	0.482	REJECT
0.25	235	4	1.25	0.575	REJECT

0.25	245	4	0.85	0.591	REJECT
0.25	245	4	1	0.669	ACCEPT
0.25	245	4	1.25	0.623	ACCEPT
0.25	50	1.5	0.85	0.659	ACCEPT
0.25	50	1.5	1	0.518	REJECT
0.25	50	1.5	1.25	0.497	REJECT
0.25	58	1.5	0.85	0.657	ACCEPT
0.25	58	1.5	1	0.586	REJECT
0.25	58	1.5	1.25	0.413	REJECT
0.25	65	1.5	0.85	0.357	REJECT
0.25	65	1.5	1	0.605	ACCEPT
0.25	65	1.5	1.25	0.353	REJECT
0.5	228	4	0.85	0.745	ACCEPT
0.5	228	4	1	0.771	ACCEPT
0.5	228	4	1.25	0.635	ACCEPT
0.5	235	4	0.85	0.381	REJECT
0.5	235	4	1	0.422	REJECT
0.5	235	4	1.25	0.492	REJECT
0.5	245	4	0.85	0.302	REJECT
0.5	245	4	1	0.406	REJECT
0.5	245	4	1.25	0.624	ACCEPT
0.5	50	1.5	0.85	0.628	ACCEPT
0.5	50	1.5	1	0.448	REJECT
0.5	50	1.5	1.25	0.649	ACCEPT
0.5	58	1.5	0.85	0.468	REJECT
0.5	58	1.5	1	0.592	REJECT
0.5	58	1.5	1.25	0.526	REJECT
0.5	65	1.5	0.85	0.486	REJECT
0.5	65	1.5	1	0.466	REJECT
0.5	65	1.5	1.25	0.364	REJECT
1	228	4	0.85	0.473	REJECT
1	228	4	1	0.4	REJECT
1	228	4	1.25	0.433	REJECT
1	235	4	0.85	0.514	REJECT
1	235	4	1	0.482	REJECT
1	235	4	1.25	0.575	REJECT
1	245	4	0.85	0.591	REJECT
1	245	4	1	0.669	ACCEPT
1	245	4	1.25	0.623	ACCEPT
1	50	1.5	0.8s5	0.659	ACCEPT
1	50	1.5	1	0.518	REJECT
1	50	1.5	1.25	0.497	REJECT
1	58	1.5	0.85	0.657	ACCEPT
1	58	1.5	1	0.586	REJECT
1	58	1.5	1.25	0.413	REJECT
1	65	1.5	0.85	0.357	REJECT

1	65	1.5	1	0.605	ACCEPT
1	65	1.5	1.25	0.353	REJECT

Table A.7 Width Arithmetic Mean Results with Parameter Combinations

Conc.	Nozzle_Speed	Nozzle_Diameter	H_D_Ratio	Width_Arithmentic_ Mean_Deviation	Label
0	228	4	0.85	0.242413541	ACCEPT
0	228	4	1	0.353030525	ACCEPT
0	228	4	1.25	0.318526495	ACCEPT
0	235	4	0.85	0.288078336	ACCEPT
0	235	4	1	0.271724468	ACCEPT
0	235	4	1.25	0.320459638	ACCEPT
0	245	4	0.85	0.362350659	ACCEPT
0	245	4	1	0.256536882	ACCEPT
0	245	4	1.25	0.281398008	ACCEPT
0	50	1.5	0.85	2.180282742	REJECT
0	50	1.5	1	2.149847113	REJECT
0	50	1.5	1.25	2.163626165	REJECT
0	58	1.5	0.85	2.151009608	REJECT
0	58	1.5	1	2.18274042	REJECT
0	58	1.5	1.25	2.143698078	REJECT
0	65	1.5	0.85	2.196721661	REJECT
0	65	1.5	1	2.200132308	REJECT
0	65	1.5	1.25	2.21118904	REJECT
0.25	228	4	0.85	1.271076604	REJECT
0.25	228	4	1	1.351047327	REJECT
0.25	228	4	1.25	1.384179859	REJECT
0.25	235	4	0.85	1.279614838	REJECT
0.25	235	4	1	1.359033646	REJECT
0.25	235	4	1.25	1.267081067	REJECT
0.25	245	4	0.85	1.287854992	REJECT
0.25	245	4	1	1.20028469	REJECT
0.25	245	4	1.25	1.2484684	REJECT
0.25	50	1.5	0.85	1.658350342	REJECT
0.25	50	1.5	1	1.499456281	REJECT
0.25	50	1.5	1.25	1.900070436	REJECT
0.25	58	1.5	0.85	1.702977984	REJECT
0.25	58	1.5	1	1.381651704	REJECT
0.25	58	1.5	1.25	1.458005136	REJECT
0.25	65	1.5	0.85	1.242505719	REJECT
0.25	65	1.5	1	1.826389744	REJECT
0.25	65	1.5	1.25	1.621443652	REJECT
0.5	228	4	0.85	0.700645645	ACCEPT
0.5	228	4	1	0.690584677	ACCEPT
0.5	228	4	1.25	0.662608134	ACCEPT

0.5	235	4	0.85	0.778147429	ACCEPT
0.5	235	4	1	0.765260378	ACCEPT
0.5	235	4	1.25	0.728179528	ACCEPT
0.5	245	4	0.85	0.805934389	REJECT
0.5	245	4	1	0.813915279	REJECT
0.5	245	4	1.25	0.745529447	ACCEPT
0.5	50	1.5	0.85	1.786509362	REJECT
0.5	50	1.5	1	1.726876223	REJECT
0.5	50	1.5	1.25	1.770545084	REJECT
0.5	58	1.5	0.85	1.717131149	REJECT
0.5	58	1.5	1	1.832249988	REJECT
0.5	58	1.5	1.25	1.759163782	REJECT
0.5	65	1.5	0.85	1.727595415	REJECT
0.5	65	1.5	1	1.782171184	REJECT
0.5	65	1.5	1.25	1.775396887	REJECT
1	228	4	0.85	1.271076604	REJECT
1	228	4	1	1.351047327	REJECT
1	228	4	1.25	1.384179859	REJECT
1	235	4	0.85	1.279614838	REJECT
1	235	4	1	1.359033646	REJECT
1	235	4	1.25	1.267081067	REJECT
1	245	4	0.85	1.287854992	REJECT
1	245	4	1	1.20028469	REJECT
1	245	4	1.25	1.2484684	REJECT
1	50	1.5	0.85	1.658350342	REJECT
1	50	1.5	1	1.499456281	REJECT
1	50	1.5	1.25	1.900070436	REJECT
1	58	1.5	0.85	1.702977984	REJECT
1	58	1.5	1	1.381651704	REJECT
1	58	1.5	1.25	1.458005136	REJECT
1	65	1.5	0.85	1.242505719	REJECT
1	65	1.5	1	1.826389744	REJECT
1	65	1.5	1.25	1.621443652	REJECT

Table A.8 Width Root Mean Square Results with Parameter Combinations

Conc.	Nozzle_Speed	Nozzle_Diameter	H_D_Ratio	Width_Root_Mean _Square_Deviation	Label
0	228	4	0.85	0.303629971	ACCEPT
0	228	4	1	0.427540598	ACCEPT
0	228	4	1.25	0.382581511	ACCEPT
0	235	4	0.85	0.357616543	ACCEPT
0	235	4	1	0.340618343	ACCEPT
0	235	4	1.25	0.39356558	ACCEPT
0	245	4	0.85	0.423289019	ACCEPT
0	245	4	1	0.334914669	ACCEPT

0	245	4	1.25	0.361134741	ACCEPT
0	50	1.5	0.85	2.202088349	REJECT
0	50	1.5	1	2.179588514	REJECT
0	50	1.5	1.25	2.181549584	REJECT
0	58	1.5	0.85	2.174050861	REJECT
0	58	1.5	1	2.197847434	REJECT
0	58	1.5	1.25	2.16695654	REJECT
0	65	1.5	0.85	2.215598974	REJECT
0	65	1.5	1	2.221584245	REJECT
0	65	1.5	1.25	2.235723098	REJECT
0.25	228	4	0.85	1.293308518	REJECT
0.25	228	4	1	1.386987433	REJECT
0.25	228	4	1.25	1.420156538	REJECT
0.25	235	4	0.85	1.331184403	REJECT
0.25	235	4	1	1.405024384	REJECT
0.25	235	4	1.25	1.335091382	REJECT
0.25	245	4	0.85	1.362012346	REJECT
0.25	245	4	1	1.268360888	REJECT
0.25	245	4	1.25	1.300421394	REJECT
0.25	50	1.5	0.85	2.029398608	REJECT
0.25	50	1.5	1	1.780878369	REJECT
0.25	50	1.5	1.25	2.478749532	REJECT
0.25	58	1.5	0.85	2.110278261	REJECT
0.25	58	1.5	1	1.590871132	REJECT
0.25	58	1.5	1.25	1.676665128	REJECT
0.25	65	1.5	0.85	1.283134911	REJECT
0.25	65	1.5	1	2.297046206	REJECT
0.25	65	1.5	1.25	2.066071614	REJECT
0.5	228	4	0.85	0.736575389	ACCEPT
0.5	228	4	1	0.743939705	ACCEPT
0.5	228	4	1.25	0.720071166	ACCEPT
0.5	235	4	0.85	0.831007858	ACCEPT
0.5	235	4	1	0.811363182	ACCEPT
0.5	235	4	1.25	0.77541455	ACCEPT
0.5	245	4	0.85	0.880601329	ACCEPT
0.5	245	4	1	0.861377492	ACCEPT
0.5	245	4	1.25	0.787831095	ACCEPT
0.5	50	1.5	0.85	1.808761141	REJECT
0.5	50	1.5	1	1.754903087	REJECT
0.5	50	1.5	1.25	1.79325398	REJECT
0.5	58	1.5	0.85	1.740806648	REJECT
0.5	58	1.5	1	1.853986671	REJECT
0.5	58	1.5	1.25	1.786555164	REJECT
0.5	65	1.5	0.85	1.751071874	REJECT
0.5	65	1.5	1	1.807806988	REJECT
0.5	65	1.5	1.25	1.799187715	REJECT

1	228	4	0.85	1.293308518	REJECT
1	228	4	1	1.386987433	REJECT
1	228	4	1.25	1.420156538	REJECT
1	235	4	0.85	1.331184403	REJECT
1	235	4	1	1.405024384	REJECT
1	235	4	1.25	1.335091382	REJECT
1	245	4	0.85	1.362012346	REJECT
1	245	4	1	1.268360888	REJECT
1	245	4	1.25	1.300421394	REJECT
1	50	1.5	0.85	2.029398608	REJECT
1	50	1.5	1	1.780878369	REJECT
1	50	1.5	1.25	2.478749532	REJECT
1	58	1.5	0.85	2.110278261	REJECT
1	58	1.5	1	1.590871132	REJECT
1	58	1.5	1.25	1.676665128	REJECT
1	65	1.5	0.85	1.283134911	REJECT
1	65	1.5	1	2.297046206	REJECT
1	65	1.5	1.25	2.066071614	REJECT

Table A.9 Thickness Mode Results with Parameter Combinations

Conc.	Nozzle_Speed	Nozzle_Diameter	H_D_Ratio	Thickness_Mode	Label
0	228	4	0.85	4.533685893	ACCEPT
0	228	4	1	4.031029619	ACCEPT
0	228	4	1.25	4.263015873	ACCEPT
0	235	4	0.85	4.749831012	REJECT
0	235	4	1	4.625991348	REJECT
0	235	4	1.25	4.635766276	REJECT
0	245	4	0.85	4.143853635	ACCEPT
0	245	4	1	5.688182817	REJECT
0	245	4	1.25	5.083107238	REJECT
0	50	1.5	0.85	1.770334363	REJECT
0	50	1.5	1	1.736266862	REJECT
0	50	1.5	1.25	2.585910829	REJECT
0	58	1.5	0.85	1.755946937	REJECT
0	58	1.5	1	1.889715578	REJECT
0	58	1.5	1.25	1.946946991	REJECT
0	65	1.5	0.85	2.837941725	REJECT
0	65	1.5	1	2.12115374	REJECT
0	65	1.5	1.25	2.873957831	REJECT
0.25	228	4	0.85	4.250223499	ACCEPT
0.25	228	4	1	4.047491635	ACCEPT
0.25	228	4	1.25	4.013891036	ACCEPT
0.25	235	4	0.85	4.439332975	ACCEPT
0.25	235	4	1	4.627008508	REJECT

0.25	235	4	1.25	4.385476312	ACCEPT
0.25	245	4	0.85	4.613116908	REJECT
0.25	245	4	1	4.413796009	ACCEPT
0.25	245	4	1.25	4.516562798	ACCEPT
0.25	50	1.5	0.85	1.702616196	ACCEPT
0.25	50	1.5	1	1.569672936	ACCEPT
0.25	50	1.5	1.25	1.619907935	ACCEPT
0.25	58	1.5	0.85	1.629784468	ACCEPT
0.25	58	1.5	1	1.638502995	ACCEPT
0.25	58	1.5	1.25	2.607859385	REJECT
0.25	65	1.5	0.85	3.902040081	REJECT
0.25	65	1.5	1	1.880706266	REJECT
0.25	65	1.5	1.25	1.816396662	REJECT
0.5	228	4	0.85	4.855523534	REJECT
0.5	228	4	1	4.459296141	ACCEPT
0.5	228	4	1.25	4.306424936	ACCEPT
0.5	235	4	0.85	4.291207686	ACCEPT
0.5	235	4	1	4.822023481	REJECT
0.5	235	4	1.25	4.555791465	ACCEPT
0.5	245	4	0.85	4.35578937	ACCEPT
0.5	245	4	1	4.553939071	ACCEPT
0.5	245	4	1.25	4.257735657	ACCEPT
0.5	50	1.5	0.85	1.763767686	REJECT
0.5	50	1.5	1	2.038217023	REJECT
0.5	50	1.5	1.25	1.399050782	ACCEPT
0.5	58	1.5	0.85	2.855519387	REJECT
0.5	58	1.5	1	1.94960017	REJECT
0.5	58	1.5	1.25	1.713554608	ACCEPT
0.5	65	1.5	0.85	3.699889616	REJECT
0.5	65	1.5	1	1.822849382	REJECT
0.5	65	1.5	1.25	2.062606373	REJECT
1	228	4	0.85	4.250223499	ACCEPT
1	228	4	1	4.047491635	ACCEPT
1	228	4	1.25	4.013891036	ACCEPT
1	235	4	0.85	4.439332975	ACCEPT
1	235	4	1	4.627008508	REJECT
1	235	4	1.25	4.385476312	ACCEPT
1	245	4	0.85	4.613116908	REJECT
1	245	4	1	4.413796009	ACCEPT
1	245	4	1.25	4.516562798	ACCEPT
1	50	1.5	0.85	1.702616196	ACCEPT
1	50	1.5	1	1.569672936	ACCEPT
1	50	1.5	1.25	1.619907935	ACCEPT
1	58	1.5	0.85	1.629784468	ACCEPT
1	58	1.5	1	1.638502995	ACCEPT
1	58	1.5	1.25	2.607859385	REJECT

1	65	1.5	0.85	3.902040081	REJECT
1	65	1.5	1	1.880706266	REJECT
1	65	1.5	1.25	1.816396662	REJECT

Table A.10 Thickness Consistency Results with Parameter Combinations

Concentration	Nozzle_Speed	Nozzle_Diameter	H_D_Ratio	Thickness_Consistency	Label
0	228	4	0.85	0.856	ACCEPT
0	228	4	1	0.533	REJECT
0	228	4	1.25	0.803	ACCEPT
0	235	4	0.85	0.791	ACCEPT
0	235	4	1	0.891	ACCEPT
0	235	4	1.25	0.777	ACCEPT
0	245	4	0.85	0.384	REJECT
0	245	4	1	0.727	REJECT
0	245	4	1.25	0.819	ACCEPT
0	50	1.5	0.85	0.662	REJECT
0	50	1.5	1	0.757	ACCEPT
0	50	1.5	1.25	0.414	REJECT
0	58	1.5	0.85	0.623	REJECT
0	58	1.5	1	0.422	REJECT
0	58	1.5	1.25	0.162	REJECT
0	65	1.5	0.85	0.354	REJECT
0	65	1.5	1	0.412	REJECT
0	65	1.5	1.25	0.4	REJECT
0.25	228	4	0.85	0.587	REJECT
0.25	228	4	1	0.502	REJECT
0.25	228	4	1.25	0.508	REJECT
0.25	235	4	0.85	0.578	REJECT
0.25	235	4	1	0.584	REJECT
0.25	235	4	1.25	0.558	REJECT
0.25	245	4	0.85	0.657	REJECT
0.25	245	4	1	0.732	REJECT
0.25	245	4	1.25	0.664	REJECT
0.25	50	1.5	0.85	0.703	REJECT
0.25	50	1.5	1	0.496	REJECT
0.25	50	1.5	1.25	0.538	REJECT
0.25	58	1.5	0.85	0.85	ACCEPT
0.25	58	1.5	1	0.783	ACCEPT
0.25	58	1.5	1.25	0.58	REJECT
0.25	65	1.5	0.85	0.208	REJECT
0.25	65	1.5	1	0.587	REJECT
0.25	65	1.5	1.25	0.253	REJECT
0.5	228	4	0.85	0.861	ACCEPT
0.5	228	4	1	0.809	ACCEPT

0.5	228	4	1.25	0.764	ACCEPT
0.5	235	4	0.85	0.415	REJECT
0.5	235	4	1	0.518	REJECT
0.5	235	4	1.25	0.669	REJECT
0.5	245	4	0.85	0.25	REJECT
0.5	245	4	1	0.414	REJECT
0.5	245	4	1.25	0.787	ACCEPT
0.5	50	1.5	0.85	0.646	REJECT
0.5	50	1.5	1	0.482	REJECT
0.5	50	1.5	1.25	0.656	REJECT
0.5	58	1.5	0.85	0.366	REJECT
0.5	58	1.5	1	0.514	REJECT
0.5	58	1.5	1.25	0.787	ACCEPT
0.5	65	1.5	0.85	0.311	REJECT
0.5	65	1.5	1	0.493	REJECT
0.5	65	1.5	1.25	0.347	REJECT
1	228	4	0.85	0.587	REJECT
1	228	4	1	0.502	REJECT
1	228	4	1.25	0.508	REJECT
1	235	4	0.85	0.578	REJECT
1	235	4	1	0.584	REJECT
1	235	4	1.25	0.558	REJECT
1	245	4	0.85	0.657	REJECT
1	245	4	1	0.732	REJECT
1	245	4	1.25	0.664	REJECT
1	50	1.5	0.85	0.703	REJECT
1	50	1.5	1	0.496	REJECT
1	50	1.5	1.25	0.538	REJECT
1	58	1.5	0.85	0.85	ACCEPT
1	58	1.5	1	0.783	ACCEPT
1	58	1.5	1.25	0.58	REJECT
1	65	1.5	0.85	0.208	REJECT
1	65	1.5	1	0.587	REJECT
1	65	1.5	1.25	0.253	REJECT

Table A.11 Thickness Arithmetic Mean Results with Parameter Combinations

Conc.	Nozzle_Speed	Nozzle_Diameter	H_D_Ratio	Thickness_Arithmentic_Mean_Deviation	Label
0	228	4	0.85	0.294393667	ACCEPT
0	228	4	1	0.270901979	ACCEPT
0	228	4	1.25	0.275329765	ACCEPT
0	235	4	0.85	0.276689277	ACCEPT
0	235	4	1	0.257250695	ACCEPT
0	235	4	1.25	0.232995442	ACCEPT
0	245	4	0.85	0.283370986	ACCEPT

0	245	4	1	0.269104137	ACCEPT
0	245	4	1.25	0.253277253	ACCEPT
0	50	1.5	0.85	2.792020454	REJECT
0	50	1.5	1	2.798061515	REJECT
0	50	1.5	1.25	2.79525337	REJECT
0	58	1.5	0.85	2.749838894	REJECT
0	58	1.5	1	2.796688328	REJECT
0	58	1.5	1.25	2.59700431	REJECT
0	65	1.5	0.85	2.825696289	REJECT
0	65	1.5	1	2.753941758	REJECT
0	65	1.5	1.25	2.778651487	REJECT
0.25	228	4	0.85	0.447528761	ACCEPT
0.25	228	4	1	0.390994196	ACCEPT
0.25	228	4	1.25	0.395661685	ACCEPT
0.25	235	4	0.85	0.412064377	ACCEPT
0.25	235	4	1	0.435236468	ACCEPT
0.25	235	4	1.25	0.593960711	ACCEPT
0.25	245	4	0.85	0.583276378	ACCEPT
0.25	245	4	1	0.765141137	REJECT
0.25	245	4	1.25	0.563660397	ACCEPT
0.25	50	1.5	0.85	4.406349226	REJECT
0.25	50	1.5	1	4.014842178	REJECT
0.25	50	1.5	1.25	4.190579604	REJECT
0.25	58	1.5	0.85	4.430765584	REJECT
0.25	58	1.5	1	4.172028909	REJECT
0.25	58	1.5	1.25	4.029744117	REJECT
0.25	65	1.5	0.85	2.974414408	REJECT
0.25	65	1.5	1	4.375539671	REJECT
0.25	65	1.5	1.25	3.656777813	REJECT
0.5	228	4	0.85	0.770948938	REJECT
0.5	228	4	1	0.710830155	REJECT
0.5	228	4	1.25	0.767909415	REJECT
0.5	235	4	0.85	0.637205544	REJECT
0.5	235	4	1	0.645522205	REJECT
0.5	235	4	1.25	0.675875948	REJECT
0.5	245	4	0.85	0.663238497	REJECT
0.5	245	4	1	0.712421206	REJECT
0.5	245	4	1.25	0.743670391	REJECT
0.5	50	1.5	0.85	3.197877309	REJECT
0.5	50	1.5	1	3.288055768	REJECT
0.5	50	1.5	1.25	3.256033763	REJECT
0.5	58	1.5	0.85	3.208801913	REJECT
0.5	58	1.5	1	3.192190227	REJECT
0.5	58	1.5	1.25	3.211125687	REJECT
0.5	65	1.5	0.85	3.185790604	REJECT
0.5	65	1.5	1	3.233153103	REJECT

0.5	65	1.5	1.25	3.226570865	REJECT
1	228	4	0.85	0.447528761	ACCEPT
1	228	4	1	0.390994196	ACCEPT
1	228	4	1.25	0.395661685	ACCEPT
1	235	4	0.85	0.412064377	ACCEPT
1	235	4	1	0.435236468	ACCEPT
1	235	4	1.25	0.593960711	ACCEPT
1	245	4	0.85	0.583276378	ACCEPT
1	245	4	1	0.765141137	REJECT
1	245	4	1.25	0.563660397	ACCEPT
1	50	1.5	0.85	4.406349226	REJECT
1	50	1.5	1	4.014842178	REJECT
1	50	1.5	1.25	4.190579604	REJECT
1	58	1.5	0.85	4.430765584	REJECT
1	58	1.5	1	4.172028909	REJECT
1	58	1.5	1.25	4.029744117	REJECT
1	65	1.5	0.85	2.974414408	REJECT
1	65	1.5	1	4.375539671	REJECT
1	65	1.5	1.25	3.656777813	REJECT

Table A.12 Thickness Root Mean Square Results with Parameter Combinations

Conc.	Nozzle_Speed	Nozzle_Diameter	H_D_Ratio	Thickness_Root_Mean_Square_Deviation	Label
0	228	4	0.85	0.410284092	ACCEPT
0	228	4	1	0.325046893	ACCEPT
0	228	4	1.25	0.384478655	ACCEPT
0	235	4	0.85	0.404465386	ACCEPT
0	235	4	1	0.459343163	ACCEPT
0	235	4	1.25	0.46200976	ACCEPT
0	245	4	0.85	0.358321988	ACCEPT
0	245	4	1	0.403491816	ACCEPT
0	245	4	1.25	0.442217154	ACCEPT
0	50	1.5	0.85	2.815375576	REJECT
0	50	1.5	1	2.813359786	REJECT
0	50	1.5	1.25	2.827093159	REJECT
0	58	1.5	0.85	2.779691296	REJECT
0	58	1.5	1	2.811748743	REJECT
0	58	1.5	1.25	2.678375693	REJECT
0	65	1.5	0.85	2.832926841	REJECT
0	65	1.5	1	2.780237627	REJECT
0	65	1.5	1.25	2.79684009	REJECT
0.25	228	4	0.85	0.56795297	ACCEPT
0.25	228	4	1	0.563721804	ACCEPT
0.25	228	4	1.25	0.538119077	ACCEPT
0.25	235	4	0.85	0.554417045	ACCEPT

0.25	235	4	1	0.571379842	ACCEPT
0.25	235	4	1.25	0.700114714	ACCEPT
0.25	245	4	0.85	0.946368226	REJECT
0.25	245	4	1	1.331932853	REJECT
0.25	245	4	1.25	0.68414966	ACCEPT
0.25	50	1.5	0.85	5.534278352	REJECT
0.25	50	1.5	1	4.699987581	REJECT
0.25	50	1.5	1.25	5.138834365	REJECT
0.25	58	1.5	0.85	5.577838226	REJECT
0.25	58	1.5	1	5.309440832	REJECT
0.25	58	1.5	1.25	4.863033492	REJECT
0.25	65	1.5	0.85	3.104923079	REJECT
0.25	65	1.5	1	5.51336538	REJECT
0.25	65	1.5	1.25	4.753290762	REJECT
0.5	228	4	0.85	0.813751656	REJECT
0.5	228	4	1	0.773851186	ACCEPT
0.5	228	4	1.25	0.823601495	REJECT
0.5	235	4	0.85	0.72912343	ACCEPT
0.5	235	4	1	0.758085526	ACCEPT
0.5	235	4	1.25	0.748748301	ACCEPT
0.5	245	4	0.85	0.82255247	REJECT
0.5	245	4	1	0.821437069	REJECT
0.5	245	4	1.25	0.795498507	ACCEPT
0.5	50	1.5	0.85	3.216006579	REJECT
0.5	50	1.5	1	3.308887619	REJECT
0.5	50	1.5	1.25	3.269471741	REJECT
0.5	58	1.5	0.85	3.231107317	REJECT
0.5	58	1.5	1	3.208232713	REJECT
0.5	58	1.5	1.25	3.233946438	REJECT
0.5	65	1.5	0.85	3.198683876	REJECT
0.5	65	1.5	1	3.250611625	REJECT
0.5	65	1.5	1.25	3.249697633	REJECT
1	228	4	0.85	0.56795297	ACCEPT
1	228	4	1	0.563721804	ACCEPT
1	228	4	1.25	0.538119077	ACCEPT
1	235	4	0.85	0.554417045	ACCEPT
1	235	4	1	0.571379842	ACCEPT
1	235	4	1.25	0.700114714	ACCEPT
1	245	4	0.85	0.946368226	REJECT
1	245	4	1	1.331932853	REJECT
1	245	4	1.25	0.68414966	ACCEPT
1	50	1.5	0.85	5.534278352	REJECT
1	50	1.5	1	4.699987581	REJECT
1	50	1.5	1.25	5.138834365	REJECT
1	58	1.5	0.85	5.577838226	REJECT
1	58	1.5	1	5.309440832	REJECT

1	58	1.5	1.25	4.863033492	REJECT
1	65	1.5	0.85	3.104923079	REJECT
1	65	1.5	1	5.51336538	REJECT
1	65	1.5	1.25	4.753290762	REJECT

Code A.1: MATLAB Code for Data Labeling

```
% Clear variables from the workspace

clear

clear all

clc

% Read the data generated from the experiment

T=readtable("C:\Users\smitt\Downloads\SHIVANI-REVISED\SHIVANI-
REVISED\DISCRIMINANTANALYSIS\DATALABELLING\WIDTH\ResultSheetWidthAV
ERAGE.xlsx")

%%%%%%%%%%%%%%%%%%%%%%%%%%%%%%%%%%%%%%%%%%%%%%%%%%%%

% Assign variable to the predictors and response

%%%%%%%%%%%%%%%%%%%%%%%%%%%%%%%%%%%%%%%%%%%%%%%%%%%%

Concentration=T.Concentration;

Nozzle_Speed=T.Nozzle_Speed;

Nozzle_Diameter=T.Nozzle_Diameter;

H_D_Ratio =T. H_D_Ratio;

% Width_Mode (or any other shape fidelity metric)

Width_Mode=T.Width_Mode;

% Preallocate memory to store the labels

Label=categorical(zeros(size(T,1),1));

% Calling loop to each row of the table

for k=1:size(T,1)
```

```
    % Reference response
    a1=T.Nozzle_Diameter(k);
    % Measured response
    a2=T.Width_Mode(k);
    % Percentage difference between reference and measured response
    da=(abs(a1-a2)/a1)*100;
    % Criteria for assigning label to data based on the acceptable and unacceptable limits
    if (da <=10)
        Label(k,1)=char('ACCEPT');
    else
        Label(k,1)=char('REJECT');
    end
end
% Create table using the predictors and response variables as well as the variable for labels
TL=table(Concentration, Nozzle_Speed, Nozzle_Diameter, H_D_Ratio, Width_Mode,Label);
% Write the new table to the file
writetable(TL,'C:\Users\smitt\Downloads\SHIVANIREVISED\SHIVANIREVISED\DISCRMINANTANALYSIS\DATALABELLING\WIDTH\ResultSheetWidthAVERAGEwithLabels.xlsx')
```

Code A.2: MATLAB Code to split data into training and testing for LDA

```
% Clear variables from workspace
clear
clear all
clc
```

```
% Read table that contains labels
T=readtable("C:\Users\smitt\Downloads\SHIVANIREVISED\SHIVANIREVISED\DISCRIMINANTANALYSIS\SPLITTRAINTEST\WIDTH\WIDTHMODE\ResultSheetWidthAVERAGEwithLabels.xlsx");
% Assign variable to the labels in the table
Labels=T.Label;
% Create indices for the 10-fold cross-validation.
indices=crossvalind('Kfold',Labels,10);
%%%%%%%%%%%%%%%%%%%%%%%%%%
% DEFINE PARTITION
%%%%%%%%%%%%%%%%%%%%%%%%%%
% Preallocate memory to 10-fold partition
Partition=zeros(size(Labels,1),10);
% Calling loop to each indices
for k1 = 1:10
   % Current test index
   test=(indices==k1);
   % Indices in the data belonging to the test set
   indTe=find(test);
   % Assign the test set indices to the 10-fold partition
   Partition(indTe,k1)=1;
   % Current training index
   train=~test;
   % Indices in the data belonging to the training set
   indTr=find(train);
```

```
    % Assign the training set indices to the 10-fold partition
    Partition(indTr,k1)=0;
end
% Preallocate memory to store the classification accuracy for each fold
Acc1=zeros(1,10);
% Calling loop to each of the 10 fold
for k2=1:size(Partition,2)
    %%%%%%%%%%%%%%%%%%%%%%%%%%%%%%%%%%%%%%%%%%%%%%%%%%%%
    % SPLIT DATA INTO TRAINING AND TEST SETS
    %%%%%%%%%%%%%%%%%%%%%%%%%%%%%%%%%%%%%%%%%%%%%%%%%%%%
    % Training set indices
    indTrain=find(Partition(:,k2)==0);
    % Test set indices
    indTest=find(Partition(:,k2)==1)
    % Training set
    TrainSet=T(indTrain,1:5);
    % Training set labels
    TrainSetResponse=T(indTrain,6);
    % Test set
    TestSet=T(indTest,1:5);
    % Test labels
    TestSetResponse1=T(indTest,6);
    % True labels converted from table to cell format
    labels=table2cell(TestSetResponse1)
```

```
%%%%%%%%%%%%%%%%%%%%%%%%%%%%%%%
% TRAIN CLASSIFIER
%%%%%%%%%%%%%%%%%%%%%%%%%%%%%%%
Mdl=fitcdiscr(TrainSet,TrainSetResponse);
%%%%%%%%%%%%%%%%%%%%%%%%%%%%%%%%%
% TESTING - EVALUATE CLASSIFIER
%%%%%%%%%%%%%%%%%%%%%%%%%%%%%%%%%
PredLabels = predict(Mdl,TestSet);
%%%%%%%%%%%%%%%%%%%%%%%%%%%%
% EVALUATION PARAMETERS
%%%%%%%%%%%%%%%%%%%%%%%%%%%%
% Compute the confusion matri
ConfMatrixT=confusionmat(labels,PredLabels);
% Invert to define true positive as 'ACCEPTABLE' and true negative as 'REJECT'
ConfMatrixT=ConfMatrixT';
% Compute the evaluation parameters
[ACC2,TPR2,TNR2,Prec_Accpt2,Prec_Rejt2]=ConfMatrix2EvalutionParam(ConfMatrixT);
% Accuracy
ACC1(1,k2)=ACC2;
% True positive rate
TPR1(1,k2)=TPR2;
% True negative rate
TNR1(1,k2)=TNR2;
% Precision Accept
```

```
    Prec_Accpt1(1,k2)=Prec_Accpt2;
    % Precision Reject
    Prec_Rejt1(1,k2)=Prec_Rejt2;
end
% Average acccuracy
ACC=mean(ACC1)
% Average true positive rate
TPR=mean(TPR1)
% Average true negative rate
TNR=mean(TNR1)
% Average precison accept
Prec_Accpt=mean(Prec_Accpt1)
% Average precison reject
Prec_Rejt=mean(Prec_Rejt1)
```

Code A.3: MATLAB Code for computing five performance evaluation parameters from the confusion matrix

```
%%%%%%%%%%%%%%%%%%%%%%%%%%%%%%%%%%%%%%%%%%%%%%%%%%%%%
function [ACC,TPR,TNR,PrecFem,PrecMale]=ConfMatrix2EvalutionParam(ConfMatrix)
%%%%%%%%%%%%%%%%%%%%%%%%%%%%%%%%%%%%%%%%%%%%%%%%%%%%%
% This matlab code computes five performance evaluation parameters from the
% confusion matrix
%%%%%%%%%%%%%%%%%%%
% INPUT
%%%%%%%%%%%%%%%%%%%
```

```
% ConfMatrix - Confusion matrix

%%%%%%%%%%%%%%%%

% OUTPUT

%%%%%%%%%%%%%%%%

% ACC - Accuracy

% TPR - True positive rate

% TNR - True negative rate

% PrecFem - Precision female

% PrecMale - Precision male

% Copyright © 2022 by Dr. Michael Osadebey

% MatrixSpec Solutions Inc.

% All rights of this code belong to MatrixSpec Solution Inc.

%%%%%%%%%%%%%%%%%%%%%%%%%%%%%%%%%%%%%%%%%%%%%
%%%%%%%%%%%%%%%%%%%%%%%%%%%%%%%%%%%%

% Compute the evaluation parameters

% ACC

ACC=(ConfMatrix(1,1)+ConfMatrix(2,2))/sum(ConfMatrix(:));

% TPR

TPR=ConfMatrix(2,2)/sum(ConfMatrix(2,:));

% TNR

TNR=ConfMatrix(1,1)/sum(ConfMatrix(1,:));

% Precision Female

PrecFem=ConfMatrix(2,2)/sum(ConfMatrix(:,2));

% Precision Male

PrecMale=ConfMatrix(1,1)/sum(ConfMatrix(:,1));
```